Titre: Title:	Ascending Aorta Parametric Modeling and Fluid Dynamics Analysis in a Child Patient with Congenital BAV and Ascending Aorta Aneurysm
Auteur: Author:	Rosario Criscione
Date:	2013
Type:	Mémoire ou thèse / Dissertation or Thesis
Référence: Citation:	Criscione, R. (2013). Ascending Aorta Parametric Modeling and Fluid Dynamics Analysis in a Child Patient with Congenital BAV and Ascending Aorta Aneurysm [Mémoire de maîtrise, École Polytechnique de Montréal]. PolyPublie. https://publications.polymtl.ca/1313/

UNIVERSITÉ DE MONTRÉAL

ASCENDING AORTA PARAMETRIC MODELING AND FLUID DYNAMICS ANALYSIS IN A CHILD PATIENT WITH CONGENITAL BAV AND ASCENDING AORTA ANEURYSM

ROSARIO CRISCIONE
INSTITUT DE GÉNIE BIOMÉDICAL
ÉCOLE POLYTECHNIQUE DE MONTRÉAL

MÉMOIRE PRÉSENTÉ EN VUE DE L'OBTENTION
DU DIPLÔME DE MAÎTRISE ÈS SCIENCES APPLIQUÉES
(GÉNIE BIOMÉDICAL)
DÉCEMBRE 2013

UNIVERSITÉ DE MONTRÉAL

ÉCOLE POLYTECHNIQUE DE MONTRÉAL

Ce mémoire intitulé :

ASCENDING AORTA PARAMETRIC MODELING AND FLUID DYNAMICS ANALYSIS IN A CHILD PATIENT WITH CONGENITAL BAV AND ASCENDING AORTA ANEURYSM

présenté par : CRISCIONE Rosario
en vue de l'obtention du diplôme de : Maîtrise ès sciences appliquées
a été dûment accepté par le jury d'examen constitué de :

M. TRÉPANIER Jean-Yves, Ph.D, président
Mme PÉRIÉ-CURNIER Delphine, Doctorat, membre et directrice de recherche
M. YAHIA L'Hocine, Ph.D, membre et codirecteur de recherche
M. MIRO Joaquim, M.D., membre

To Gabriella and Luciano,
without you, I would have never
amounted to anything.

ACKNOWLEDGMENTS

First of all, I want to thank all the members of the jury who assessed my work, jury president Docteur Jean-Yves Trépanier, Docteurs L'Hocine Yahia, Delphine Périé-Curnier and Joaquim Miró.

I would especially like to thank my research director, Docteur Delphine Périé-Curnier, for her support throughout all my work and for being a truly comprehensive and sensitive person.

Thank you to Eddy, for introducing and helping me with the mesh and fluid-dynamics test environment. Thank you also to Hadrien for having shared his expertise in CATIA with me.

Thank you to my family, for allowing me to have this great experience. Without you and your support, this would never have been possible.

Thank you to Marina, who motivated me throughout our similar journeys in Montreal.

Mei, thank you for your strength and your admirable constancy. Daniela, thank you for your 360 degree support in every circumstance. Giulia, thank you for your elegant smiles. You were my secret weapon during this period.

RÉSUMÉ

L'anévrisme de l'aorte ascendante ($AAoA$) est une déformation qui affecte la partie de l'aorte entre la valve aortique et le tronc brachiocéphalique. L'incidence de cette maladie est plus élevée dans les cas de patients atteints de la pathologie de la Bicuspidie Valvulaire Aortique (BVA). BVA est la malformation cardiaque congénitale la plus commune dans le monde avec une prévalence entre *0.5%* et *2%*. De nombreux patients atteints de l'AAoA sont des enfants comme cela se produit plus souvent à un plus jeune âge.

La chirurgie invasive est actuellement considérée comme l'étalon-or pour le traitement de la déformation de l'aorte. Cette intervention chirurgicale a un taux de mortalité élevé, entre *2.5%* et *5%* des cas traités, en raison du danger intrinsèque de l'opération qui pourrait prendre plus de 5 heures. L'avènement des techniques chirurgicales à invasion minimale au cours des dernières années a pour but de réduire la nécessité d'une chirurgie invasive en utilisant des dispositifs tels que des stents et des greffes qui sont implantables par cathétérisme. L'utilisation de ces nouvelles techniques d'intervention présente des avantages significatifs par rapport à la chirurgie conventionnelle, comme la diminution du risque de mortalité opératoire et la durée totale de l'intervention et de l'hospitalisation. Cependant, un processus de simulation précisant toutes les conditions possibles dans lesquelles le dispositif implanté pourrait fonctionner est nécessaire.

Ce projet de recherche consiste à développer un modèle de l'aorte ascendante par Conception Assistée par Ordinateur (CAO) qui permet de simuler, avec une grande fiabilité, les propriétés mécaniques et morphologiques de cette partie de l'aorte. Ce modèle de l'aorte ascendante peut interagir avec un modèle CAO de tout type de dispositif (par exemple, un stent) pour simuler les effets sur l'aorte. En outre, le modèle peut être utilisé pour des évaluations de Computational Fluid Dynamics (CFD) ainsi que pour mesurer la contrainte de cisaillement à la paroi (WSS) et la vitesse du sang. Dans la littérature, il existe plusieurs exemples de modèles de l'aorte, toutefois, il n'existe aucune preuve actuelle d'une analyse CFD dans laquelle la maladie de BVA est modélisée dans un modèle CAO de l'aorte ascendante dans le cas d'un anévrisme.

Pour ce projet de recherche, une base de données de 140 patients a été consultée. Les patients étaient âgés de zéro à dix-huit ans et ont montré plusieurs anomalies tels que le syndrome de Marfan, la BVA, la dilatation de l'aorte et l'anévrisme, *etc.* Un ensemble d'Images à Résonance Magnétique (IRM) d'un enfant avec un anévrisme de l'aorte ascendante évidente et une BVA a été choisi comme cas spécifique. Le processus de segmentation d'images a été réalisé dans le logiciel *Slice-O-Matic* afin d'obtenir un nuage de points qui a ensuite été utilisé

pour construire le modèle CAO. Ce dernier a été conçu en utilisant différentes techniques de reconstruction de surface exécutées par le logiciel de modélisation *CATIA* tout en conservant la plus grande précision possible. Différents maillages ont été générés dans le logiciel de maillage *Ansys ICEM CFD* afin de mieux réaliser l'analyse de la Méthode Méthode des Volumes Finis (*FVM*, Finite Volume Method). Le modèle maillé a ensuite été importé dans *Ansys Fluent* pour effectuer une évaluation CFD dans des conditions d'écoulement transitoire du sang tout en simulant la présence d'un anévrisme et d'une BVA.

Plusieurs étapes de corroboration et de vérification ont été effectuées pour évaluer la qualité du processus complet de la reconstruction. Les résultats de cette analyse ont montré une erreur très faible lorsque l'on compare les dimensions de l'anévrisme du modèle de CAO avec la partie correspondante segmentée (erreur inférieure à 1%), comme avec la dimension de l'anévrisme du modèle de CAO et les images IRM (erreur inférieure à 3%) ainsi que les images segmentées et les images IRM (erreur inférieure à 3%). Une analyse CFD a montré de très bons résultats par rapport aux résultats dans la littérature. Des valeurs des lignes de courant de la vitesse du sang, de WSS et de la vitesse du sang sont alignées sur les résultats dans la littérature. Les lignes de courant observées dans l'anévrisme frappent la paroi de l'aorte et créent des hélices comme décrit dans la littérature. Les valeurs de WSS dans la région touchée étaient plus élevées par rapport à la zone à côté et les valeurs de la vitesse du sang sortant de la valve étaient plus élevées comparées à un cas normal. Dans les deux cas, ces valeurs étaient alignées sur les mêmes résultats dans la littérature. Deux ouvrages publiés dans la littérature ont été choisis comme référence pour comparer les résultats de la présente étude.

En conclusion, après avoir obtenu des résultats qui concordent avec des œuvres publiées, il est possible d'affirmer que le modèle CAO de l'aorte thoracique développé est un point de départ intéressant pour étudier plus profondément la présence simultanée d'un AAoA et d'une BVA. Même si tous les objectifs de cette étude ont été atteints, le modèle CAO, les maillages et l'analyse CFD peuvent toujours être affinés ou développés dans des études complémentaires.

ABSTRACT

Ascending Aorta Aneurysm (*AAoA*) is a deformation which affects the portion of the aorta between the aortic valve and the brachiocephalic trunk. The incidence of this disease is higher in cases of patients with the Bicuspid Aortic Valve (*BAV*) pathology. BAV is the most common congenital heart deformation in the world with a prevalence between *0.5%* and *2%*. Many patients with AAoA are children as it occurs more frequently at a younger age.

Invasive surgery is currently considered the gold standard for aortic deformation treatment. This surgical procedure has a high mortality rate, between *2.5%* and *5%* of the treated cases, because of the intrinsic danger of the operation which could take more than 5 hours. The advent of minimally invasive surgical techniques in recent years aims to reduce the need for invasive surgery using devices such as stents and grafts which are implantable by catheterization. The use of these new interventional techniques has significant advantages compared to conventional surgery, such as a decreased risk of operative mortality, total time of intervention and hospitalization. However, an accurate simulation process of all the possible conditions in which the implanted device could operate is required.

This research project consists of developing a Computer-Aided Design (*CAD*) model of the ascending aorta which can simulate, with high reliability, the mechanical and morphological properties of the ascending aorta. This model of the ascending aorta can interact with a CAD model of any type of device (eg. stent) to simulate its effects on the aorta. Furthermore, the model can be used for Computational Fluid Dynamics (*CFD*) evaluations in order to assess Wall Shear Stress (*WSS*) and blood velocity measurements. In literature, there are several examples of aortic models, however, there is no present evidence of a CFD analysis in which the BAV disease is modeled into a CAD model of the ascending aorta within an aneurysm.

For this research project, a database of 140 patients was consulted. Patients were aged between zero and eighteen years old and showed several anomalies, like Marfan syndrome, BAV disease, aortic dilatation and aneurysm, *etc.* A set of Magnetic Resonance Images (*MRIs*) of a child patient with an evident ascending aortic aneurysm and BAV disease was chosen as a patient-specific case. The image segmentation process was performed within the software *Slice-O-Matic* in order to obtain a cloud of points, which then was used to build the CAD model. The latter was conceived using different surface reconstruction techniques executed by the modeling software *CATIA* while maintaining the highest possible accuracy. Different kinds of meshes were generated into the *Ansys ICEM CFD* meshing software to better achieve the Finite Volume Method (*FVM*) analysis. The meshed model was then

imported into *Ansys Fluent* to perform a CFD evaluation in transient blood flow conditions while simulating the presence of an aneurysm and a BAV.

Several corroboration and verification steps were taken to assess the quality of the entire reconstruction process. Results from this analysis showed a very low error when comparing the dimensions of the aneurysm of the CAD model with the corresponding segmented part (error less than 1%), as with the dimension of the aneurysm of the CAD model and the MRI images (error less than 3%) as well as the segmented images and the MRI images (error less than 3%). CFD analysis showed very good results compared to the findings in literature. Blood velocity streamlines, WSS and blood velocity values were aligned with the results in literature. The streamlines observed in the aneurysm hit the aorta wall and created helices as observed in literature. The WSS values in the affected region were higher when compared with the nearby region and the speed of the blood exiting the valve was higher when compared with a normal case. In both cases, the values aligned with the same results in literature. Two works published in literature were chosen as references to compare the results in the present study.

In conclusion, having achieved results which agreed with the published works, it is possible to affirm that the thoracic aorta CAD model developed is a valuable starting point to investigate the simultaneous presence of an AAoA and a BAV. Even if all the objectives of this study were achieved, the built CAD model, the meshes and the CFD analysis can be still refined or further developed in complementary studies.

TABLE OF CONTENTS

LIST OF TABLES

LIST OF FIGURES

LIST OF ACRONYMS

AAoA	*Ascending Aorta Aneurysm*
aROI	*anatomical Region Of Interest*
ASCII	*American Standard Code for Information Interchange*
BAV	*Bicuspid Aortic Valve*
BMI	*Body Mass Index*
BSA	*Body Surface Area*
CAD	*Computer Aided Design*
CAO	*Conception Assistée par Ordinateur*
CFD	*Computational Fluid Dynamics*
CT	*Computed Tomography*
DICOM	*Digital Imaging and COmmunications in Medicine*
FEA	*Finite Element Analysis*
FEM	*Finite Element Method*
MDCT	*Multi-Detector Computed Tomography*
MR	*Magnetic Resonance*
MRI	*Magnetic Resonance Images*
NO	*Nitric Oxide*
NUPBS	*Non Uniform Polynomial B-Spline*
OSI	*Oscillatory Shear Index*
PDEs	*Partial Differential Equations*
RBCs	*Red Blood Cells*
SIMPLE	*Semi-Implicit Method for Pressure Linked Equations*
STL	*STereoLithography*
TAV	*Tricuspid Aortic Valve*
TGF	*Transforming Growth Factor*
UDFs	*User Defined Functions*
vmtk	*Vascular Modeling Toolkit*
VSMCs	*Vascular Smooth Muscle Cells*
WSS	*Wall Shear Stress*

CHAPTER 1

INTRODUCTION

THE PRESENT research work studies the consequences of two pathologies, the ascending aorta thoracic aneurysm ($AAoA$) and the bicuspid aortic valve (BAV) on the values of wall shear stress and blood velocities in the case of the manifestation of two pathologies. The AAoA is characterized by an abnormal enlargement of the wall in the ascending portion of the aorta. As a result of this enlargement, as in classical aneurysmal diseases, the fluid dynamic of the blood is altered. Moreover, the bicuspid pathology contributes in modifying blood ejection out of the left ventricle. In this study, the changes in the hemodynamics that occur in the case of both the pathologies were evaluated. More specifically, the values studied in this project are the wall shear stress in the wall region affected by the aneurysm and the blood flow velocity in the thoracic aorta region. In order to accomplish the fluid dynamics evaluations assessments, a parametric CAD model of the ascending aorta was created using MRI images of a child patient.

1.1 Definitions and Basic Concepts

The aorta is the largest artery in the human body. It distributes oxygenated blood to all parts of the human body, providing the necessary blood supply to all areas of the bloodstream, except for the pulmonary region that is oxygenated by the pulmonary circulation. The aorta originates from the orifice of the aortic valve, which separates it from the left ventricle. In this region (sinus of Valsalva), the first collateral circulation, or the right and left coronary arteries, that feed directly into the heart via the coronary circulation, originate. The portion of the aorta immediately above the sinus of Valsalva, represents the origin of the ascending aorta region, which continues till the aortic arch from where originates the supra-aortic vessels (ie. truck brachiocephalic, left common carotid artery, left subclavian artery) that supply the brain and the bloodstream of the upper limbs with (oxygenated) blood. The aortic arch then continues to the descending aorta until it reaches the abdomen, where it becomes the abdominal aorta and then bifurcates at the pelvic level (iliac bifurcation) so as to make up the circulation of the lower limbs.

The fundamental units of the aortic wall tissue are the elastic lamellae, which, thanks to their composition (ie. smooth muscle and elastic matrix), render the mechanical properties of the aorta distinctive. In particular, the smooth muscle component is activated to provide

viscoelasticity and stiffness to the aortic wall, while the elastic matrix is responsible for the remarkable elastic properties of the aortic tissue. This key feature allows the aorta to accomplish its function of distribution of blood throughout the body and heart. In fact, when the blood flow is ejected during systole at great speed and pressure from the left ventricle to the aorta, the latter stores the energy of the flow thanks to its elastic component. In this fundamental mechanism, known as the Windkessel effect, the kinetic energy of the blood flow (pulsatile) is transformed into elastic potential energy, as the flow is damped by the walls of the aorta. The elastic matrix in the aorta expands, playing the classic compliant role to accommodate the pressure of the flow, then decreases again thus distributing the blood at a sufficient pressure even during diastole. Despite being aware that the Windkessel effect does not represent the only mechanism involved in the distribution of blood from the heart through the aorta, it is still possible to state that the elastic component of the aortic tissue plays a major role in the proper functioning of the aorta.

The aneurysmal pathology is characterized by a dramatic decrease of the elastic properties of the aortic tissue. In almost all cases, the formation of atherosclerotic plaques, and more generally, a manifestation of arteriosclerosis are the precursors of this disease, which generates atrophy of smooth cells and especially a deficit of the elastic matrix. The loss of the peculiar properties of the aortic tissue related to the elastic components cause a surge of mechano-biological factors that are mainly characterized by the increase in the diameter of the vessel concerned (an aneurysm is considered when the diameter of the vessel increases by more than the 50% of its original diameter) and the loss of parallelism between its walls.

Among the mechanical factors, the most influential is undoubtedly the changing ability of the aortic wall to play its compliant role, which induces anomalies in the fluid dynamics of the blood flow (eg. pulsatile component damped, mean velocity, wall shear stress on the wall) and in the pressor components (eg. radial pressure against the wall, internal pressure in the vessel). The imbalances in the fluid cause a malfunction of the normal distribution of blood not only to the organs but also to the vasa vasorum system that supplies blood to the aorta itself. This cascade of factors leads to the worsening of the aorta and, subsequently, the conditions of the aneurysm as well. When the conditions are very severe, the aneurysm tears, causing a hemorrhage that quickly becomes fatal and therefore immediately emphasizes the degeneration of this disease.

In order to evaluate changes in blood flow and pressure regime that involve an aneurysm, one needs to recreate the conditions of the aorta in the presence of this disease. Hence, it is imperative to have a model of the pathological aorta, on which to measure necessary fluid dynamics data. There are several approaches to building a model (ie. mathematical model, computational model, experimental model, in vivo model). The model described and used in

this research is based on the approach that is commonly referred to as computational. The computational approach allows one to create a three-dimensional model, which is as close as possible to reality. To accomplish this, the model is constructed starting from biomedical images (eg. CT, MRI, ultrasound) of the patient, usually acquired in a hospital. Using the appropriate software, one then proceeds to the sorting of the set of images considered, to be better based on the quality of the biomedical image itself and according to the characteristics of the organ desired to be modeled. The chosen set of images is then processed by a second software in what is commonly referred to as the segmentation process. In this critical process, the images previously selected are processed (manually or using semi-automatic methods) in order to cut (segmenting) only the affected organ, thus neglecting the background image. From this process, one will get a first 3D model represented as a cloud of points.

The process following the segmentation, usually is the construction of a three-dimensional model starting from the segmented images. Different ways are actually available to accomplish this step. The most used two are : direct reconstruction of the model within the segmentation software and CAD reconstruction by importing the segmentation results into a dedicated software. The latter option, even if it is more complicated and time consuming, gives the opportunity to personalize the model in order to satisfy specific research requirements. The further step is the adaptation of this model for CFD analysis. During this delicate process, the boundary conditions are simulated, which regulate the physics of the bloodstream, and thus, its interaction with the model. The key step in the realization of a test setup using a CFD model is to obtain a mesh. A mesh is a reticulation that follows the geometry of the model, formed by the repetition of three-dimensional figures note (eg. hexahedral, tetrahedral, prism) that fill the volume and the surface of the model. The three-dimensional figures (called elements) are chained to each other creating a sequence of vertices, edges and faces that constitute the mesh. The adjacent vertices of each element are joined to form the fundamental unit of a mesh, which is the node. The number of nodes that can form each element corresponds to the number of vertices of the geometric figure, a relation that forms the base of the concept of precision of the mesh (eg. four nodes in the case of the tetrahedron, eight in the case of the hexahedron). At constant quality of the mesh, in other words, the precision of a mesh is dictated by the number of nodes that it possesses.

Once the mesh is obtained and the boundary conditions that govern the problem are set, the CFD test can be performed. Often, two different softwares are used to generate the mesh and to set the CFD problem. In this case, the mesh is imported into the CFD software following specific file extensions (eg .msh, .uns). The resolution of the CFD problem, in the end, allows one to know the distribution of the values of the blood flow and, in particular, of the WSS and the blood velocity during the cardiac cycle. With the knowledge of this

distribution, it tries to refine, if necessary, the model in its parts. We therefore identify any errors in the various steps of the modeling process, which induce a detachment of the values sought by the values that scientific literature proposes. If the gap was to be accepted, the model would be considered valid. The power of validation of a model is given by the percentage of detachment from the values in literature, assumed to be real values. The greater the difference between the values resulting from the model and the values proposed by literature, the higher the percentage of detachment and therefore reducing the credibility of the model. In engineering applications, the power of a model is a parameter as fundamental as it is difficult to keep under control, because even in less complex applications, it depends on a number of significant factors, which are found subsequently in the various steps of the modeling process. This way, generating an error upstream, even if negligible initially, can be crucial at the end of the simulation process. To check the various steps in the modeling process and simulation, one runs the validation tests. There are several types of validation tests that depend largely on what needs to be validated. More in general there are three different type of accrediting a scientific work. Without entering in the details, the three methods written following the increase accreditation power, are : corroboration (also called confirmation), verification and validation. In the corroboration step, results obtained are compared to same works already present in the literature. The next step, verification, extend the comparison to *in-vitro* and/or *in-vivo* tests. Validation is the last and most significant step as it contemplates the results of a statistical analysis obtained by investigating a large group of patients.

In the biomedical field, one of the methods to corroborate the accuracy with which the biomedical images were segmented is to take the measurements in the original image and then the same measurement in the corresponding part of the reconstructed model, evaluating the difference with a certain degree of approximation. If the degree of approximation is accepted (and hence the mistake), then the step is considered validated. Validating a CAD model is a much more complex operation and will be widely covered in section 4.2.

1.2 Elements of the Problematic

This research project tackles the enlargement of the ascending aorta. Already recognized in the medical field, this disease is widely studied in order to fully understand its etiology. Medical research has established correlations between the development of an aneurysm of the ascending aorta and the presence of some common factors of the pathology. It is important to understand that they are simply correlations and currently nothing has been scientifically proven. Among the factors common to the ascending aortic aneurysm (ie. genetic dysfunctions, systemic blood pressure), the most important is surely the presence of a bicuspid aortic

valve. This disease is characterized by a deformation of the aortic valve and, more generally, by a disorder in the evolutionary process of the cardiac tissue. Addressing the issue of the enlargement of the ascending aorta is therefore a field that connects the various triggers of causes (unknown) that generate the aneurysm. Being able to monitor these factors and somehow monitor their effects would result in a victory with respect to the development of the disease. However, the variability of the factors stated above combined with the difficulty in finding correlations between them turns out to be one of the major problems in the study of an aneurysmal disease. This region of the human body, being cardiovascular, is certainly among the most difficult to study because it involves the conditions related to fluid mechanics unique throughout the body and linked to the presence of the nearby heart. These conditions concern the fluid dynamics and pressures involved as well as the deformations and transitions.

The fluid dynamics of the cardiovascular organ is unique in its kind. The blood flow ejected from the heart that passes through the aortic valve with a flow rate of approximately 70 ml per second is a (specific) type of pulsatile flow. Ejected at maximum pressure and with virtually no resistance, the blood flow impacts the aortic wall to then be distributed along the aorta following the natural bifurcations. A small part of the ejected volume fluid is dedicated to the needs of the heart through the coronary tree that begins at the aortic root (ie. sinus of Valsalva). The blood flow that impacts the aortic wall presents the zones of turbulence and then takes on the typical characteristics of pulsatility that distinguish the hemodynamics of all collateral vessels (to the aorta) and the descending portion of the aorta. In pathological conditions, particularly in the presence of BAV, the blood flow is modified by the different geometry of the aortic valve. In some cases, for example, the flow in the first portion of the ascending aorta becomes helical or changes its fluid dynamics regime increasing the zone of turbulence while in other cases, the flow is not directed properly from the valve and the impact with the aortic wall becomes more violent. One of the major issues addressed in this project is choosing the best approximation for cardiovascular hemodynamics. Correctly modeling the cardiovascular fluid dynamics undoubtedly represents a significant challenge in biomedical research.

1.3 Research Objectives

The global objective of this project is to implement a specific patient study seeking to create a parametric CAD model of the thoracic arterial tree, which represents a pathological situation of an aneurysm of the ascending aorta and, subsequently, to develop a CFD analysis of the model, simulating the presence of both the ascending aortic thoracic aneurysm and the bicuspid aortic valve pathology.

Complementary to the global objective, five sub-objectives are formulated. The first is to conceive a highly reliable CAD model of the ascending aorta aneurysm, starting from MRI images of a selected patient. Then, to parametrize this model allowing the user to change the diameter of the aneurysm, is the second sub-objective. The third is to achieve the most reliable mesh of the model, which does not need to be entirely regenerated if the CAD model changes. The fourth sub-objective, relating to the third, is to achieve a convergence and a sensibility analysis of the mesh. The last sub-objective is to obtain blood speed and wall shear stress values, from the CFD analysis, which are comparable with results in literature.

From an accurate analysis of the available literature today, we can state that there is no evidence of a parametric CAD model of the ascending aorta aneurysm. In addition, to the best of the author's knowledge, there are no previous works related to the study described in this paper.

1.4 Thesis Outline

This thesis is divided into six parts. The first part, the Introduction, takes a look at the problem investigated in this work and the general purpose of this research. The second part is the Literature Review in which an in depth look of the problem treated in this thesis is described. In the Literature Review, both the ascending aorta aneurysm and the bicuspid aortic valve pathologies are reviewed. Then, the state of the art CAD and CFD modeling is widely described, as well as the principal models adopted to approximate the blood viscosity and describe the blood dynamic. The third part, Materials and Methods, describes all of the processes achieved to conceive the 3D model, from image segmentation to mesh generation, through the building of the CAD model and finally, the CFD analysis. The results from the study are presented in the fourth part. Both the results from the computation of the blood velocity and the wall shear stress are shown together with the results from the corroboration step. The fifth part is the Discussion where results from the previous section are discussed and a panorama of the accomplished study is provided. This part ends with the limitations of the present study and its potential future developments. Lastly, in the sixth part, the Conclusion details a synthesis of the global experience during the development of this thesis. In the next page, the thesis outline in a graphical form, with the principal sections, is shown.

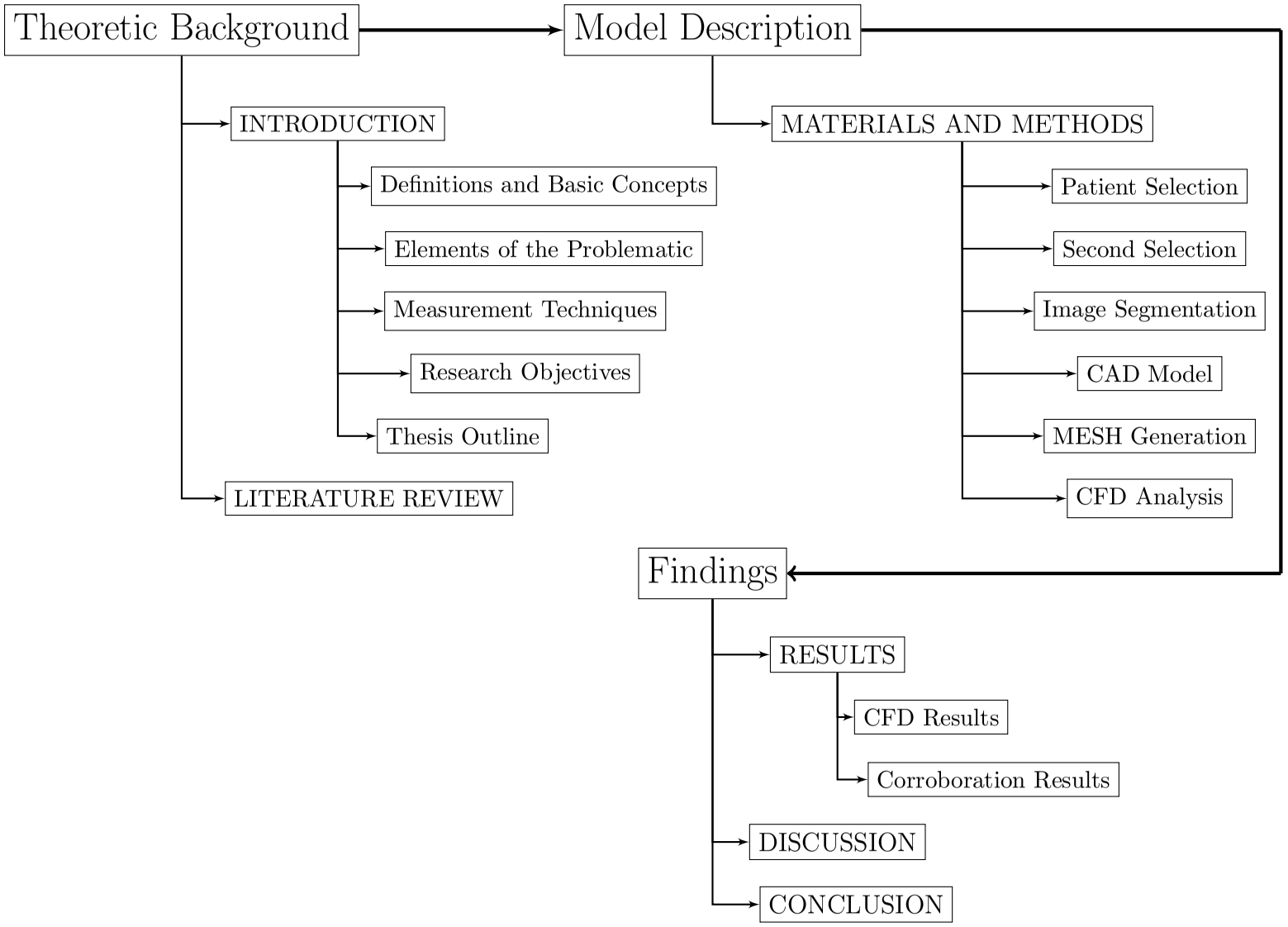

Figure 1.1: Thesis Outline. Clicking on the box will bring to the corresponding section in the thesis.

CHAPTER 2

LITERATURE REVIEW

In order to help the reader focus on the most important aspects of this thesis, the literature review was divided into 13 sub-sections. Each sub-section can be read independently, according to the reader's preferences. In the first section, the physiology of the aorta is described, with particular interest in the layers that form the aorta as they are the entities most affected by an aneurysm. Two ways of classifying the aorta were also cited.

The second section refers to the classical measurement techniques to establish the severity of the aortic dilatation. Then, non-conventional systems to predict aortic diseases are described. The third sub-section mentions the aorta's biomechanics in relation to its structure and an accredited model, which attempts to explain the steps that lead to the formation of the aortic aneurysm, is cited. In the fourth sub-section, the vast panorama of degenerative diseases related to the aorta's pathologies is given. Diseases such as the Marfan syndrome, the Ehlers-Danlos, the Loeys-Dietz and the Turner syndrome are described, due to their importance in the aorta's pathology. The fifth sub-section introduces atherosclerosis disease, which is related to the aorta and subsequently, the bicuspid aortic valve disease is presented.

Researchers are actually following two approaches to establish a link between AAoA and BAV. One approach investigates histological disorders in the aneurysm and in the BAV speculating that a common path needs to be followed. Researchers following the second approach try to relate the changes in hemodynamics due to BAV and AAoA formation.

In the sixth and seventh sub-sections, the findings from the first and the second methods, respectively, are presented. In the eight sub-section, the wall shear stress parameter is introduced in depth since it is widely considered to be one of the principal indicators of blood flow anomalies, even in an aneurysmatic pathology. The state of the art CAD and CFD models investigating aortic aneurysm and aortic valve pathologies, are presented in the ninth sub-section.

These models try to best reproduce the complex hemodynamics in the region of the aorta, facing a large quantity of difficulties while modeling blood flow. For this reason, approximations need to be made when a computational model of the hemodynamics of the aorta is accomplished. These approximations are principally linked to the blood viscosity and to the dynamics of the blood flow. The tenth and eleventh sub-sections describe the two ways of modeling the blood flow dynamics, the steady flow and the transient flow, respectively. The twelfth and thirteenth sub-section, finally, depict the two models most often used when ap-

proximating the blood flow viscosity, namely the Newtonian and the non-Newtonian blood models.

2.1 Physiology of the Aorta

The human aorta is the largest artery in the body, showing a physiological diameter ranging between 25 and 35 mm in adults. From the aortic valve to the iliac bifurcation, the human aorta measures an average of 75 cm. Along this path, the aorta distributes oxygenated blood to all other minor arteries (except those of the lungs) supplying the heart via the coronaries, the brain via the supra-aortic vessels and all the organs of the abdominal region via the abdominal aorta.

The human aorta can be classified in two ways. According to anatomical regions, the thoracic aorta goes from the heart to the diaphragm where it enters the abdominal region, becoming the abdominal aorta which runs until the aortic bifurcation. The other way of classifying the aorta follows the normal path of the blood flow ejected from the aortic valve. The aorta begins as the ascending aorta, turns into the aortic arch and takes an inferior course where the descending aorta starts its vertical trajectory before ending at the bifurcation of the two common iliac arteries. The ascending aorta originates in the upper part of the left ventricle, from which is separated by the aortic valve. This area, namely the aortic root, does not have the classical tubular shape yet, but follows a bulb shaped geometry. This region is quite important as its particular shape allows the blood that recoils to be collected from the ascending aorta and supplies heart via the coronary arteries. The tubular shape, typical of the aorta, starts when the aortic root ends at the sinotubular junction. The ascending aorta can be considered developed where the sinotubular junction ends and runs until it starts to curve and bifurcates into the aortic arch and the supra-aortic vessels, respectively. In figure 2.1, the thoracic aorta is shown.

The aortic tissue is made of three different layers, from the outermost to the innermost they are : the tunica adventitia, the tunica media and the tunica intimate. The adventitia is mostly composed of collagen fibers, the thick media layer, responsible for the aorta's elastic properties, is made of smooth muscle cells and elastic tissue. Finally, the thin intima layer, which is in direct contact with the blood flow, is mainly made of endothelial cells. The media layer accomplishes the compliant function of the aorta and, for this reason, reaches its largest thickness at the ascending aorta walls, which are the most solicited of the entire aorta. Consequently, on the basis of the vessel remodeling theory, various research works speculate that different values of the blood flow can vary the ascending aorta wall properties. It is widely known that pathologies like the aortic dissection or the aortic aneurysm, are related

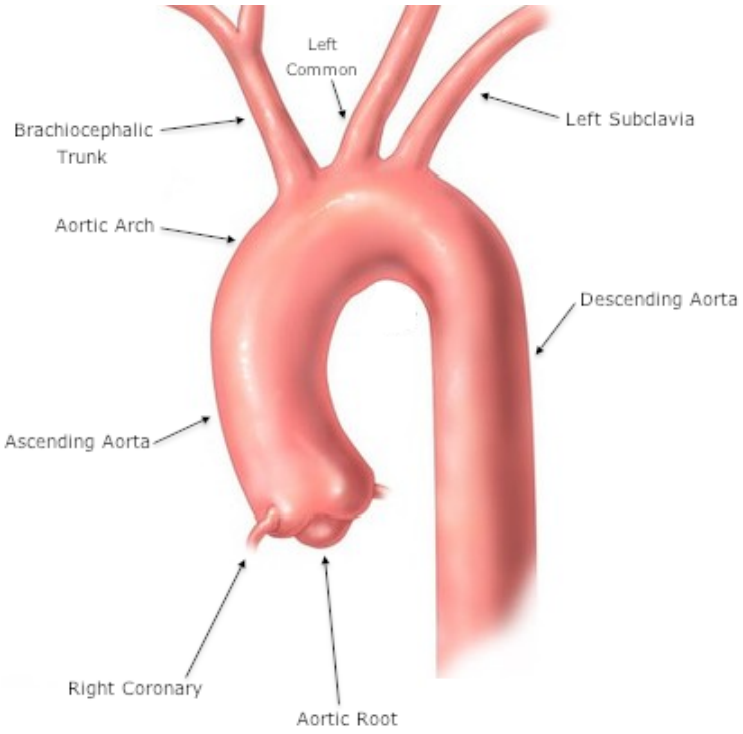

Figure 2.1: A physiologic thoracic aorta is represented. The aortic root with its particular trilobate shape, which recoils blood, and the two main coronaries are shown. It should be noted that the aortic diameter is almost constant along all of the thoracic course. Adapted from *http ://tinyurl.com/pz443s2*

to changes in aorta wall properties (Roberts, 1981), (Busuttil *et al.*, 1982), (Campa *et al.*, 1987). Aortic dissection appears when the inner layer of the aortic wall rips and blood starts to leak into the aortic layers. When the dissection begins in the ascending aorta, it is the most severe case and it is called type A dissection. The ascending aorta aneurysm is defined as a dilatation of the ascending portion of the aorta, which produces an enlarged vessel diameter 1.5 times greater than the original diameter. An ascending aorta whose diameter is between 1.1 and 1.5 times the original size is considered to be dilated or ectatic. Figure 2.2 shows an example of ascending aorta aneurysm.

2.2 Measurement Techniques

Normal aorta dimensions have been established over the years applying different techniques that use biomedical images. Roman *et al.* (1989) have carried out the measurements of the aortic root in young people and adults with the technique of echocardiography in two dimensions. This study showed that the results obtained using the echocardiography in two dimensions are more reliable than those gathered with the technique based on the M-mode

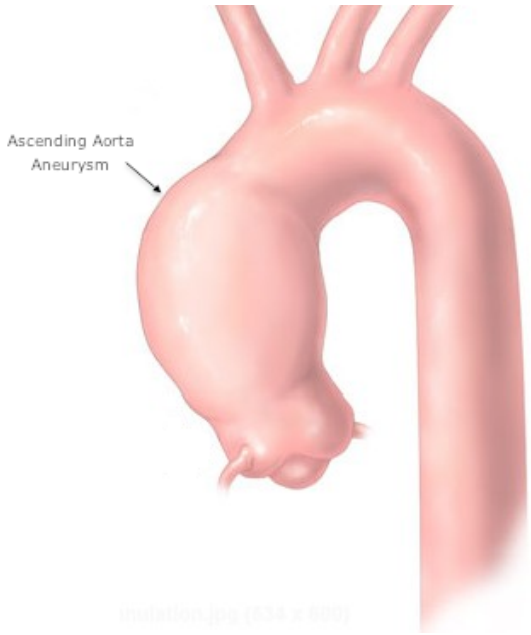

Figure 2.2: A typical example of an ascending aorta aneurysm is shown in the image. The diameter suddenly changes after the aortic root, causing the jet to behave abnormally. Adapted from*http ://tinyurl.com/o95482x*

echocardiography nomograms. The study conducted by Lin *et al.* (2008) instead highlights traditional techniques such as Computed Tomography (CT) that provides less accurate values than the evolved Multi-Detector Computed Tomography ($MDCT$) technique. In particular, the measurements carried out on a sample of 103 healthy adults have provided reference values classified by age and sex, regarding the size of the vessels of the thoracic part of the aorta. Reference values were also identified using the Magnetic Resonance Imaging (MRI) technique in the work by Burman *et al.* (2008) team on 120 healthy volunteers while using, for the first time, transecting scanning planes as well as planes aligned with the axis of the aortic root.

The reference values, indicated in the studies previously stated, represent the standards used to date to diagnose diseases of the aorta. However, some studies propose more effective systems to predict diseases, not only based on dimensional measurements (eg. root diameter, volume of Valsalva cusps, *etc.*), but also on factors that depend on the mechanical properties of the aortic wall (eg. wall shear stress). Pape *et al.* (2007) examined 591 cases of type A dissection of the aorta evaluating the validity of the indications to operate for aortic diameters greater than 5.5 cm. The study highlights the probability of failure of the threshold based on the measurement of the diameter and propose further deepening of predictive techniques based on genetic testing, biomarkers or studies on the functionality of the aorta. The team

of Fillinger *et al.* (2002) had previously shown that the values of wall stress measured on aneurysms in vivo close to the time of rupture were greater than those measured for patients that underwent elective repair, thus demonstrating that clinical indices for the diagnosis of aortic aneurysms should be reconsidered. The same team (Fillinger *et al.*, 2003) later subjected 103 patients to a CT scan, this time, making evident the superiority of an analysis based on the values of wall stress rather than the traditional standardized values of the diameter of the aneurysm. Aneurysmal diseases of the aorta, therefore, are not easy to measure, but it is clear that cases of spontaneous aortic rupture remain events with an extremely poor prognosis for the patient.

2.3 Biomechanics and Biological Models

The incidence of ascending aortic aneurysms has been estimated to be 10.4 in 100.000 cases per year (Clouse *et al.*, 1998). The AAoA is the most common form of thoracic aortic aneurysm (60%), followed by the aneurysm of the descending portion (30%), the aortic arch (10%) while the remaining 10% involves the thoraco-abdominal tract (Bonow *et al.*, 2011). Because the etiology of the AAoA is mostly unknown, it is classified as an idiopathic disease largely related to hemodynamic factors, changes in the biomechanics properties of aortic tissue and in the aortic valve (Patel et Deeb, 2008). The biomechanics properties of the ascending aorta are unique in their kind as it (the aorta) differs from other aortic segments in structure and biochemistry, presenting a thinner intimate in favor of a thicker media and a greater quantity of lamellar units when compared to the abdominal aorta. The ascending aorta shows a greater amount of elastin and collagen with respect to the abdominal portion, but a smaller collagen-elastin ratio (Ghorpade et Baxter, 1996). As shown in Gittenberger-de Groot *et al.* (1999) and Bergwerff *et al.* (1998)'s research, the Vascular Smooth Muscle Cells (*VSMCs*) in the ascending aorta originate from the neural crest while the cells of the descending and abdominal aorta originate from mesoderm and endothelial cells.

To the best of our knowledge to date, it is not yet possible to correlate these differences with the different pathophysiology of the ascending aorta compared to other traits. The best model attempting to correlate most of the factors that play a part in the formation of an aneurysm today remains perhaps the model proposed in 2006 by Shimizu *et al.* (2006). In this article, a two-step model is presented that would explain the pathogenesis of an abdominal aortic aneurysm. The first step involves genetic or environmental factors that cause the initial damage to the endothelial cells and of the aortic wall. The inflammatory response consists of VSMCs trying to eliminate the injuring agents. During this crucial passage, the behavior of the ascending aortic tissue differs a great deal from that of the abdomen. While

the inflammatory response, mediated by a particular class of T-lymphocytes (ie. TH-0, Th-1, Th-2) in the abdominal tissue, generates more frequently an atherosclerotic lesion, the ascending tract's initial damage may result in medial degeneration (Libby *et al.*, 2002). The second step involves solely environmental factors that aggravate the damage and increase the aortic inflammatory response. Shimizu *et al.* (2006) conclude that the genomic polymorphism ultimately predisposes certain individuals to the formation of aortic aneurysms.

2.4 Degenerative Diseases

The AAoAs are for the most part degenerative (Yun, 2002) and have a specific pathological profile. By the late 1920s, doctors Otto Gsell and Jacob Erdheim studied the histology of the aortic tissue describing the aneurysm as a cystic medial necrosis. In fact, from the moment there is neither necrosis nor cyst formation, to date the most appropriate term seems to be elastic type medial degeneration (Tadros *et al.*, 2009). This compromises the mechanical vascular degeneration of the aorta : the aortic distensibility decreases as its diameter increases and the wall stress rises as a consequence of increased blood pressure, according to Laplace's law (Koullias *et al.*, 2005). Absi *et al.* (2003) have shown how the components of the aneurysmal tissue differ in the case of an ascending aneurysm or an abdominal aneurysm. Their findings show that the formation of both types of aneurysms is characterized by the alteration in the expression of certain genes which are different in the case of the ascending aorta rather than the abdominal aorta.

The results of studies to indicate whether the elastic type medial degeneration is related with a decreased density of VSMCs in an aortic media and an apoptosis of VSMCs, are nevertheless contradictory. The results of Lesauskaite *et al.* (2001) assert that the decrease in VSMCs during the formation of an AAoA is secondary if compared to the transition of these cells from the contractile type to the synthetic type, by reason of increased matrix metalloproteinase production. Tang *et al.* (2005) have come to similar conclusions stating that apoptosis in a thoraco-abdominal aortic aneurysm was not significant, but rather have noticed an increased amount of leukocytes at the expense of the non-notable unchanged density of VSMCs. However, He *et al.* (2006) reported that the presence of inflammatory cells and markers of apoptotic cell death in the vascular tunica media of the AAoA can lead to the elimination of VSMCs and, therefore, to the degeneration of the aneurysm.

An alteration of the aortic tissue often related to the presence of AAoA (especially in adolescent patients) is the Marfan syndrome. Marfan syndrome is the most common inherited connective tissue disease with an incidence of 1 in 10000 (Franco et Verrier, 2003). It is caused by a mutation of the gene encoding fibrillin-1 (ie. FBN1) (Judge et Dietz, 2005),

the main component of the extracellular matrix. Recently, it has been discovered that the mutation of FBN1 generates alterations to the Transforming Growth Factor-β (TGF-β). The blocking of the TGF-β signal (via Losartan) in a sample of mice attenuated the development of the thoracic aneurism. Premature elastic medial degeneration, disorganized elastic fibres and a resulting complex of musculoskeletal, ocular, cardiovascular and central nervous system abnormalities, are the typical phenotypic manifestations of Marfan syndrome (Judge et Dietz, 2005). Several studies confirmed that almost all patients with Marfan syndrome develop, in the course of their life, some aortic disease (ie. aortic aneurysm, aortic dissection, rupture), which leads to a drastically reduced life expectancy : about 32 years without treatment and up to 60 years with optimal treatment (Brooke *et al.*, 2008), (Silverman *et al.*, 1995).

Ehlers-Danlos syndrome is an inherited connective tissue disorder in which type III collagen synthesis is impaired. In the past, there were more than 10 recognized types of Ehlers-Danlos syndrome, but in 1997 they were classified as six different types and were given different names (eg. the dermatosparaxis type, the hypermobility type, *etc.*) (Beighton *et al.*, 1998). The syndrome that affects the blood vessels is the vascular type (formerly Ehlers-Danlos syndrome type IV) and occurs between 1 in 100,000 to 1 in 200,000 patients (Lawrence, 2005). According to Pepin *et al.* (2000), it is detrimental to arterial dissections and ruptures (65%) and, in addition, the rupture of organs (21%) occurs more frequently in the descending segment of the aorta although some cases have been reported in the ascending aorta Pepin *et al.* (2000) as well.

More recently, Loeys-Dietz syndrome has been identified as an autosomal dominant genetic aortic aneurysm syndrome. This disease, caused by mutation of the transforming growth factor beta receptor genes 1 and 2 (TGF-β R1 and TGF-β R2), has been correlated to the presence of aortic aneurysms. The mutation of these genes leads to a overproduction of collagen, elastin and disarray in the alignment of the elastic fibers (Loeys *et al.*, 2006). These disorders cause generalized arterial tortuosity (84%) and an aggressive aneurysm (98%) of the great vessels (Loeys *et al.*, 2005). Turner syndrome is a sex chromosome aneuploidy syndrome that affects 1 in 2000 live-born girls (Matura *et al.*, 2007). Patients with this syndrome show cardiovascular abnormalities in 75% of cases, including bicuspid aortic valve, coarctation of the aorta and thoracic aortic aneurysms and dissections (Ho *et al.*, 2004). Throughout the development of this disease, there appears to be a general expansion that could lead to an aneurysm of the major vessels including the aorta (Matura *et al.*, 2007). However, the exact origin of the aortic defects caused by Turner syndrome is still unknown, despite the fact that the histopathology has demonstrated a cystic medial degeneration similar to that seen in Marfan's syndrome (Matura *et al.*, 2007).

The development of an aneurysmal disease may be related to genetics, but in a non-

syndromic way (Barbour *et al.*, 2007). Familial thoracic aortic aneurysm disorders are primarily associated with ascending aorta aneurysms and dissections (Coady *et al.*, 1999). They are caused by various genetic mutations (eg. MYH11, ACTA2, *etc.*), but, at the moment, details of this genetic mechanism are only partially known (Hiratzka *et al.*, 2010). In a database of 1600 patients with thoracic aortic aneurysms and dissections, Elefteriades (2002) of Yale University, noted a certain genetic aneurysmal disease. In his review, Elefteriades (2002) explains that from a genetic analysis of the cases in the database, 21% of patients with thoracic aortic aneurysm have first-order family members with an arterial aneurysm. This data stipulates that the family history of a patient can be correlated with a certain predisposition to the formation of aneurysms.

2.5 Atherosclerosis and Bicuspid Aortic Valve

One of the major diseases that affects blood vessels is certainly the atherosclerosis. It frequently affects the coronary tree, ultimately causing a heart attack. The atherosclerosis is most often associated with aneurysms of the descending and the abdominal tract (Alcorn *et al.*, 1996), (Reynolds *et al.*, 2001) while the ascending portion is spared (Agmon *et al.*, 2004). In the presence of AAoA, according to Achneck *et al.* (2005) results, the systemic atherosclerosis even seems to decrease. It is obvious that, as previously mentioned, the factors which bring a greater contribution to the characterization of an AAoA are the alterations in the aortic tissue discussed above and the hemodynamics of the vessel, which are directly linked to the presence of a well-known pathology of the aortic valve, named bicuspid aortic valve (BAV).

BAV is the most common congenital cardiac abnormality in the world having an incidence between 0.46 to 1.37% (Lloyd-Jones *et al.*, 2010), (Nistri *et al.*, 2005). It consists of the fusion of two of the three aortic valvular leaflets which form the normal tricuspid aortic valve. Due to this fusion, the aortic valve results in a bicuspid configuration, as is shown in figure 2.3.

This disease alone shows more morbidity and mortality than all other congenital heart diseases known combined together (Ward, 2000) and it mainly occurs in male children (Tutar *et al.*, 2005), (Basso *et al.*, 2004), (Stewart *et al.*, 1984). Coupling this information about BAV with what was stated earlier above about AAoA establishes a link between BAV and AAoA development, suggesting that many patients with ascending aortic diseases are children. This link could be fundamental for two important reasons. First, as it was mentioned earlier, a BAV abnormality shows a very high incidence meaning that a lot of people could benefit from a potential solution preventing AAoA. Second, an aortic aneurysm (and, more generally, aortic dilatation) has a high risk of dissection and rupture and linking BAV disfunction with

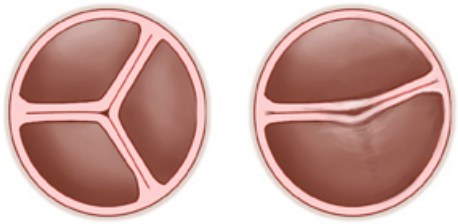

Figure 2.3: On the left, a normal tricuspid valve is displayed while, on the right, a bicuspid aortic valve is represented. One can easily see the differences in the valve conformation, which causes the blood flow to assume non-conformational paths. Adapted from *http ://tinyurl.com/o4fhkzz*

aortic dilatation adds value to the prevention of this potentially fatal disease.

To better understand how much research is been conducted in this field trying to prove the existence of this link, a database research in PubMed suffices. At the time this research project was written, there were 219 journal articles that could be retrieved, considering only the PubMed database.

2.6 Aortic Tissue and BAV Related Disorders

In a Canadian follow-up study of 88 BAV patients aged 0-18 years, doctors Warren *et al.* (2006) found that in 13 years since the first echocardiographic acquisition, 74% of the children followed showed a dilated ascending aorta. Moreover, they noticed the dilatation tended to worsen over time. This data attests that in AAoA and BAV patients, the growth rate of the aneurysm is faster than in non-BAV patients, which is supported by a great deal of literature, both for pediatric (Holmes *et al.*, 2007), (Beroukhim *et al.*, 2006) studies and adult (Davies *et al.*, 2007), (Yasuda *et al.*, 2003) ones. In a prospective study, Santarpia *et al.* (2012) found some associations between 40 BAV patients and a control group formed by 40 normal subjects. The BAV group was selected with no particular evidence of complications and matched for age, gender and body surface area. Santarpia *et al.* (2012)'s insights point to the aorta's mechanical properties and, in particular, to stiffness and aortic properties. In fact, they found that patients with BAV showed an increased aortic stiffness and a reduction in tissue deformation properties, like aortic compliance, when compared with the control group. In addition, from this research, it is possible to affirm that a reduction of aortic strain isn't necessarily related only to the diastolic aortic diameter, but is a combination of the reduced aortic valve area (very frequent in BAV) and the increase of the diastolic aortic diameter (as seen for dilations or aneurysms). Santarpia *et al.* (2012) concluded that aortic strain is not only related to the diastolic aortic diameter, but its reduction in combination with the

reduced aortic valve area, noticed in BAV patients, is able to predict an altered left ventricular remodeling.

The ascending aorta and the aortic valve share something in common : they both have a common embryonic origin. In fact, they both develop from neural crest cells (Kirby et Waldo, 1990) and as mentioned above, some researchers believe that VSMCs that cause elastic medial degeneration of the ascending aorta (and lastly, AAoA) are of neural crest origin as well. The ascending aorta and the aortic valve in fact, exhibit common aspects and strong associations as demonstrated in a substantial quantity of works that can be found in literature (Bonderman *et al.*, 1999), (de Sa *et al.*, 1999), (BECKER *et al.*, 1970). For instance, Gleason (2005) demonstrated certain histological changes in the ascending aortas of BAV patients such as elastic fibre fragmentation and elastic medial degeneration, loss of VSMCs and changes in their orientation. Analysis of the aortic media conducted by Niwa *et al.* (2001)'s team has revealed abnormalities of elastic lamellae in patients with BAV disfunction and loss of elastic tissue compared to patients with a tricuspid aortic valve (TAV). AAoA specimens of 20 patients, half TAV, the other half BAV, were examined by Schmid *et al.* (2003) team in order to asses the histopathologic and biologic condition of AAoA associated with BAV or TAV. Results confirmed medial tissue destruction, elastic fragmentation and disorientation.

Once again, related to these findings is a constant lack of VSMCs in the aneurysmal tissue and an increased number of apoptosis in BAV specimens rather than TAV specimens. In the last decade, some researchers started paying attention to the activity of the Nitric Oxide (NO) molecule belonging to the cardiac system. In our research group at the *LIAB* (Institut de génie biomédical at École Polytechnique de Montréal, 2900, Boulevard Edouard-Montpetit, Montréal), researchers are focusing on hemocompatibility and, more generally, on NO biocompatibility. Nitric Oxide is known to play a role in regulation of several vascular properties, like inhibition of VSMCs and proliferation of endothelial cells (Dudzinski *et al.*, 2006), (Gewaltig et Kojda, 2002). A link between NO (in particular between endothelial Nitric Oxide Synthase, eNOS) and BAV was then found by Aicher *et al.* (2007) in addition to another between WSS and NO regulation (Ranjan *et al.*, 1995) ; in particular, high levels of eNOS correspond to an adaptive response of body to an imminent VSMCs apoptosis, which occurs in aneurysmatic sites (as described above) because eNOS inhibits VSMCs apoptosis. Following these associations, Mohamed *et al.* (2012) based his research work trying to link AAoA, BAV and eNOS. He examined 19 aortic aneurysm patients specimens (14 with BAV and 5 with TAV) and interesting insights were uncovered. Mohamed *et al.* (2012) found that the eNOS levels show high variance in the different parts of the ascending aorta for BAV specimens while they are quite regular in TAV patients. A conclusion stating that in BAV

patients, irregular WSS values may lead to VSMCs apoptosis could be assessed.

Choudhury *et al.* (2009) examined 16 ascending aorta samples obtained from five healthy TAV patients without ascending aorta dilation, six dilated TAV patients and six dilated BAV patients. They mechanically tested these samples finding local variations in the ascending aorta thickness and the mechanical properties between the three groups. Interestingly, the data collected showed thinning of BAV aortic tissue while TAV tissue, also when dilated, was more capable of preserving normal mechanical properties, like thickness and elasticity. This finding, confirmed that local differences between dilated ascending aorta tissue in BAV and TAV cases exist, leading to changes in passive mechanical properties between the two tissues. Results like the ones found by Choudhury *et al.* (2009) are quite interesting in surgical decision making and should be deeply investigated while looking at the genetics characteristics of both tissues.

2.7 Changes in Blood Flow Patterns

Two hemodynamic phenomena that occur in BAV and AAoA patients are being documented by researchers : the eccentricity of blood flow jets ejected by functioning BAV and the helical systolic flow. Throughout the first phenomenon, instead of moving along the central ascending aorta axis, the jet deviates hitting the aorta wall. During the second phenomenon, which is more evident in dilated or aneurysmatic cases, the ejected flow forms spirals moving towards the aortic arch. Although it was frequently demonstrated that a bicuspid aortic valve generates certain hemodynamics changes in ascending aortic blood flow, some researchers attempt to point out that prior to hemodynamics factors, the causes of ascending aortic dilation (and lastly, aneurysm) must be found in the intrinsic BAV pathology. Such is the case of Keane *et al.* (2000)'s research work, in which 118 BAV patients were examined. Within this group, 18 patients only had BAV without any more evident complications. The other 100 patients had aortic regurgitation, aortic stenosis, or mixed lesions. Keane *et al.* (2000) took measurements of the diameter along the aorta's entire length and he concluded that beyond other abnormalities (which influence hemodynamics in the ascending aorta), BAV is responsible for the dilation of the proximal part of the aorta. In figure 2.4 histological findings by Keane are presented. Despite Keane *et al.* (2000) conclusions, some researchers found links between hemodynamic forces and aneurysm formation as in the work of Hoshina *et al.* (2003) where WSS and relative wall strain properties were examined and almost directly linked to endothelial cell and VSMCs proliferation in aneurysm sites. WSS and blood flow properties were also examined by the Sho *et al.* (2004)'s research group, whom concluded that hemodynamic forces (expressed through WSS and blood flow) may lead to aneurysm dilation via

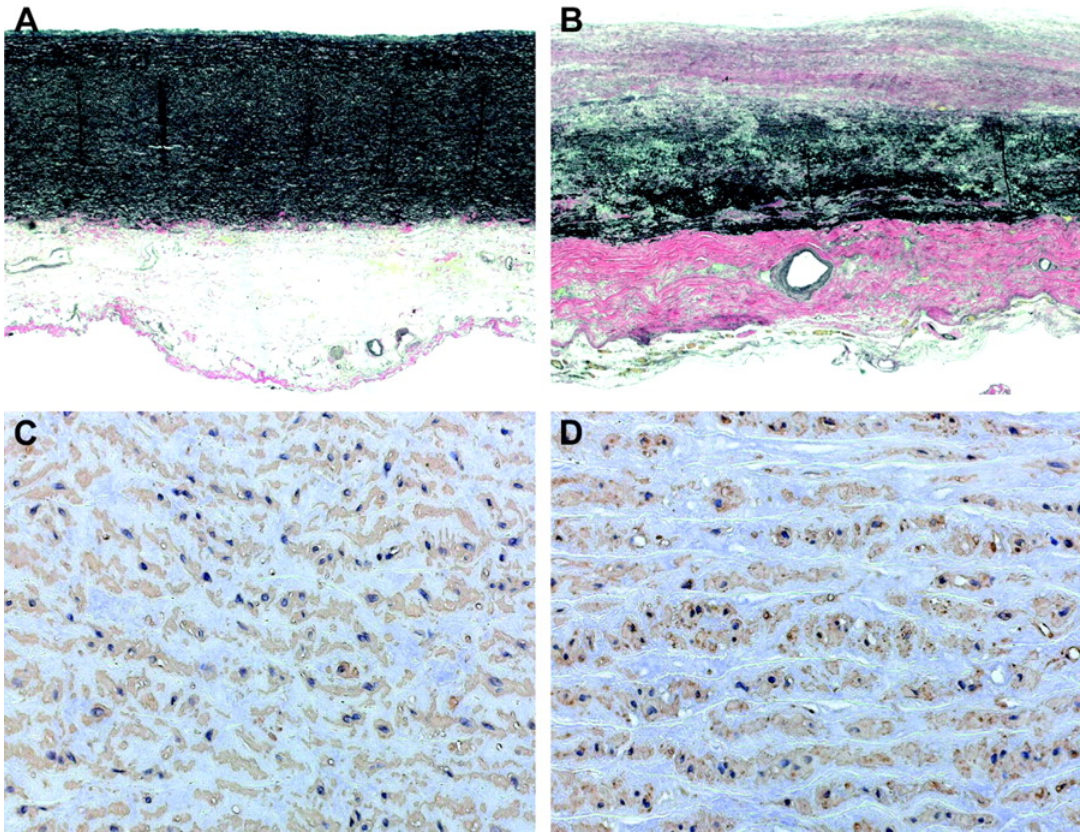

Figure 2.4: In figures A and C, two sections of a non-aneurysmal aortic tissue are compared with images B and D, taken from an aortic aneurysmal tissue. The differences between the two images are evident, especially in the elastin component (darkest area), which is a thinner layer in the aneurysmal tissue.

regulation of intimal macrophage adhesion or transmural migration. A fundamental conclusion can be assessed looking at Tang *et al.* (2005)'s research work, in which a morphometric analysis was performed on 28 physiologic ascending aortas and 29 ascending aortic aneurysms measuring thickness of vascular layers, cellular and matrix media tissue composition. Tang *et al.* (2005)'s conclusion is that a regulation system acts when mechanical properties are compromised by vascular dilation : an adaptive response (to minimize increased WSS and blood flow velocity values) which leads to hyperplastic cellular remodeling of the media layer in AAoA.

Other researchers investigate aortic flux, focusing more on flow properties, than aortic tissue ones. Hope *et al.* (2010) used four-dimensional flow magnetic resonance imaging (formerly time-resolved 3D phase-contrast magnetic resonance) to investigate the association between blood flow exiting from the bicuspid aortic valve and AAoA. A total of 53 individual systolic blood flow patterns were analyzed in this innovative work forming three distinct groups : 20

BAV patients, 25 TAV patients and eight volunteers. Among the group afflicted by BAV, seven patients have also an ascending aortic dilatation as well as four patients in the TAV group. It is interesting to observe that 15 of the 20 BAV patients showed a nested helical systolic flow while none of the other 33 individuals showed this same pattern. Among the seven patients with a BAV abnormality and an ascending aortic dilatation, six showed a right-handed nested helical systolic flow. Although these flow patterns should be referred to as flow streamlines, which is slightly different, Hope *et al.* (2010)'s study is very interesting to begin understanding the behavior of the blood in BAV and AAoA cases. In figure 2.5 blood streamlines from Hope's findings are displayed. It is important to point out that the helicity found in this study is not due to the BAV's altered fluid dynamics. As was stated in certain publications, in vitro (Morbiducci, 2007) and in vivo (Morbiducci *et al.*, 2009), helicity occurs because it is the best way to dissipate the relatively high content of energy in this specific portion of the aorta, where Reynolds number reaches its highest value and because helicity represents one of the mechanisms the body uses to avoid atherosclerosis plaque formation in the aorta. In a previous similar study, using the same magnetic resonance technique, Hope *et al.* (2007) found several differences between the blood streamlines of a group of 19 healthy volunteers and 13 AAoA patients. These differences refer to, above all, the average velocity of the blood from the ascending aorta and the transverse aorta, which was found to decrease in the normal volunteer group as opposed to increase in the AAoA group.

Weigang *et al.* (2008) demonstrated that in AAoA patients, blood streamlines reveal considerable differences compared to healthy individuals. In this study, 6 patients were examined with a flow sensitive MRI system. Results were compared with representative material of one healthy volunteer and with a series of 19 volunteers taken from previous studies. They found a possible correlation between known pathologies (1 patient suffered from Marfan syndrome, 2 from atherosclerosis, 1 from BAV) and the development of irregular blood flow streamlines which lead to flow acceleration, increased vortex formations within Valsalva's sinuses and a helical flow pattern in the middle aorta.

Stalder *et al.* (2008)'s research work is interesting because it shows the normal streamlines which blood follows in a non pathologic aorta nor aortic valve, referencing normal blood velocity paths and values while analyzing the WSS value. Stalder *et al.* (2008) collected very reliable results combining b-spline interpolation and Green's integral theorem to perform one of the first in vivo quantifications of blood flow and vessel wall parameters.

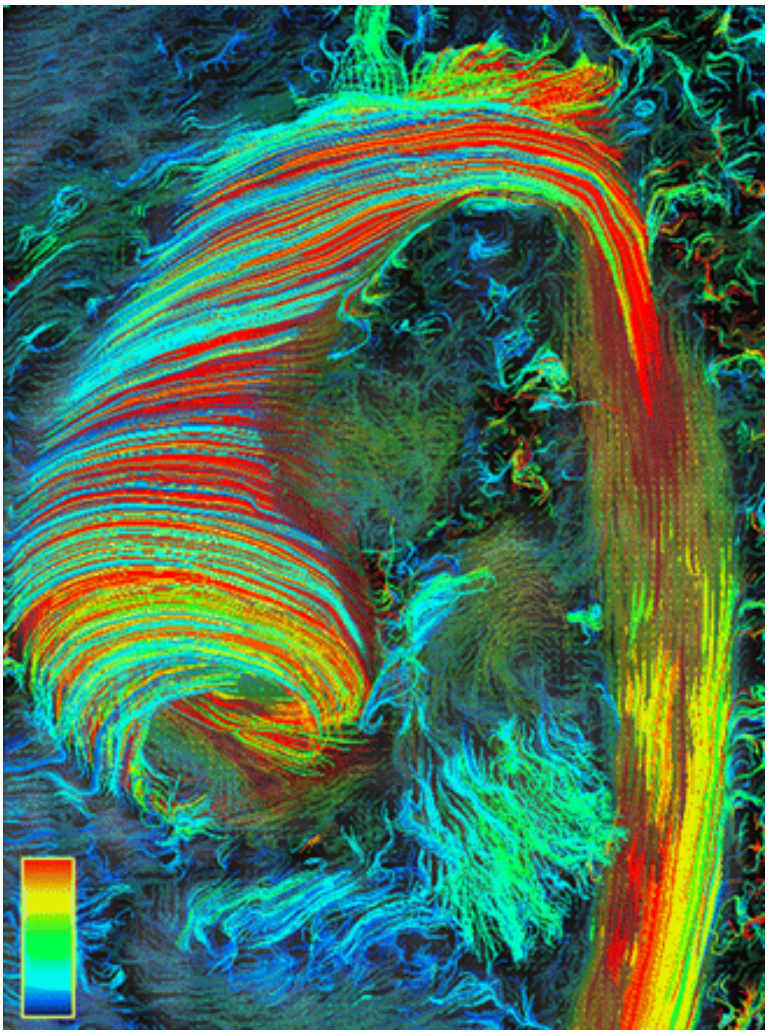

Figure 2.5: Hope's findings in blood streamlines are shown in this image. The flow starting at the aortic root suddenly became helicoidal, thus confirming the numerous speculations on this argument.

2.8 Changes in Wall Shear Stress

The variations that a bicuspid aortic valve induces in the ascending aorta also concern some mechanicals properties, like WSS. The latter, is one of the most important factors when treating aneurysms. It was demonstrated that WSS is actually one of the principal factors contributing to aneurysmal growth (Prado *et al.*, 2006). It is not completely understood yet if BAV induced WSS, can influence, in some way, AAoA growth. According to the classical

formulation of the WSS :

$$\tau_w = \mu \frac{\partial u}{\partial y}\Big|_{y=0}$$

where μ is the dynamic viscosity and y represents the generic distance from the boundary, the WSS depends on the velocity of the fluid (u) and, since changes in blood velocity due to BAV are already well documented, some researchers are trying to investigate the alterations in WSS caused by BAV and/or AAoA. Some works have already investigated correlations between WSS and atherosclerosis (Cheng *et al.*, 2006), (Malek *et al.*, 1999) or vascular remodelling, more in general (Ishida *et al.*, 1997), (Nerem *et al.*, 1998). They found correlations between high WSS values and faster vascular remodeling but lower atherosclerosis plaque formation.

In a pioneering study, Barker *et al.* (2012) examined 60 subjects, divided into 4 equal groups : 15 BAV patients, 15 TAV healthy subjects, 15 normal TAV age-appropriate subjects and 15 TAV patients with AAoA. The study aimed to demonstrate that BAV abnormality causes changes in WSS and blood flow patterns in AAoA patients comparing the BAV group results with other groups and particularly with the group of TAV patients with AAoA. For the first time, despite the low number of patients for each group, results were significant when compared to each other. Barker *et al.* (2012) found higher WSS values among all the patients in the BAV group compared to the other groups. He also found that the modified flow jet impacting the aorta wall is responsible for the high WSS values in the impacted area. In a pilot study of 30 individuals two years before, Barker *et al.* (2010) detected interesting differences between the BAV group and the control group in terms of WSS. They measured the circumferentially averaged WSS in the ascending aorta of the 15 BAV patients and repeated the same measurement for the group of 15 control patients finding statistically significative differences. In figure 2.6 the blood flow streamlines reconstructed by Barker are shown. In the study of Bissell *et al.* (2013), other differences were found in a group of 142 subjects, 47 healthy and 93 patients with BAV. They described the well known right/left handed helical blood streamlines that are modulated by an bicuspid aortic valve as they focused their attention to the circumferentially averaged WSS. In the healthy group, they found a lower WSS with an increasing ascending aorta diameter while, in the BAV patients, constant high WSS values were found with an increasing ascending aorta diameter, confirming once again that different blood flow patterns caused by BAV, influence the WSS for, at least, the first segment of the aorta (ie. ascending aorta). When considering AAoA, interesting insights were found by Bieging *et al.* (2011), observing 11 patients with AAoA (of which, 7 had BAV) and 10 healthy volunteers. In this particular case, they found higher values of WSS in the patients group, both during diastole and systole, which correlates the increased helical blood flow patterns. WSS alterations in AAoA patients without BAV were also investigated. Bürk *et al.* (2012)'s research examines 33 AAoA patients with an MR based technique where they

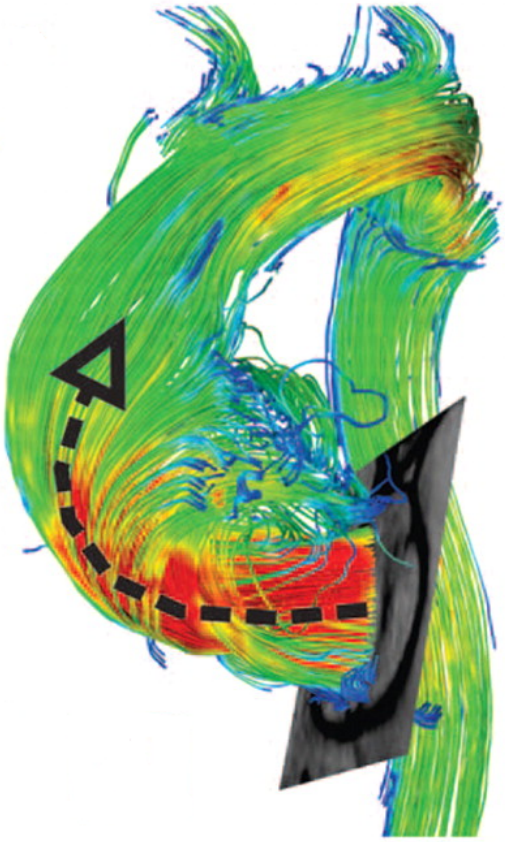

Figure 2.6: In the study by Barker, spectacular reconstructions of the blood flow streamlines were made, confirming Hope's findings. The black arrow points to the direction of the jet, which impacts the ascending aorta walls and then goes up in a helical form.

found comparable WSS results with the Barker *et al.* (2010) and Bissell *et al.* (2013) studies.

Comparable results can also be extracted from Harloff *et al.* (2010)'s report. In their research, they were investigating if WSS values are related to atherosclerotic plaques formation in the ascending and the arch aorta of patients without any valve diseases. The WSS values are comparable to the previously described research works in which they included BAV patients. This leads to an important question : does BAV play a role in determining WSS values in the AAoA ? Following Bürk *et al.* (2012) and Harloff *et al.* (2010)'s findings, BAV does not seem to play a fundamental role in modifying WSS values in AAoA mecanobiology. In a discordant manner, Barker *et al.* (2010) and Bissell *et al.* (2013)'s results lead to the opposite direction. Further studies may help to understand the exact mechanism in which AAoA and the hemodynamics of the ascending aorta is influenced by BAV.

2.9 CAD and CFD Modeling

The most significant part of this research project consisted of an ascending aorta computer aided design (*CAD*) model and computational fluid dynamics (*CFD*) analysis. CAD modeling has been used since the early '80s to reduce the persons needed to make detailed technical plans or drawings and, above all, to reduce the growing number of errors due to the increased complexity of industrial parts. Beginning with industrial parts, CAD has boomed since being the preferred tool to design almost any single piece imaginable, from the mechanical to civil field, in the military, in the arts, in electronics. CAD is now also being used in biomedical engineering applications, ranging from customized medical implant design and design optimization (such as stents, prosthetics, medical devices or supports), clinical medicine for a medical environment design (such as surgical rooms or, more generally, hospitals), tissue engineering for scaffold design and tissue modeling (Sun *et al.*, 2004), (Hollister *et al.*, 2000), (Lal et Sun, 2004), (Taguchi et Chida, 2003).

CFD analysis represents one of the most powerful engineering tools ever created. Originally for the aviation industry in the late '60s, it has grown rapidly with the spread of calculators and, consequently, computational possibilities. "*A work of fiction*" were models defined in 1983 by Nancy Cartwright in her famous book *How the Laws of Physics Lie* (Cartwright *et al.*, 1983). According to Cartwright *et al.* (1983), models are like simulacra, because the success of a model strictly depends on how much and how precisely it can reproduce reality. Today, keeping in mind the cardinal idea that a model is always an approximation of reality (Oreskes *et al.*, 1994), CFD analysis within models allows the simulation of almost every type of problem in which a fluid is involved, in all engineering domains. The fundamental role of CFD analysis in the biomedical field was assessed in 1999 by Taylor *et al.* (1999), when they created a medical breakthrough in previous surgery planning for the treatment of cardiovascular disease and the new paradigm of preventative medicine, which anticipates a reasonable outcome of treatment plans for patient-specific cases, by using computational tools like anatomic models and fluid dynamics analysis. In this research work, a pathology was modeled and to the best of the author's knowledge today, no other studies published show the same characteristics of the present work, except for one (published after this research was already started) that shows a similar research context.

In an interesting article, Faggiano *et al.* (2012) presented results from a CFD investigation of 4 BAV patients with dilated ascending aorta which they compare with CFD results from 4 TAV subjects representing the control group. In particular, they attempted to relate the observed den Reijer *et al.* (2010) phenomenon of blood jet asymmetry in BAV patients with the dilated ascending aorta to the systolic helical flow observed with magnetic reso-

nance techniques. Figure 2.7 shows the systolic jet hitting the aorta wall at "high" speed (red) in a reconstruction by Faggiano, compared with a normal systolic jet. A unique sur-

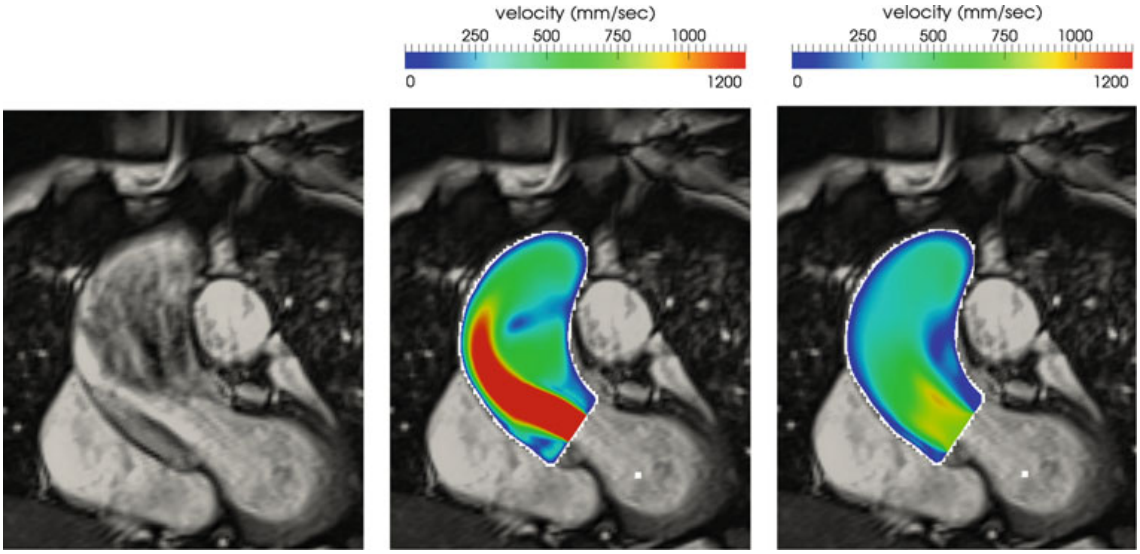

Figure 2.7: In the image on the left, the jet exiting from the bicuspid aortic valve is visible. The second image shows the quantification of this jet while the image on the right portrays the quantification of the jet in a tricuspid case.

face model of one patient's ascending aorta and aortic valve was obtained from the MR images using a segmentation technique provided by the Vascular Modeling Toolkit (vmtk, *http ://www.vmtk.org*). The valve orifice was manually conceived starting from the valve plane previously selected and using a tool which allows one to choose the valve morphologies and position. The valve leaflets weren't modeled and the valve was considered in an off position when closed (end diastolic phase) and in an on position during the rest of the cardiac cycle. Afterwards, a 1.36×10^6 elements tetrahedral volume mesh was generated by using, once again, vmtk and unsteady CFD were performed using the finite elements library LifeV (LifeV, *http ://www.lifev.org*). In this work, blood was modeled as Newtonian, homogeneous and incompressible and the vessel wall was considered rigid. To better describe the fluid dynamics in the ascending aorta, Faggiano *et al.* (2012)'s team introduced useful indices that quantify the flow reversal ratio, the flow eccentricity, the wall shear stress and the helical flow patterns as well as represent one of the most interesting innovations in that work. Developing ways to better understand quantities which aren't immediately explicit adds value to projects that really want to contribute to research.

Related to Faggiano *et al.* (2012)'s work, Viscardi *et al.* (2010) conducted a study during which they investigated the dependance of the aortic flow pattern on the aortic valve leaflets' orientation. In particular, two different BAV configurations (ie. antero-posterior BAV, latero-

lateral BAV) and a TAV case were modeled, using two softwares, vmtk and LifeV. Vergara *et al.* (2012)'s research project was also based on understanding the role played by BAV disease in the ascending aorta's fluid dynamics. Vergara *et al.* (2012)'s team merged the aortic model obtained from magnetic resonance images segmentation with different valve areas and orientations.

2.10 Steady State Blood Flow Modeling

The heart pump, due to its cyclic nature, creates pulsatile conditions in all arteries. The heart ejects (velocity) and is filled (pressure) with blood in alternating cycles, lasting about 0.8 s, called systole, which lasts about 0.3 s and diastole, which lasts the remaining 0.5 s. Hence, blood flow and pressure have unsteady characteristics, bearing pulsatile shapes that vary greatly in different parts of the arterial system. In general, the first flow out of the heart is intermittent with a positive acceleration component which goes to zero when the aortic valve is closed (diastole). Blood pressure, in physiological cases, does not go to zero during the diastole, due to the compliant nature of the systemic arteries. These arteries have a high downstream resistance during rest and the flow may be modeled as on or off with each cycle. Nevertheless, a CFD blood analysis in which blood flow is considered to have steady flow conditions, constitutes an approximation of reality.

Johnston *et al.* (2004) and Johnston *et al.* (2006) presented two papers in which they examined the characteristics of both steady and unsteady flow conditions in a non-Netwonian blood model. For both papers, a 3D model of the right human coronary artery (without branches) was reconstructed starting from magnetic resonance images and using the centre lines reconstruction method. This method, widely used when reconstructing cylinder shape models, is quite fast and automatic, even if it shows some significant approximations especially the low quality perimeter definition which could be an important parameter when considering an atherosclerotic plaque, for example. Johnston compared five different non-Newtonian blood models as well as the Newtonian model. For each model, they evaluated the blood flow velocity and WSS results in both steady and unsteady configurations in order to asses which one shows the best approximation compared to simulations done in the same artery segment of four different patients. In the first study, using steady blood flow characteristics in CFD analysis, allowed Johnston *et al.* (2004) to conclude that for a slow blood velocity rate (mainly at the inlet), the non-Newtonian effects are not negligible. However, the question he posed in the second paper was to what extent are these effects important over an entire cardiac cycle ?

To answer the question, they proposed a different method in the second publication. Firstly, only the Generalized Power Law and the Newton model for blood viscosity were

used in the CFD simulations. Secondly, for the four CFD analyses of each arterial model, they added two more simulations using two of these artery models, one representative of the normal arteries and the other of an ectatic artery. They used these two simulations to study the differences between the two blood models when a pulsatile regime is imposed. So a distribution of WSS values was built during some fixed time of the cardiac cycle. These values were chosen as they are representative of key points through the cardiac cycle. At the end of the cycle, Johnston *et al.* (2006) affirmed that only little visual difference between the two distributions was noticed and that the WSS results for the two models, were different during 30% of the cardiac cycle. For the rest of the cycle, when using a pulsatile regime, both blood model behaviors were fine. As a matter of fact, in the second paper it is stated that although there is an effective and non-negligible difference in WSS stress distribution through cardiac cycle, it could be argued that in the particular region of the right coronary artery, the difference in the WSS values isn't significant, due to the low overall magnitudes of the WSS compared to other anatomic points. Consequently, from this study, it could be concluded that a Newtonian model for blood viscosity is an adequate approximation for transient (pulsatile regime) simulations.

2.11 Transient Blood Flow Modeling

Research articles by Faggiano *et al.* (2012), Viscardi *et al.* (2010) and Vergara *et al.* (2012) are all characterized by unsteady blood flow conditions. In particular, a waveform describing blood flow velocity in a cardiac cycle, is given at the inlet boundary condition. As described in these projects, the velocity waveform has a quite regular trend : it increases rapidly during systole to the peak systole value after about 0.16 s with a flow rate a little less than 400 $cm^3 s^{-1}$. It then starts to decrease, reaching the maximum deceleration rate and the lowest flow rate value after approximately 0.32 s. The flow rate value starts to be negative after 0.3 s, which means that the blood flow inverses his direction for a while (about 0.1 s) and then rises slowly again to reach the zero flow rate value until the cycle begins again. Assessing the cardiac cycle with a pulsatile waveform of the type described, is without a doubt, the most precise approximation possible when a CFD vascular analysis is settled.

Shahcheraghi *et al.* (2002) described the three-dimensional unsteady characteristics of blood flow in all of the human thoracic aorta and the three major branches (ie. brachio-cephalic, carotid, subclavian). Rigid aortic walls and no-slip conditions were assumed and interesting boundary conditions were imposed : at the inlet were imposed both a parabolic flow profile and a complete pulsatile waveform characterized by accelerating, decelerating, reversed and zero blood flow regions. Since the inlet mass flow was known (as the geometric

characteristics of the cross-sectional area), pressure gradients were calculated inside the ascending aorta with the meshed model in order to impose the same axial pressure gradient at the entrance of the ascending aorta. The three-dimensional model was reconstructed beginning with a series of two-dimensional slices obtained with in vivo CT scan images of a patient-specific case. It's interesting to note in Shahcheraghi *et al.* (2002)'s article a tracer was introduced to better investigate the blood flow regime in large arteries. They numerically injected a non interactive tracer into the flow, by imposing the tracer as a wall boundary condition in the unsteady convection-diffusion equation they used. They were able to visually see the tracer evolution during the CFD analysis, by interpreting the CFD results when the convection-diffusion equation converges. Particularly, range between 0 and 1 was given to the tracer value, where 0 means no diffusion of the tracer into the aorta walls and no backward flow convection (for example, if the flow is too fast to interact with the aorta walls, such as during early systole) and 1 means maximum tracer diffusion into the aorta walls and backward flow convection (for example, in the aortic arch for peak systole).

Walsh *et al.* (2005), in a patient-specific study of a human aorta model, compared the results obtained varying some characteristics of the model geometry accomplishing both steady and unsteady flow conditions. The first aorta model reconstruction showed no axial nor area smoothing, the second one had both axial and area smoothed and the final model was built assuming all cross sections were circular with axial and area smoothing. They also varied the blood flow characteristics with the first simulation being steady and pulsatile in the second. Results showed that a particular emphasis should be brought upon the model geometry. Walsh *et al.* (2005) compared the WSS results obtained for the three models in both the blood flow regimes, showing that WSS values in the less smoothed model when paired with pulsatile flow regime, was almost not calculable due to wall geometry effects to the fluid. They also evaluated the velocity waveform in various segments of the aorta and noticed the different shapes due to the two different blood flow regimes. In particular, the waveform showed major differences between steady and unsteady flow in the aortic arch region. Walsh *et al.* (2005) concluded that steady flow solutions underestimated blood recirculation and reverse flow regions and that the radius of curvature along the aortic arch is one of the main influencing factors when studying aortic fluid dynamics and therefore, appropriate care should be taken when reconstructing an aorta model from MR images.

2.12 Newtonian Blood Models

A fluid is defined as Newtonian when the shear stress and shear rate ratio are constant. Plotting shear stress versus shear rate on a graph (at a given temperature, defined as 25°

Celsius) gives a straight line with a constant slope. The values of the viscosity of the fluid for which the plot was graphed belong to that straight line. All gases are Newtonian as are some common liquids, such as water and the majority of pharmaceutical syrups. However, many important fluids such as polymers, paints and fluids we eat show a non-Newtonian viscosity. This means that the slope of the shear stress against shear rate is no longer constant. When the viscosity of these types of fluids decreases as the shear rate increases, the fluid is called shear-thinning. On the other hand, when the viscosity increases as the fluid is subjected to a higher shear rate, the fluid is called shear-thickening. Blood is a non-Newtonian fluid showing a shear-thickening behavior (Chien *et al.*, 1970), (Pedley, 1980) and consisting of an elastic particulate cell suspension in a liquid known as plasma.

Blood is made of two phases : a particulate phase and a continuous phase. The latter is the plasma, which, for human blood, is about 91% water, 7% proteins while the balance consists of inorganic solutes and other minor organic substances (Mazumdar, 1992). Some studies have demonstrated that plasma is a Newtonian fluid with a viscosity as a function of temperature (De Gruttola *et al.*, 2005). The particulate phase of blood consists of Red Blood Cells *(RBCs)* or erythrocytes (which are the major component, 99% in the blood particulate phase), white blood cells or leukocytes and platelets. Red blood cells have a biconcave discoid shape with a diameter ranging from 6 to 9 μm and a thickness between 1.84 and 2.84 μm ; comprising of an elastic membrane which encloses the hemoglobin molecule and makes RBCs deformable. This particular property, combined with the aggregatable nature of RBCs, play a significant role in blood rheology. RBCs aggregation, in fact, causes an evident increase in blood viscosity at low shear rates (Zydney *et al.*, 1991). As the shear rate increases, the RBCs forms small units called rouleaux which, thanks to the elastic membrane, start to assume a cluster form (C, 1993) ; at which point, the more the shear rate increases, the more these clusters begin to lose rouleaux units, until they are converted again into single RBCs and dispersed throughout the plasma separately (Kang, 2002). Hence, it can be understood that both the viscosity and the shear-thinning blood behaviors largely depend on the blood's rheology (hematology) and on the blood's composition properties such as hematocrit levels (Crowley et Pizziconi, 2005), temperature and shear rate (Cho et Kensey, 1990), plasma viscosity (Baskurt et Meiselman, 2003), cell orientation (Baskurt et Meiselman, 1997), aggregation and deformation (Chien *et al.*, 1970), vessel geometry (O'Callaghan *et al.*, 2006), *etc.*

A suitable blood model should include non-Newtonian properties of blood. Despite the well known blood rheology, there does not appear to be a common consensus in literature on the importance of non-Newtonian properties when studying blood flow in large arteries. Some studies found non-Newtonian rheology important (Rodkiewicz *et al.*, 1990), (Gijsen *et al.*, 1999), while others found that it is relatively unimportant in determining blood flow

behavior in large arteries, especially when unsteady flow conditions are imposed (Perktold *et al.*, 1997), (Ballyk *et al.*, 1993). In particular, in his innovative study, Perktold *et al.* (1997) used a 3D human carotid bifurcation model to accomplish a detailed analysis of the blood flow regime and the wall shear stress distribution during the cardiac cycle. To build the basic geometrical data and the pulsatile flow conditions, they used data from Ku *et al.* (1985) and modeled blood as a non-Newtonian fluid (using the Casson model). Afterwards, blood was modeled as Newtonian, giving a constant viscosity $\mu_N = 0.035$ Poise and the non-Newtonian and Newtonian results were then compared. The comparison demonstrated that in the human carotid, the Newtonian simplification yields no change in the essential flow characteristics. According to Perktold *et al.* (1997), the most evident differences can be seen in the secondary flow velocity, which varies from 4 to 48%; also, in reversed flow velocity, a difference between 18 and 31% can be observed. However, as Perktold affirm, these local deviations do not play a fundamental role in the entire flow field. In terms of WSS results, Perktold concluded that Newtonian results underestimate WSS of about 10% of the same non-Newtonian results.

Another very interesting work, whose results go in the opposite direction from the Perktold ones, was conducted by Gijsen *et al.* (1999). In their research work, they used the Laser Doppler technique and finite elements simulations to investigate the differences between Newtonian and non-Newtonian properties of blood concerning the axial velocity distribution. A carotid bifurcation model made on plexiglas (for laser investigation) was used and an analogous blood fluid was recreated using a solution of potassium thiocyanate in water, for the Newtonian fluid, and the same solution with 250 ppm of Xanthan gum added (as described in Brookshier et Tarbell (1993) was used as the non-Newtonian fluid. Moreover, a CFD analysis using the Carreau-Yasuda model was made, without simulating the viscoelastic blood properties. A comparison between the experimental models and the numerical ones was made, showing an agreement between both the Newtonian and the non-Newtonian fluid.

The first conclusion from the results demonstrates that the shear-thinning property of the blood analog fluid seems to be the dominant non-Newtonian property of blood (under steady flow conditions), since, in the computational model, only shear-thinning was included and viscoelasticity was ignored. Secondly, from the comparison between the computational and the experimental results, it can be noticed that, in the common carotid artery, the differences between the velocity distribution of the Newtonian and the non-Newtonian fluid are evident, which contrasts Perktold's conclusions. Using the same parameters Perktold used in addition to the same non-Newtonian blood model (but with the blood analog fluid), ultimately allowed Gijsen to obtain comparable results in terms of axial velocity and shear rate. Gijsen then made an important conclusion affirming that the shear thinning properties of blood, which mostly describe the blood velocity distribution in larger arteries, are strongly influenced by

little variations in the shear rate. Thus, a CFD blood simulation in large arteries (such as the thoracic aorta) should take into account the fundamental role played by the blood shear rate.

2.13 Non-Newtonian Blood Models

Several models have been proposed over the past years to predict blood behavior, but none has been universally accepted yet. This perhaps explains the reason blood is often assumed as a Newtonian fluid in CFD simulations, which, in any case, is an approximation. However, this approximation is acceptable when considering some shear rate ranges. In fact, when shear rate does not exceed a limiting value, the blood behaves like a Newtonian fluid. This limiting value of shear rate, which determines the blood apparent viscosity, is a function of a large quantity of factors as it was described above. In literature, the limiting value of shear rate is not yet properly assessed, varying from 50 s^{-1} (Long *et al.*, 2004) to 100 s^{-1} (Chan *et al.*, 2007) or in the range of 100 to 300 s^{-1} (Crowley et Pizziconi, 2005).

Considering the average high shear rate values in large arterial blood vessels (ie. vessel diameter $\geq$ 1 mm), blood is often modeled as Newtonian fluid by assuming a constant blood viscosity. Some studies attempted to estimate Newtonian blood viscosity as a function of plasma viscosity and cell density. One of the first and most famous studies was conducted by Einstein in 1906 on monodisperse rigid spheres, in which the effective viscosity of a very dilute suspension of rigid and non-interacting spherical particles, irrespective of absolute size and relative size distribution, is $\eta = \eta_0(1+2.5\phi)$, where η is the effective suspension viscosity, η_0 denotes the viscosity of the suspending medium, which is pure liquid and ϕ is the volume fraction of the solid phase (the rigid spheres). This relation was the starting point for several of Einstein's derived viscosity formulations still being used today (Lee et Steinman, 2007). Several of these studies on Newtonian blood viscosity were extended to the non-Newtonian case, trying to model the role of certain fundamental variables, the first being shear rate. As previously stated, in large arterial blood vessels, the instantaneous shear rate range varies between zero and around 1000 s^{-1} over the cardiac cycle (Cho et Kensey, 1990)). This means that during the cardiac cycle, blood behaves as a shear-thinning fluid exhibiting low shear rate values in arterial vessels ; this conclusion is also valid when considering particular vascular regions such as bifurcations or regions affected by pathologies like aneurysms and stenoses (Leondes, 2000). In these areas, blood non-Newtonian properties are more evident and the shear-thinning properties have to be considered in the CFD analysis.

To describe the relationship between blood viscosity and shear-thinning properties, a constitutive equation is required. In addition, shear-thinning behavior is not the only one

blood demonstrates. Some researchers also considered the thixotropic (Chen *et al.*, 1991) and elastic (Ai et Vafai, 2005) behavior characteristics of blood, which allow the classification of blood models into another two non-Newtonian subcategories : time-independent and time-dependent flow behavior models. In time-independent models, the apparent blood viscosity depends on the shear rate values. Three distinct regions are described as follows : the lower and upper Newtonian region (where shear rate is low or high, respectively) the viscosity constant region and the middle region where the apparent blood viscosity decreases while shear rate increases. To represent with high accuracy the entire blood flow scenario in the human body within an acceptable approximation, the time-independent flow behavior models are the most used models in CFD analysis. Models like the Power Law, the Carreau-Yasuda, the Ballyk Model (or Generalised Power Model), the Casson model and the Cross model are only a fraction of the time-independent models in existence adapted to be used with blood and vascular geometries. The second non-Newtonian subcategory is the time-dependent flow behavior model, which is used to best approximate the thixotropic and viscoelastic blood behavior. Examples of this subcategory are the blood-adapted models of Huang (Huang *et al.*, 1986), Weltman (Rao, 2007), Rosen (Braun et Rosen, 2008). In the already cited research works of Faggiano *et al.* (2012), Viscardi *et al.* (2010) and Vergara *et al.* (2012), no apparent blood viscosity model was considered and a constant blood viscosity was assumed. This assumption is considerably realistic since blood does not demonstrate a non-Newtonian behavior at all flow rates and all vascular geometries. Blood's non-Newtonian behavior is appreciable in almost every microcirculatory system, in regions where very low shear rates occur such as small branches or capillaries, for instance.

2.14 Rationale

From the literature review, it can be assessed that there are two principal currents of research. The one that believes the growth of an AAoA is the result of a complex series of hemodynamic factors which interact together (above all the presence of a bicuspid aortic valve). On the other hand, researchers believe that, beyond hemodynamic factors, genetic factors have to be considered to understand the mechanism of AAoA formation in BAV patients. The latter was the most popular explanation over the last decade and can now be assumed as the dominant one (Girdauskas *et al.*, 2011).

This project refers to the first line of thought and hence, the global objective was formulated to be consistent with the assumption that the hemodynamic factors are a possible explanation for the growth of an AAoA (see section Research Objectives). In particular five sub-objectives were formulated, to support the global objective. One of them, represents the

innovating feature of this project. In fact, to better notice the changes in hemodynamics factors due to an AAoA and a BAV, a parameterization of the CAD model was included among the sub-objectives. This parameterization, allowing to change the diameter of the ascending aorta (and then the size of the aneurysm), will show the correlation between pure geometrical factors and hemodynamic changes.

In conclusion, this study offers a support in understanding a real medical problem thanks to biomedical engineering knowledge. Its originality relies in a feature which has not been developed on the literature yet. Moreover this project, due to the complexity of simulating the physics of the human body, left different aspects to be further developed in future works.

CHAPTER 3

MATERIALS AND METHODS

3.1 Patient Selection

An initial patient selection was made at Sainte-Justine, using the software Synapse (Fujifilm Holdings America Corporation, Valhalla, New York) along with the support of a Sainte-Justine cardiologist. A database of 140 patients, obtained under the approbation of the Ethics Committee, was firstly inspected. Two criteria, age and presence of an evident ascending aorta dilatation, were used to accomplish a first basic patient selection among the 140 cases in the database. Twenty-one patients were then selected, according to the two criteria mentioned above. The Body Surface Area (BSA) and Body Mass Index (BMI) were also calculated during this step.

BSA and BMI are two indexes widely used in the practice of medicine. BSA is considered to be the best index to normalize certain physiological parameters, such as cardiac output, left ventricular mass, renal clearance and thus, estimating the necessity of certain cardiac therapies or drug dosages in therapies like chemotherapy (Cosolo *et al.*, 1994), (Daniels *et al.*, 1995), (Hallynck *et al.*, 1981). The most used formula to evaluate BSA is the Du Bois and Du Bois formula, BSA = $(W^{0.425} \times H^{0.725}) \times 0.007184$.

BMI is a simple index, largely used in practical medicine, to give initial insight into the general conditions of a subject. Hundreds of studies examine the relation between body weight and mortality trying to correlate the two (Cornoni-Huntley *et al.*, 1991),(Lee *et al.*, 1993),(Rimm *et al.*, 1995). The formula is quite simple, expressed as the subject's body mass (in Kg) divided by their height (in meters) squared, according to the first formulation by Quetelet (Eknoyan, 2008). Based solely upon two factors (weight and height), these two indexes were extensively discussed and are only considered to be indicative by doctors Levey *et al.* (1999), Willett *et al.* (1991) and Manson *et al.* (1987) and are no longer taken as pathology indicators. This is the way the two indexes were considered in this research study. In figure 3.1, the list of the 21 patients, from the second selection, is displayed.

3.2 Second Selection

Patient images were taken between 2003 and 2012 at CHU Sainte-Justine (3175, Chemin de la Côte-Sainte-Catherine, Montréal, H3T 1C5) with a Siemens Avanto 1.5T (Siemens AG, Muenchen, Germany) unit, which offered spatial resolution of $1 \times 1 \times 5$ mm (fl3d1

ID	AGE	GENDER	WEIGHT (kg)	HEIGHT (cm)	Z-SCORE	EXPECTED Z (SD)	BSA (m2)	BMI (kg/m2)	DIM.1 (mm)	DIM.2 (mm)	REPORT
1	16	F	56,8	166	6,43	2,23 (±0.31)	1,63	20,61	39	40	BAV, STÉNOSE, HV
2	18	F	47,4	155	6,31	2,11 (±0.29)	1,43	19,73	36	39	TRONC OPÉRÉ, VALVE DILATÉE, HV
3	9	F	35	142	8,44	1,95 (±0.27)	1,18	17,36	40,4	44,5	BAV, COARCTATION OPÉRÉ
4	17	F	38,7	151	4,7	2,02 (±0.28)	1,29	16,97	31	none	BAV, STÉNOSE, COARCTATION OPÉRÉ
5	17	M	98,4	180	7,53	2,52 (±0.35)	2,18	30,37	51	none	BAV, STÉNOSE, COARCTATION OPÉRÉ
6	18	F	71,2	174	6,36	2,35 (±0.33)	1,85	23,52	42	none	BAV, MÉSOCARDIE, COARCTATION OPÉRÉ
7	15	M	63	172	5,25	2,29 (±0.32)	1,75	21,30	36	38	QUASI-UNICUSPIDIE, STÉNOSE, HV
8	15	M	53,3	169	5,34	2,21 (±0,31)	1,60	18,66	35	37	BAV
9	18	M	57	169	5,42	2,24 (±0.32)	1,65	19,96	36,7	none	BAV, STÉNOSE, COARCTATION OPÉRÉ
10	16	M	81,8	168	7,67	2,39 (±0.34)	1,92	28,98	48	none	BAV, STÉNOSE, HV
11	13	F	49,7	160	5,35	2,15 (±0.30)	1,50	19,41	35	35	BAV
12	10	F	45,9	146	6,57	2,06 (±0.29)	1,35	21,53	36	39	BAV
13	11	M	40,8	132	6,22	1,96 (±0.28)	1,20	23,42	34	35	BAV, STÉNOSE, HV
14	18	M	94,9	174	6,56	2,48 (±0.35)	2,09	31,34	45	none	BAV, STÉNOSE, HV
15	15	F	57,7	151	5,25	2,17 (±0.30)	1,53	25,31	35	none	BAV, TURNER
16	17	M	54,8	164	7,59	2,2 (±0.30)	1,59	20,37	44	44	BAV, STÉNOSE, HV
17	14	M	64,3	177	7,86	2,32 (±0.32)	1,80	20,52	49	46	BAV, COARCTATION OPÉRÉ
18	15	M	74,4	183	4,11	2,41 (±0.34)	1,96	22,22	35	none	BAV, HV
19	16	M	44,8	164	2,62	2,13 (±0.30)	1,46	16,66	46	27	BAV, STÉNOSE
20	16	M	79,8	173	5,62	2,4 (±0.34)	1,94	26,66	40	40	BAV
21	17	M	64,2	178	7	2,32 (±0.32)	1,80	20,26	44	none	BAV, STÉNOSE, INSUFFISANCE
Average	15,29	8F - 13M	60,66	164,19	6,10	2,23 (±0.31)	1,65 (1,81±0,19)	22,15 (20—24,9)	39,91	38,71	

Figure 3.1: The 21-patient list is shown, in yellow the chosen patient. In green are the average values for the group. BSA and BMI average values, according to Verbraecken *et al.* (2006) are into brackets. The z-score was calculated using data from (Warren *et al.*, 2006).

sequence, ponderation T1, TR=3.19 s, TE = 1.07 s) in the midsagittal superior sectional plane projection.

The DICOM (*Digital Imaging and Communications in Medicine*) images of the final selected patient, were imported into the free version of the software OsiriX (Pixmeo, Bernex, Switzerland) to proceed with the investigation. OsiriX supplies a powerful environment in which to examine DICOM images and take measurements directly from the images. With this software, form the initial set of DICOM images, only one was chosen from the group of 21 patients (more than 900 images were studied).

The age criterion was imposed as a research constraint : only patients under the age of eighteen were included in this study. The presence of a significant dilatation of the ascending aorta was the second criterion, meaning only patients showing a dilatation of the ascending aorta greater than 30 mm in at least one of the two measured diameters were considered. In the second selection, more restrictive criteria were applied in order to obtain only one patient among the 21 already selected. Criteria based on the clinical panorama, the presence of BAV disease and more restrictive measured diameters, finally allowed to select the patient for that study.

The clinical panorama criteria was based on evidence of no further complications, with the exception of BAV, since this research paper aims to isolate, as much as possible, the ascending aorta aneurysm and BAV disease. More specifically, the selected patient showed a non stenotic bicuspid aortic valve with fusion of the right coronary with the non coronary leaflets (type 2 BAV), associated with a normal blood jet. In this second selection, the diameter criterion was chosen to be higher in order to select the patient with the most relevant dilatation. In

our case, the patient has a diameter dilatation of 40 mm in both diameter measurements, which correlates with ascending aorta dimensions for the patient's age group (Warren *et al.*, 2006), and can be considered as an ascending aneurysm at least 1.5 times greater than normal diameter value.

Due to the young age of the patients, one of the selection criteria for the images was not decided by the author, but was imposed by the quality of the set of images. In order to acquire proper MRI processing, the subject is required to remain virtually immobile, a condition not easily achieved when examining younger patients. The best quality set of images available was chosen by visually analyzing the images with respect to the previously listed selection criteria. The final selected patient was isolated from the rest of the sets of images. In sum, the selection criteria allowing the selection of the specific patient were : the age, an ascending aorta dilatation greater than 35 mm, a bicuspid aortic valve pathology and the quality of the set of images. BSA and BMI were used to compare the biometrics data.

3.3 Image Segmentation

In order to individuate and isolate the thoracic portion of the aorta needed for the study, a segmentation process was required. To segment biomedical images implies identifying body parts inside said images. Since different tissues (or the same tissues with different characteristics) are displayed with different grey scale colors in DICOM images, segmentation softwares use powerful algorithms to process the image by scanning the level of grey. Starting from the first automated segmentation method first proposed by Otsu (1975), several other segmentation techniques are used nowadays. There are approximately two categories of segmentation techniques : level based and constraint based. The first category uses low level image metadata, such as image gradient and image density data, and includes threshold methods (eg. histogram shape based algorithms, maximum entropy based algorithms), region based methods (watershed and region growing algorithms are the most famous) and edge detection methods (eg. Sobel and Laplacian filters). The second category uses a priori knowledge of the morphological and physical objects data in order to extract constraints from the processed images ; belonging to this category are multi-scale methods, deformable model based methods (eg. Snake), graph partition methods (eg. graph cuts), learning based methods (eg. k-means clustering), and template based methods (also known as atlas based methods).

The segmentation process was performed, in this case, with the software Slice-O-Matic (Tomovision, Magog, Canada). This software, allows all possible segmentation operations on DICOM images, volume reconstruction as well as mesh generation. A deformable model based method was performed, which uses active contours, implementing the Snake feature.

This feature, introduced for the first time by Kass *et al.* (1988), is a set of splines that minimize the energy near the desired local minimum using internal image constraints (eg. features such as edges, lines, particular contours) and influenced by external constraints, which typically come from the user interface. The position of a Snake can be parametrically expressed by $v_s = (x_s, y_s)$ and the functional energy (e), which the Snake aims to minimize, can be expressed as follows :

$$e = \int_0^1 e_{int}\left(\boldsymbol{v}\left(s\right)\right) \mathrm{d}s + \int_0^1 e_{ext}\left(\boldsymbol{v}\left(s\right)\right) \mathrm{d}s$$

where the first term controls the internal constraints (ie. the smoothness of the contours) and the second term controls the external constraints, which modulate the contours towards the target object (the thoracic aorta in this case) into the image. The chosen set of images (made up of 80 single slides, taken within an interval of about 0.01 s of each other) did not allow a fully automated segmentation process due to the poor quality of the grey levels (ie. internal forces). A semi-automated process was implemented : after having manually traced a couple of snakes, the *Snake Automatic Propagation* feature in Slice-O-Matic was used resulting in good contour segmentation. A new manual intervention was then required in order to best define the final organ contours. Figure 3.2 shows an example of Snake contour made for one slice and subsequently manually modified. The final (the biggest in a single slice) segmented area was taken starting from the aorta root (ie. Valsalva sinus), following the ascending aorta contours, the aortic arch and ending when the descending aorta is at the same height as the pulmonary trunk. The brachiocephalic trunk was segmented until the bifurcation of the right subclavian and the right common carotid artery. The left common carotid as well as the left subclavian artery were also segmented, maintaining the segmentation region at the same height as the brachiocephalic trunk. The *Volume 3D* feature in Slice-O-Matic was then used to generate a 3D model, figure 3.3 shows the result from this process.

Because of the relatively easy way to obtain 3D models with these segmentation softwares, this kind of models are widely used by researchers as they offer good precision entirely based on the quality of the segmentation. The 3D model obtained was used to give initial insight into the general segmentation quality and, subsequently, the geometry was saved as *ASCII* STereoLithography file (.stl). This kind of format allows the exportation of a cloud of points, which represents the discretization of each snake contour made in each of the 80 slides composing the patient's set. In figure 3.4 the cloud of points is plotted along with references for the aorta's parts.

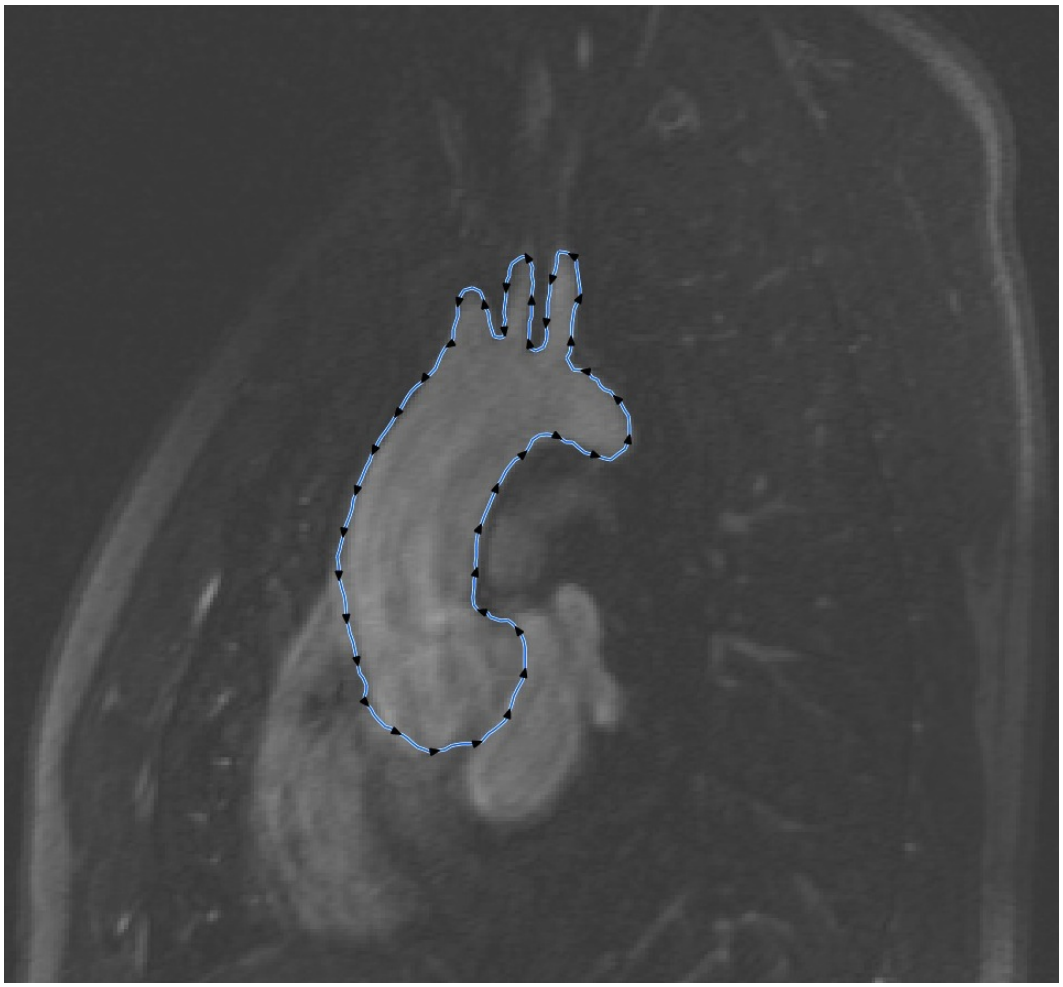

Figure 3.2: One of the slices used for the reconstruction is shown. In blue is the segmentation contour made with the Snake feature. The black triangles represent the control points inserted to better modulate the Snake.

3.4 CAD Model

To conceive and develop an ascending aorta CAD model instead of a volume developed segmentation model was decided when the parametric feature was considered for this 3D model. Volume developed segmentation models in fact, do not allow the implementation of a parametric model. Parametric signifies that certain dimensions of the final CAD model can be changed in order to simulate different characteristics. For example, if the influence of the radius of curvature while modeling the aortic arch must be investigated, a parametric model of the aortic arch is convenient, allowing one to set only the desired radius of curvature without redoing the whole model. The same goes when different grades of stenosis are examined in a vessel model : it is always possible to change the diameter parameter or the general shape

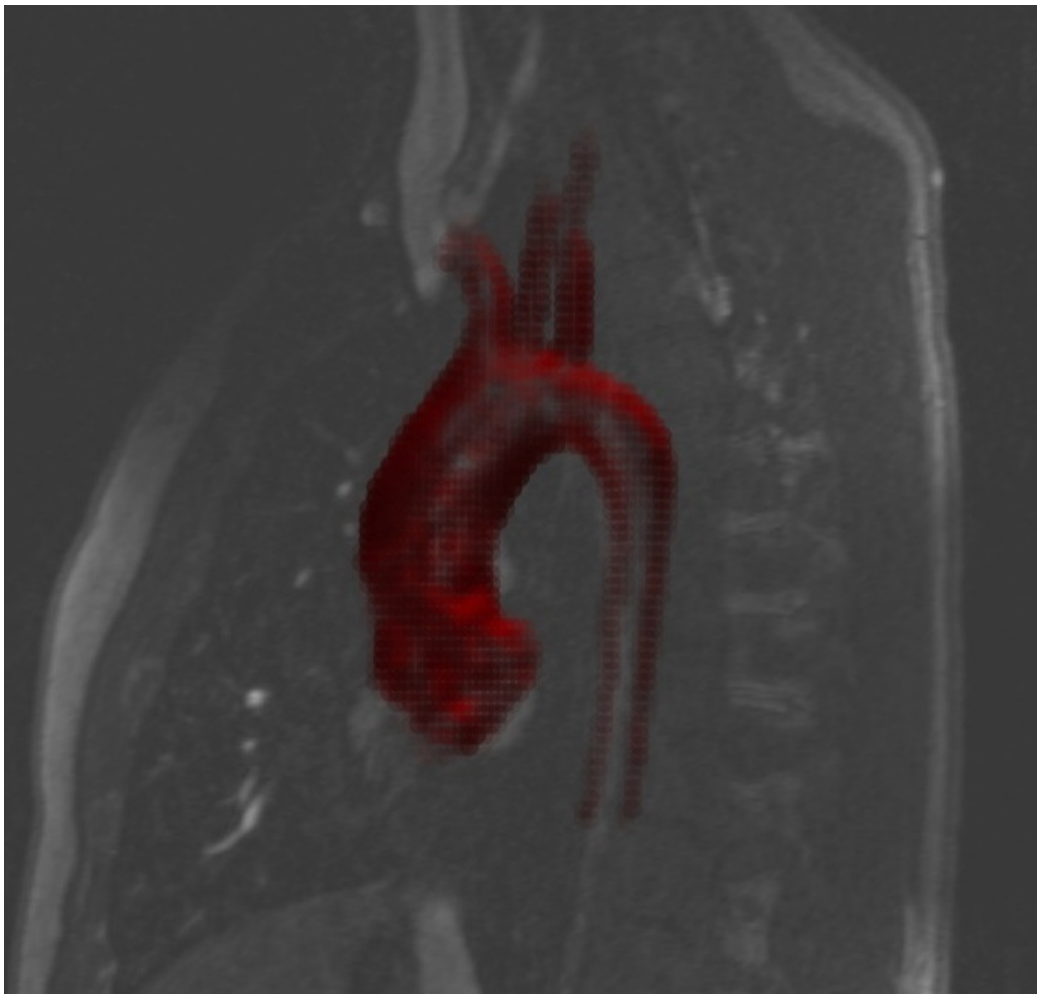

Figure 3.3: The volume reconstructed within the Volume 3D feature (in red) gives an idea of the quality of the reconstruction. The enlarged diameter of the ascending aorta due to the aneurysm is visible. The slice in the background is used to contextualize the volume.

of the stenosis if needed. When studying the impact of blood in a bifurcation to assess the various wall shear stress values or blood patterns, in a parametric model of a bifurcation, no matter how realistic the characteristics of the model, an adjustable parameter can be set for the bifurcation angle, length or inlet/outlet diameter. For the present work, the diameter of the ascending aorta aneurysm was parametrized between the pathological value and the value for whom the ascending aorta is no longer dilated.

The conception of the CAD model was realized using CATIA version 5.20 (Dassault Systemes, Vélizy-Villacoublay, France). For this thesis, two modules integrated in CATIA, were used : *Mechanical Design* and *Shape*. The first module was used to render the volume part of the model, the second was instead used to render all of the surface parts. In the latter module, the cloud of points, obtained by the the segmentation process, was imported

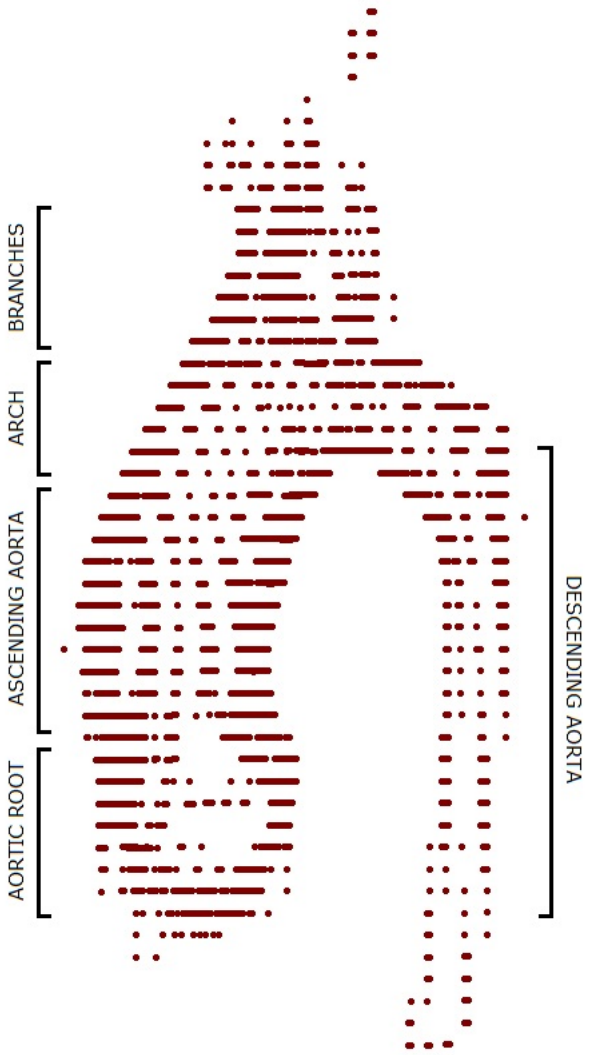

Figure 3.4: The cloud made of 1955 points. The shape of the aorta can be distinguished, in this projection, among all of the segmented parallel slices.

using the sub-module *Digitized Shape Editor*. Starting from the cloud of points, the model was conceived by separating the entire geometry in anatomic Regions Of Interest ($aROI$). In particular, seven different aROIs were individuated and thus each region was modeled separately. This process allowed the model to be handled independently, in a modular way, which resulted in an easier reconstruction. The seven aROIs, from the valve outlet to the blood flow, correspond to the aortic root, the ascending aorta, the aortic arch with the three branches (ie. the brachiocephalic trunk, the left common carotid and the left subclavian artery) and, finally, the descending aorta.

To better implement the CFD analysis, four flow extensions were added to the brachiocephalic trunk, the left common carotid, the left subclavian artery and the descending aorta aROI, which correspond to the outlets of the CFD model. Flow extensions are needed to obtain a fully developed flow, to therefore estimate the definite flow behavior even if the model boundaries do not represent the actual anatomy (Ladak *et al.*, 2000), (Antiga, 2005), (De Santis *et al.*, 2011). These outlet flow extensions were created as the last step of the model building process, in order to develop the extension from the already built model, by calculating its axis and radius from the last contours extracted from the corresponding aROI (Moore *et al.*, 1997). All four outlet flow extensions were obtained using the Extrusion tool (which retains the same characteristics as the contour profile from which it is extruded) into the *Generative Shape Design* sub-module ; the detailed dimensions of the four Extrusions are summarized in table 3.1 :

Table 3.1: Construction values for the Flow Extensions made within CATIA.

	INFLOW	OUTFLOW Brachiocephalic	OUTFLOW Left Common	OUTFLOW Left Subclavian	OUTFLOW Descending
Diameter (mm)	32.44	10.12	4.04	5.58	11.38
Lenght (mm)	150	40	40	40	50

3.4.1 Model Backbone

The model backbone was the first part to be developed. A total of three sub-modules were used : *Digitized Shape Editor*, *Quick Surface Reconstruction* and *Generative Shape Design*. As specified above, the cloud of points was imported using the sub-module *Digitized Shape Editor*, then the sub-module *Quick Surface Reconstruction* was used to implement the spline reconstruction technique. Adopting this technique created a series of parallel circular splines along the cloud of points, following the aorta's natural shape. In particular, these splines started at the level of the aortic root and ended at the extremities of the supra aortic arteries connecting all of the perimetrical points from every slide in the $x - y$ plane. Hence, each circular spline simply represents a slice of the aorta's perimeter (disregarding thickness). The spline reconstruction technique is an important step in each CAD reconstruction process beginning with a simple cloud of points. In order to give a shape to the cloud, splines are created, following the points in the cloud, building the backbone structure from where a surface and/or volume reconstruction can be achieved. CATIA uses different type of splines, in this work the Non Uniform Polynomial B-Spline (*NUPBS*) were used, in the specific form of the B-spline. A B-spline curve of n degree is a piecewise polynomial curve, whose shape is given

by a series of control points. These points drag the curve towards themselves, specifying its final shape. The aorta's cloud of points are all potential control points for the B-spline curves, which were used to build the model's backbone, are displayed in figure 3.5. To ensure conti-

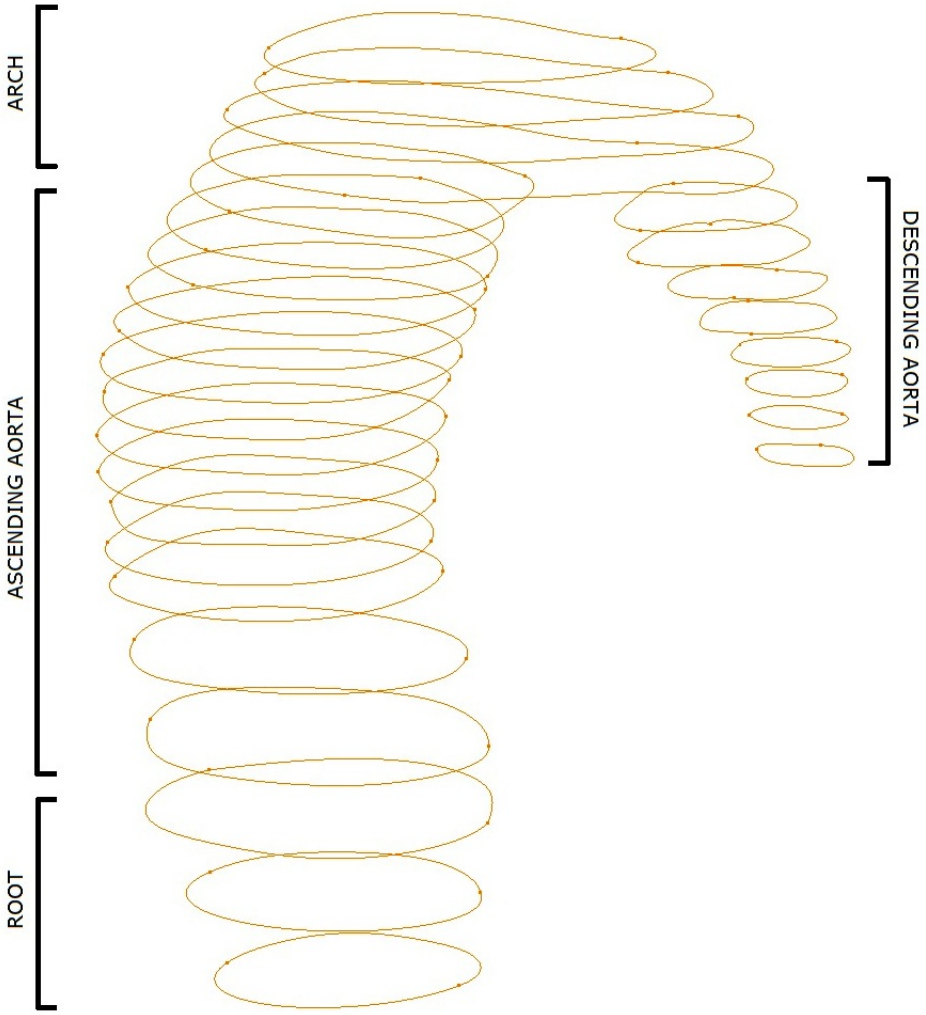

Figure 3.5: The B-spline curves built form the cloud of points. Not every segmented slice was used for the model reconstruction. For example, in the part of the aortic root, three B-splines were used due to the bad resolution of the DICOMs in this area, which could have introduced errors.

nuity in the backbone, the pieces of the curve are joined according to continuity constraints, imposed by continuity equations, in locations called joints. The continuity equations regulate curve joining, typically to render the final spline smoother (and therefore, the surface which will rely on the spline). The smoothness order in CAD applications is often referred to as Geometric continuity (G). Geometric continuity, G^n, describes the n^{th} degree ($0 \leq n \leq 2$) of smoothness between two joined curves or surfaces, the higher the number the smoother the

joint.

3.4.2 Surface Building

After having created all the necessary splines, the *Generative Shape Design* sub-module was used to build the aROIs. Each aROI was built separately, except for the aortic root and the ascending aorta's aROIs, which were created at the same time to enhance the geometric continuity of the surface. In fact, the same way curves are created by segments combined in locations called joints, surfaces (during the surface reconstruction process) are generated by patches combined together in locations called borders. To build the surface, maintaining the maximum degree of precision relative to the splines (an consequently to the cloud of points), the *Surface Multi-Sections* feature was applied. The multi-sections surface feature is one of the most powerful surface reconstruction tools available in the *Generative Shape Design* sub-module. It creates a surface between two (or more) previously defined splines through a powerful algorithm which checks the continuity of the spline and estimates the relative distance between each spline. Hence, by projecting the perimetric points of one spline onto the perimeter of the other, creates a surface between the selected splines according to the direction imposed by the user and increasing the steps along the perimeter until reaching the starting point. The surface created by the multi-sections algorithm, is a NUPBS surface, which is a spline that, instead of evolving only in one parametric direction (as the B-spline does), evolves into two, creating a parametric surface made of splines. Similarly, as control points influence the shape of a spline, the NUPBS surfaces are modulated by the splines (namely control splines) to which they refer.

In this project, the entire surface of the model was made of NUPBS surfaces derived from B-splines. This feature, takes the advantage of the geometric continuity property of NUPBS surfaces. The geometric continuity concept was previously described and now it will be easier to understand the importance of that value. In a comparative study, between models conceived both from *in vivo* and *in vitro* scans of a carotid artery bifurcation, Moore *et al.* (1999) found that when reconstructing models from MRI images, noise levels were unacceptable. He performed a smoothing process both to the luminal surface of the models and to the splines that approximate the surface, finding a consistent improvement which made models' approximation acceptable. The NUPBS surfaces used in the present study, having a G^1 continuity in almost all parts of the model, gave an already smoothed luminal surface (by definition of NUPBS), which, coupled with the G^1 order imposed to the backbone splines, granted a smooth and realistic luminal surface model. The final CAD model developed is shown on figure 3.6.

Finally, the literature was considered to model the aortic valve in order to compensate the

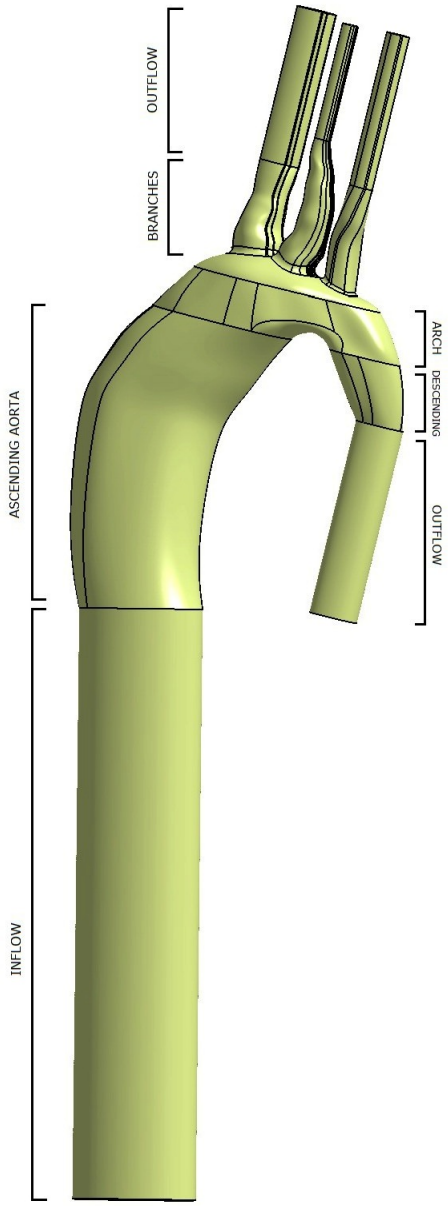

Figure 3.6: The final CAD model developed within CATIA is shown. Inflow and the four outflows are clearly visible. In black are the lines formed by the Surface Multi Section, in order to align points from different reconstructed surfaces.

lack of MRI information about valve orientation and morphology. Two articles, previously cited in CAD and CFD Modeling, mostly impacted the final shape of the valve. The important works by Vergara *et al.* (2012) about the influence of BAV geometry on the ascending aorta fluid dynamics and the study by Viscardi *et al.* (2010) on the finite element analysis of two BAV configurations relative to a normal valve, were taken into account. Then, our patient's non-stenotic second type of bicuspid valve was modeled similarly to the B1 configuration

proposed in Vergara's study (figure 3.7).

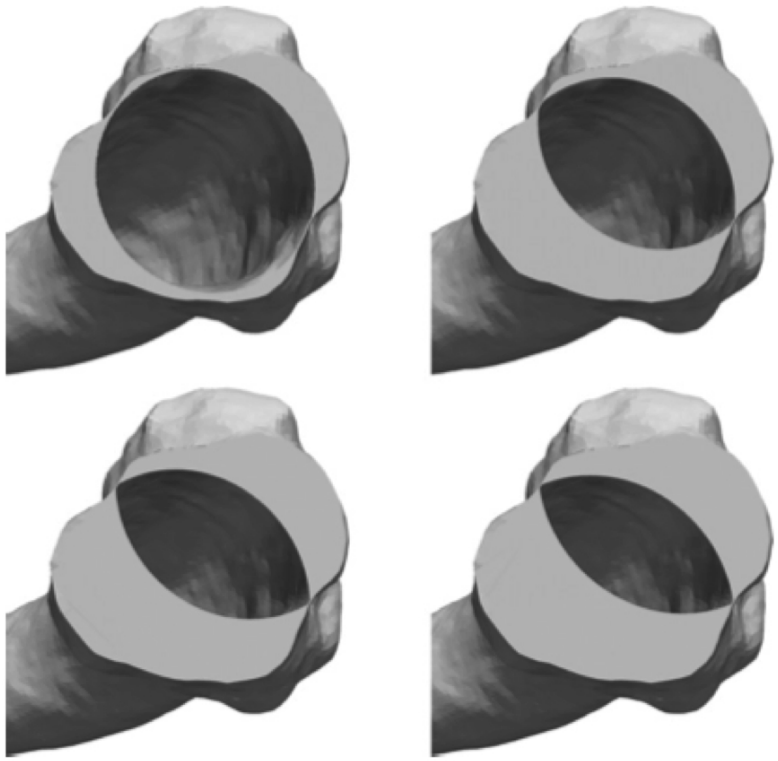

Figure 3.7: The four valves proposed by Vergara, clockwise from the top left, a physiologic tricuspid aortic valve, the B1 configuration with a remaining area of 1.9 cm^2, the B3 and the B2, with a remaining area of 1.5 cm^2 and 1.2 cm^2, respectively.

This configuration left the largest sectional area (for a bicuspid aortic valve) and this decision was made considering our patient's valve was defined as barely bicuspid since the right coronary and the non coronary leaflets were only partially fused together as seen in figure 3.8.

3.4.3 Parameterization

After having created the backbone splines for the entire model, the splines were parameterized. In CATIA version 5, almost every part of the geometry can be parameterized : surfaces, splines, points. To reach our objectives, we aimed to control the aneurysmal diameter, which is determined by the splines in the correspondent aROI. Therefore, it was decided to parameterize splines. Unfortunately, CATIA does not give the explicit option of modifying the diameter of two or more closed splines, even if they are assembled in one object. As it was previously explained, splines are controlled by control points, which in our case are the

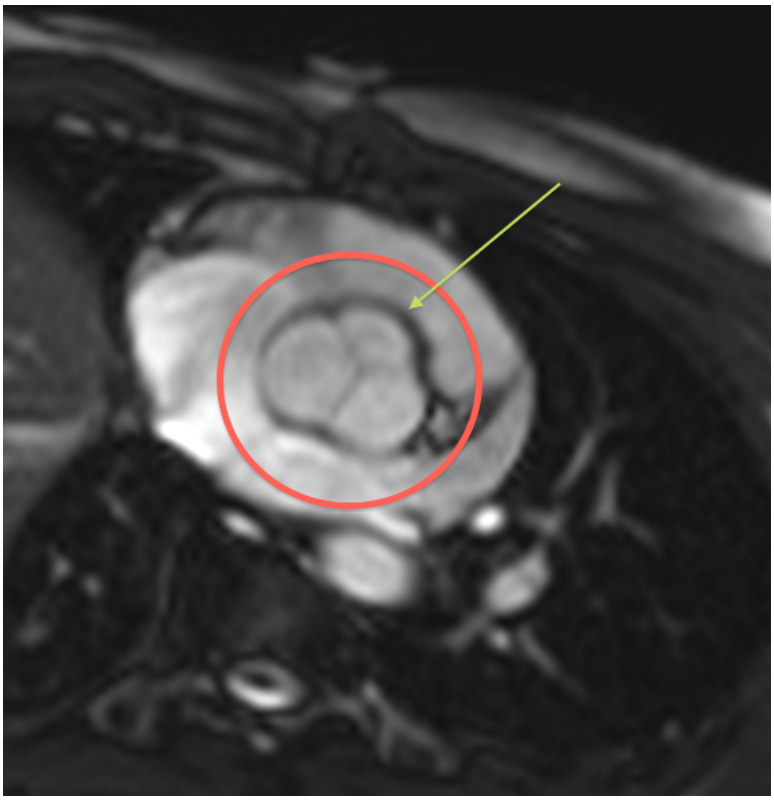

Figure 3.8: An MRI image of the selected patient in which it is possible to see the aortic valve (in the red circle). In the image, it is still possible to individuate the three leaflets, but the one pointed to by the green arrow is clearly smaller than the other two, suggesting a BAV case.

segmentation points. Controlling segmentation points means going back to the segmentation process which would be very time consuming. Instead, CATIA gives one the opportunity to control the distance between two consecutive control points of the same spline. Thus, starting from the original configuration (indicated by a certain ratio between points and curve), we imposed a percentage increase for all the points in a spline. This can be done in two different ways : by specifying the ratio between points and curves and increasing this number, or by imposing the length between two consecutive points, which does not allow one to impose a percentage increase. For this reason, the first method (imposing the ratio) was chosen. In CATIA, parameterization is handled in almost every workshop, from the Tools menu with the Expression option and then, by selecting parts of the model. We selected the spline to be modified and, from all the possible parametrizable parts, the control points were isolated. From the Add a Formula menu, the Points Construction option was selected, from which the two possible methods could be chosen. The *pointoncurveRatio* option was selected giving access to the ratio based method. Lastly, within the *pointoncurveRatio* function, the ratio

expansion percentage was imposed. We repeated this operation for all the splines that had to be parameterize. In CATIA's main screen, it is then possible to change the percentage value without repeating the entire process.

3.5 MESH Generation

The CAD volume aorta model developed represents a non discretized rigid 3D domain. The said domain is not directly exploitable for CFD simulation given the non-finite domain characteristics of the CAD volume. CFD softwares, in fact, require a discretized domain to accomplish the numerical methods employed to compute flow simulations. It is the reason why these types of numerical methods are called the finite volumes method and, most famously, the Finite Elements Method (*FEM*). FEM is based on the discretization of the Partial Differential Equations (*PDEs*) by dividing the domain into finite subregions, which, at the beginning, were triangular shaped (because the tetrahedron is the easiest tridimensional shape possible). Years later, the finite tetrahedron's domain was enriched with new possible shapes such as prisms, pyramids and cubes, which are able to better discretize certain cases in the non-finite domain. This process, to subdivide a continuous domain into a finite number of well known geometrical elements, is commonly called the meshing process and produces the mesh. The said mesh is a representation of a domain as a set of vertices, edges, faces and volumes which, all together, form a polyhedral finite domain. In nature, mesh-like structures are everywhere, figure 3.9 illustrates some well-known examples. When using FEM, mesh generation is without a doubt one of the most critical steps, especially if the domain to be meshed shows geometrical complexities such as extrusions, irregular curves, absence of symmetry, already known sub-geometries, *etc.* Oftentimes, in the biomedical environment, natural geometries do not offer symmetries and, frequently, approximating regions of the domain signifies not catching the phenomenon or missing related phenomena which carry a certain weight in the comprehension of the problem. Meshing human parts often implies the manipulation of highly variable diameters, thicknesses, bifurcations and even trifurcations, all features that can yield a lengthy meshing process.

The most critical aspect in any mesh generating process is associated with a general concept widely recognized in FEM oriented problems, which advocates the fundamental importance of a very good mesh. This imperative concept asserts the indispensable need of a meshing process otherwise jeopardizing all previous and subsequent numerical simulations, eliminating any effort done upstream and downstream to approximate the phenomenon.

In the present work, three different meshes have been generated from the same imported CAD geometry file. The meshes were created starting with the CAD model described in the

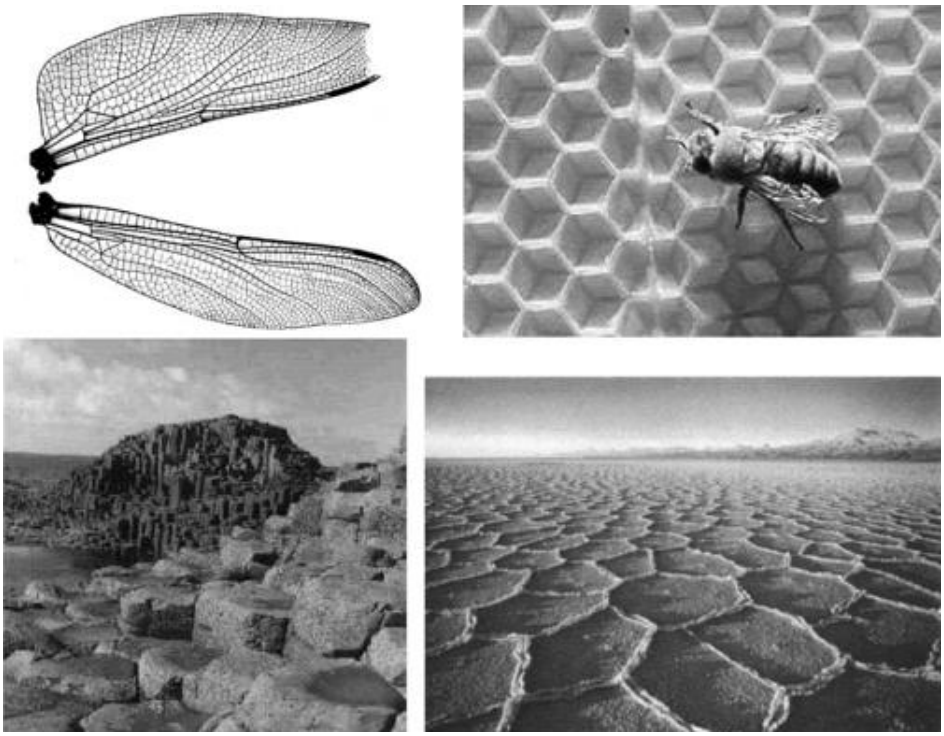

Figure 3.9: Examples of mesh like structures. Clockwise from the top left, the wings of a dragonfly, an alveolar structure then, two examples of an arrangement in nature, a basaltic rock site and a desert area. Adapted from Frey et George (2010)

previous section CAD Model. In CATIA, a binary STL file was generated and then imported into ICEM CFD (Ansys, Canonsburg, Pennsylvania), the elected software in the Ansys panorama to achieve meshes. The .stl format uses triangles to approximate the CAD model surface, similar to the way a mosaic is built. This format was chosen because, within CATIA, it is possible to adjust the quality of the volume triangles which discretize the model (.stl is a surface and not a volume rendering format) and also because CATIA possesses various powerful tools to check the generated .stl file. With these tools, namely *Mesh Smoothing*, *Mesh Cleaning* and *Fill Holes*, it is possible to ameliorate the triangulated surface or to determine whether the STL surface is completely closed, which is not always obvious when reconstructing parts from a cloud of points.

ICEM CFD can generate any type of mesh from the classical tetra-prism to the unstructured or structured hexahedral type. The three meshes generated are : a full hexahedral mesh of 157226 elements and 145008 nodes (mesh A), an hybrid hexahedral-tetrahedral mesh of 588567 elements and 146936 nodes (mesh B) and a mixed hexahedral, tetrahedral and prismatic mesh of 828176 elements and 302968 nodes (mesh C). For all three meshes, after having imported the .stl file, the model was arranged to represent the problem, therefore one inflow

and four outflows were created. The smallest diameter of the model was measured into ICEM CFD to better estimate the maximum size of one finite element. Three meshes were generated because the literature is still ambiguous with regards to the better mesh between the general unstructured tetrahedral mesh (Liu *et al.*, 2004), (Ito *et al.*, 2006) and the structured hexahedral mesh (Biswas et Strawn, 1998), (Van de Vosse *et al.*, 2003), when treating the cardiovascular domain.

3.5.1 Mesh A

Mesh A was the most difficult to accomplish due to two principal factors : the irregularity of the model's geometry and the author's lack of experience. The continuous changes in diameter and direction of the structure and the presence of trifurcations constituted a challenge when creating the typical blocks of a structured hexahedral mesh. A total of 462 structured blocks were necessary to cover the entire geometry. To better handle the blocks construction, the geometry was split into five sub-parts. For each part, non-cardinal beta splines were created in order to extract reference curves from the geometry. The beta splines were not cardinal, which means that the construction points are not equidistant from one another because ICEM CFD currently lacks the tool to create equally spaced curves. To improve the quality of the reference splines, they were projected onto the geometry, thus creating the best approximating curve, as seen in figure 3.10. Beginning from this type of curve, blocks were built using a top-down method. In short, the top down method consists of arranging blocks in the geometry by iteratively splitting blocks into smaller ones until the blocks fit perfectly in the geometry. The top down method was used to generate blocks for the entire geometry except the branches for which an extrusion method was preferred. This method in essence extracts blocks from other block faces, sharing one face with the initial block and maintaining its same shape.

Once the whole geometry was covered by blocks, various built-in tools were used to align, with respect to the geometry, the nodes and adjust node distribution in all critical edges of the structure. These two delicate operations are absolutely fundamental in obtaining the least amount of errors when carrying out the global mesh check. In particular, post processing nodes when handling a hexahedral mesh can avoid surface and volume orientation errors. The latter are the most critical errors, notably causing Fluent not to load the mesh ; they are easy to recognize because the hexahedral elements, when isolated, have almost no volume, resembling a bi-dimensional square rather than a three-dimensional hexahedron. In figure 3.11, several volume errors encountered when building mesh A are shown.

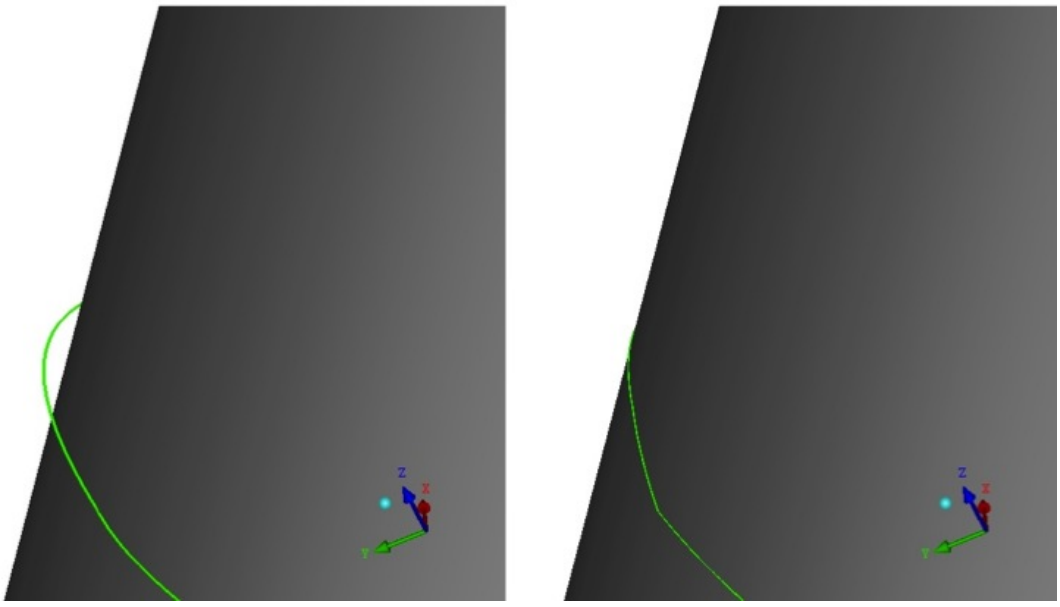

Figure 3.10: Left : the green curve not yet projected. Right : the projected curve. It is interesting to notice the difference between the two curves when approximating the surface.

3.5.2 Mesh B

Mesh B is a hybrid mesh meaning it has two (or more) different types of elements which are not mixed together in the geometry. More specifically, mesh B is organized into two large meshes which rely on two geometries obtained by splitting the CAD model. The initial geometry includes the inflow and the aneurysm while the second includes the remaining geometry. For the inflow and the aneurysm, considering that a hexahedral mesh gives better results in terms of WSS (Prakash et Ethier, 2001), (De Santis *et al.*, 2010), (Biswas et Strawn, 1998), a structured mesh (as for mesh A) was chosen.

The main difference between mesh A and B is that, for the latter, an additional step was taken after having created the blocks. In fact, mesh B was provided with an *O-Grid* structure. The O-Grid is a peculiar feature of the structured mesh, which is realized by extracting a sub-block from every block previously built. This structure is particularly efficient in cylindrical geometries for which it is possible to orient the O-Grid blocks in the (expected) predominant direction of the fluid (Ferziger et Perić, 1996), (Vinchurkar et Longest, 2008), that, in this case, is the flow ejected by the valve. Other types of Grid exist namely the C-Grid and the

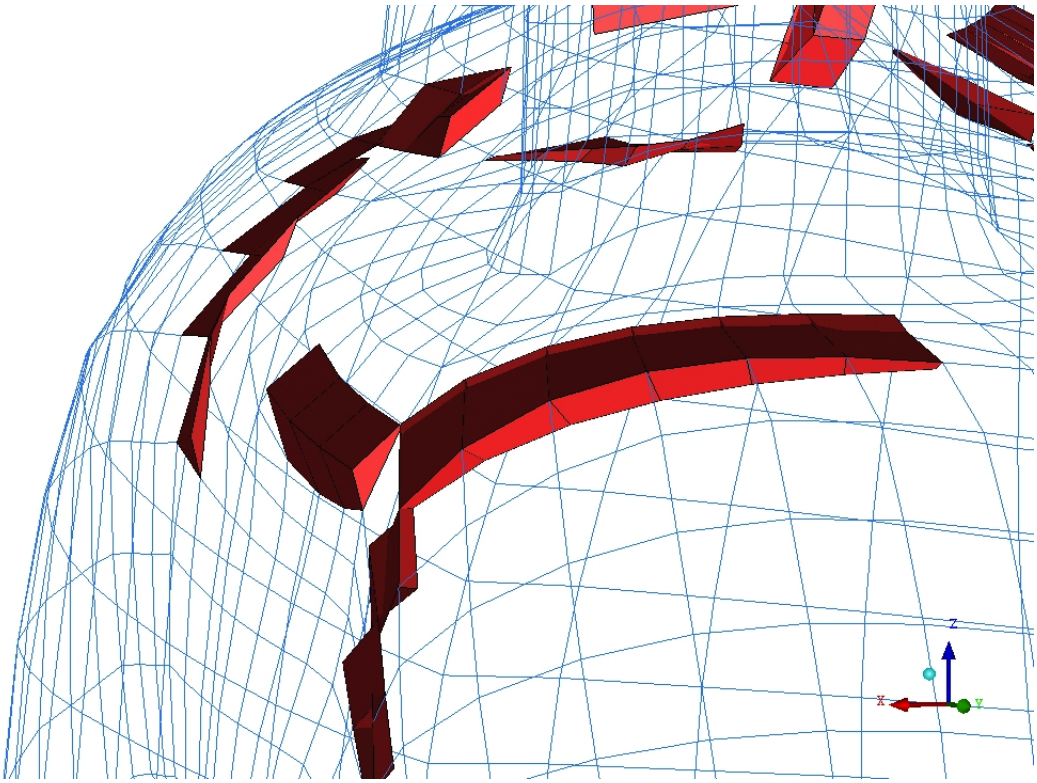

Figure 3.11: Part of the mesh structure with volume errors is highlighted (red). One can notice that they are elements without a real tridimensionality, which is why Fluent gives the error when importing the mesh. There is actually no other way, except to proceed manually, to adjust these errors.

H-Grid, which are fully supported by ICEM CFD. Conceiving an O-Grid mesh was possible seeing that the geometry, which mesh B relies on, is much simpler compared to mesh A.

In fact, as described above, mesh A was obtained with a top-down method (except for the branches), while mesh B was fully obtained with the extrusion technique starting with the inlet. These two techniques end up with a different number of blocks, which for mesh B is 20 and, for the correspondent part in mesh A, is 90. Conceiving an O-Grid mesh, as briefly explained, means building a block into another one, which corresponds to duplicating block numbers. If the structure has already a high number of blocks, as in the case of mesh A, building an O-Grid can be very time consuming and furthermore, can produce an exponential number of errors. With the dedicated function *Ogrid Block* in ICEM CFD, unstructured blocks were transformed into structured O-Grid blocks, as shown in figure 3.12. The second part of mesh B incorporates the aortic arch, the branches and the descending aorta with the relative outflows. The mesh generated in this part was Octree based. Without going into detail, the Octree algorithm is a semi-automatic mesh generating code that implements the

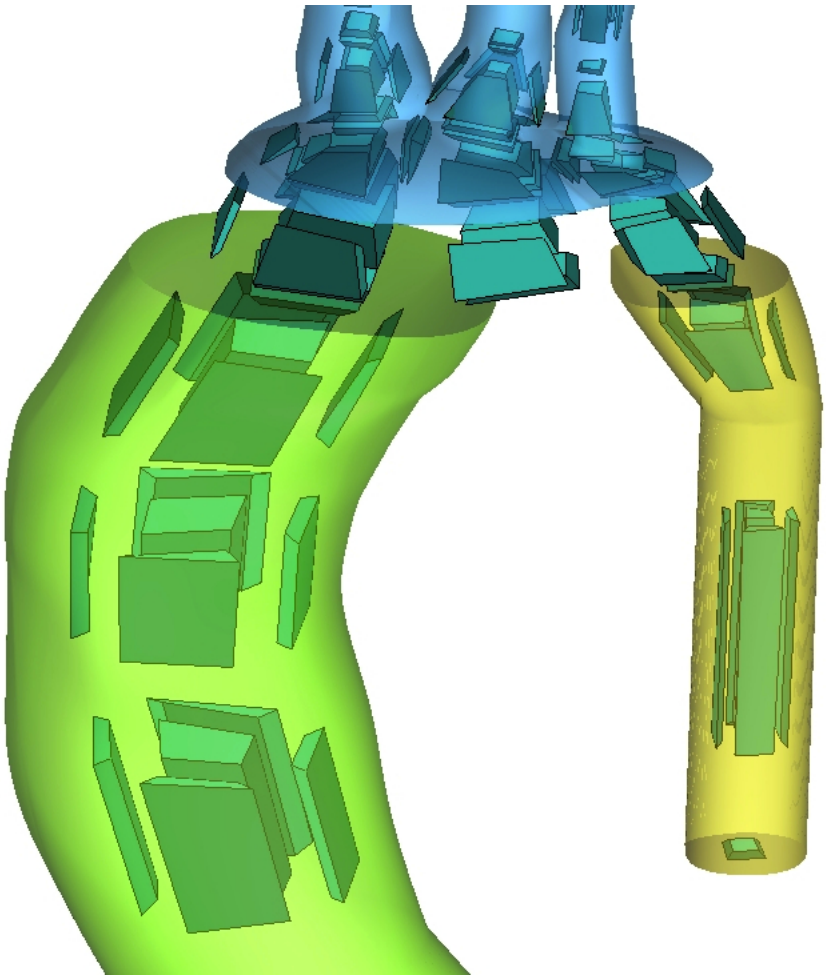

Figure 3.12: O-Grid blocks obtained while building the structured part of the mesh B. Actually, the structured part in which the O-Grid was performed is the green part (corresponding to the ascending aortic aneurysm) while, in the highest part, the blocks are automatically created by the software but are not implemented in the end. It is important to notice that every O-Grid block is made of five blocks : four represent the walls and the largest one, in the middle, discretizes the fluid.

mesh following a top-down method ; it was chosen because it is considered robust and it is widely used in the biomedical field (Zélicourt *et al.*, 2009), (Chiastra *et al.*, 2012), (Baker *et al.*, 2002). This technique, fully implemented in ICEM CFD, is relatively easy compared to the blocks technique, since it requires almost no user intervention on the geometry. A section of the Octree mesh can be seen in Mesh B. Usually, to better catch unstructured mesh deformation at the walls of cylindrical shaped geometries, a layer of prism elements is also generated at the interface between the tetra mesh and the geometry's wall. In the case of the second part of mesh B, no prisms were created because of the poor results these elements give when merged with hexahedral elements. In fact, the last step in mesh B generation consists

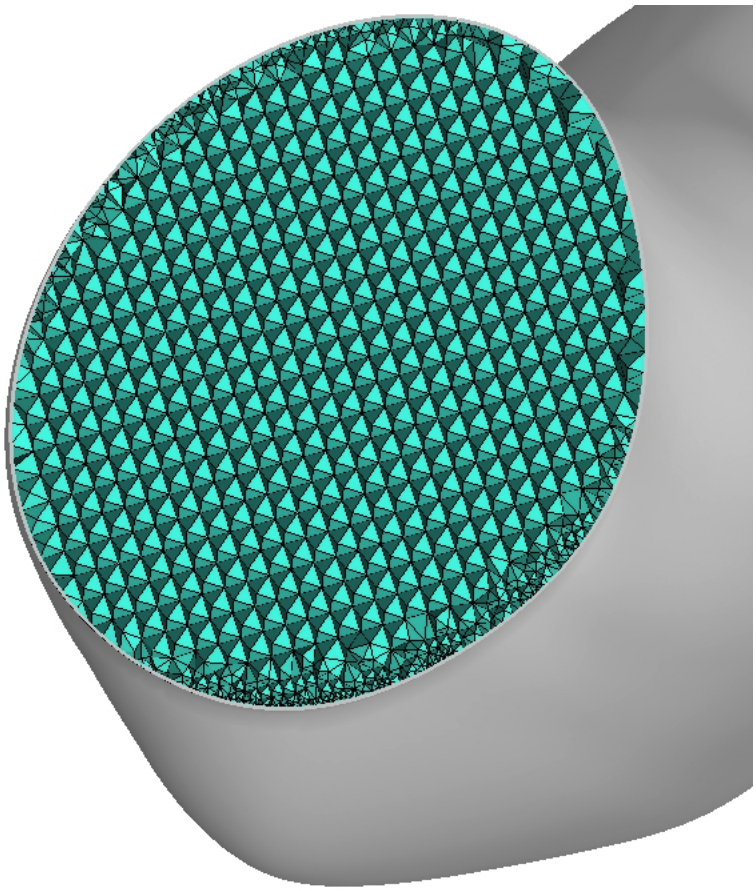

Figure 3.13: Section of the descending aorta, for mesh B. The classic square shape of the Octree elements is visible, then the mesh becomes more irregular while approaching the walls, due to the decreasing size of the tetrahedrons in order to better approximate the perimeter of the curve.

of merging the two meshes. This process was easily accomplished thanks to the function *Merge Meshes* implemented into ICEM CFD, which requires a common meshed interface as a surface where the two meshed volumes can merge.

3.5.2.1 Mesh B-1

From the same geometry as mesh B, mesh B-1 was generated. Mesh B-1 has the same features as mesh B : it is a mixed hexahedral structured and tetrahedral unstructured mesh with an O-Grid block scheme in the ascending aorta part. However, two main aspects distinguish mesh B from B-1. The first is the different geometry for the ascending part, used to build mesh B-1. The second is the different meshing of the aortic valve.

For mesh B-1, the parameterized ascending aorta geometry was loaded instead of the normal ascending dilated aorta. This is the first difference between mesh B-1 and mesh B.

Thus, for mesh B-1, the geometry loaded is an *ASCII* .stl file, similar to the other .stl files used, but with a diameter of about 25 mm, which is considered to be physiological. The advantage of splitting the CAD geometry in aROIs is evident : the mesh was generated only for the new geometry, the physiological ascending aorta. Nor the arch, the branches, the descending aorta or the inflow aROIs were involved in the mesh generation for mesh B-1.

Concerning the second big difference, the aortic valve modeling, the inflow CAD part was imported without the valve orifice at the interior, thus being a simple cylinder with the same aortic root diameter. Substantially, in mesh B-1 configuration, the aortic valve is not modeled. We considered that a physiologic aortic valve, when is opened, has a cross-sectional diameter equal to the aortic root. This configuration can be considered a good approximation of a physiological situation, in which the valve is tricuspid and the aorta's diameter ranges in the normal values.

The quality was assessed measuring orthogonality, skewness, aspect ratio and smoothness, as it was done for meshes A, B and C. The values for mesh B-1 were 0.59, 0.72, 0.66 and 0.5, respectively. Since these values are quite similar to the ones obtained with mesh B (see table 3.2), in addition to both meshes (B and B-1) being structurally comparable, it was decided not to perform neither a convergence nor a sensitivity analysis on mesh B-1.

3.5.3 Mesh C

Lastly, mesh C was obtained using three different kinds of elements : prisms, tetrahedrons and hexahedrons. Prisms were used to simulate the thickness of the aorta and the walls of the branches, hexahedrons were used to reduce computational time (notice that, as stated above, hexahedral like elements contribute, among the rest, to a drastic reduction in convergence time solving) and tetrahedrons were used to create a non-skewed interface between prisms and hexahedrons elements. The mesh was created following the Delaunay triangulation method. The Delaunay method is one of the three main approaches in which automatic mesh generation algorithms can be differentiated while the the other two are the cited Octree-based methods and the advancing front algorithms. Without claiming to be exhaustive, the Delaunay method was chosen instead of the Octree-based, since it offers both a better way of filling the volume and a smoother volume transition (when compared to the Octree-based method), but requires an Octree generation step beforehand. The Delaunay algorithm used by ICEM CFD (commonly known as Quick Delaunay) generates a tetra mesh using a bottom-up meshing approach. The first mesh generated was a surface mesh in order to better perform the prism layer. Then, a refinement was done before generating the Octree mesh. A second refinement was accomplished and the Delaunay mesh was finally obtained. In figure 3.14, a section of mesh C is shown.

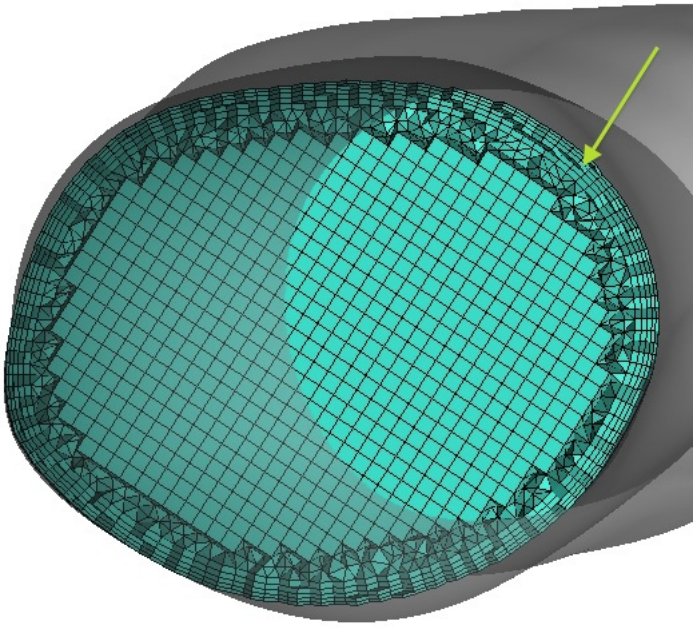

Figure 3.14: A section of mesh C where the three different elements are clearly visible. In the innermost part, the hexahedral elements discretizes the fluid, the outermost part represents the prism layer which discretizes the walls (pointed to by the green arrow). Between these two elements, a layer of tetrahedral and pyramid elements is automatically created by ICEM CFD to better couple hexahedrals and prisms.

3.5.4 Mesh Quality

When assessing mesh quality, four important parameters have to be monitored in order to obtain a better mesh convergence and to save time during the mesh validation process. These four parameters are : orthogonality, skewness, aspect ratio and smoothness. Orthogonality and skewness are respectively defined as the angle which every face of one single finite polygon forms with the immediately adjacent polygon and as the relative deviation from the common face center of two single finite adjacent polygons. The orthogonality value belongs to the Global Quality parameter. The orthogonality and skewness parameters can be applied to all kinds of meshes, whereas the aspect ratio and smoothness are meaningless if applied to the unstructured tetra mesh. Aspect ratio, in fact, is defined as the visible difference between the length and the height in one cell (then should be a prismatic or a hexahedral cell) while smoothness gives an idea of the expansion rate of the mesh as it accounts for the geometrical uniformity between contiguous cells. In a tetra mesh, this latter parameter exists, but looses value when compared with orthogonality and skewness. For the three meshes implemented in this work, the values of orthogonality, skewness, aspect ratio and smoothness are listed in table 3.2. The three meshes A, B and C can be seen in figures 3.15, 3.16 and 3.17, respectively.

Table 3.2: Average values for the quality parameters of the three meshes calculated within ICEM CFD. The Orthogonality is not displayed because it is integrated into the Global Quality parameter. This parameter ranges from 0 to 1, good values are under 0.7. Skewness good values are under 0.8. Aspect Ratio ranges from 0 to 1, good values are under 0.7. Smoothness ranges from 0 to 1, good values are under 0.8.

Quality Parameters	Mesh A	Mesh B	Mesh C
Global Quality	0.84	0.59	0.71
Skewness	0.86	0.71	0.86
Aspect Ratio	0.43	0.66	*none*
Smoothness	0.64	0.50	*none*

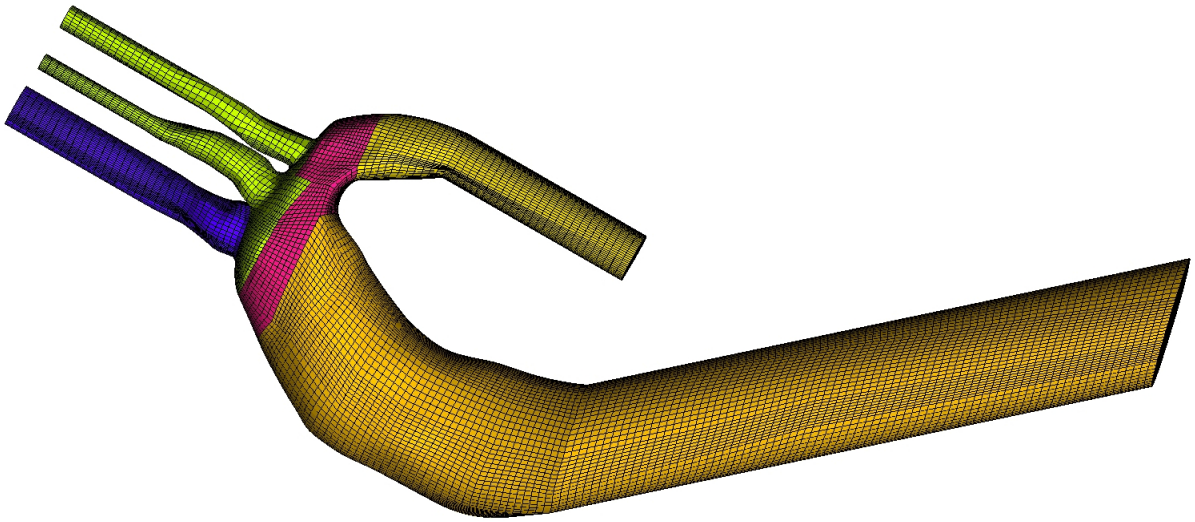

Figure 3.15: All the parts composing mesh A are clearly visible in the figure. The arch, in red, was the most difficult part to mesh, due to the presence on the top of the branches, which caused n-furcations and changes in diameter and direction.

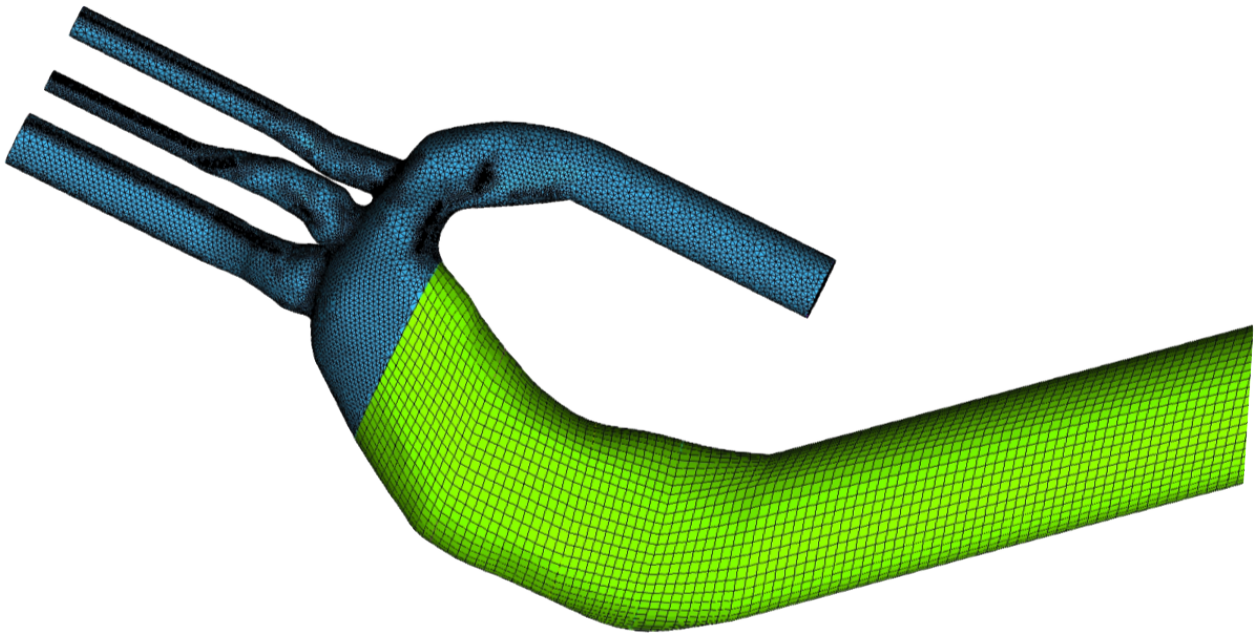

Figure 3.16: The two colors were chosen for mesh B in order to fully appreciate the difference between the two meshes (hexahedral in green and tetrahedral in blue) at the beginning of the aortic arch.

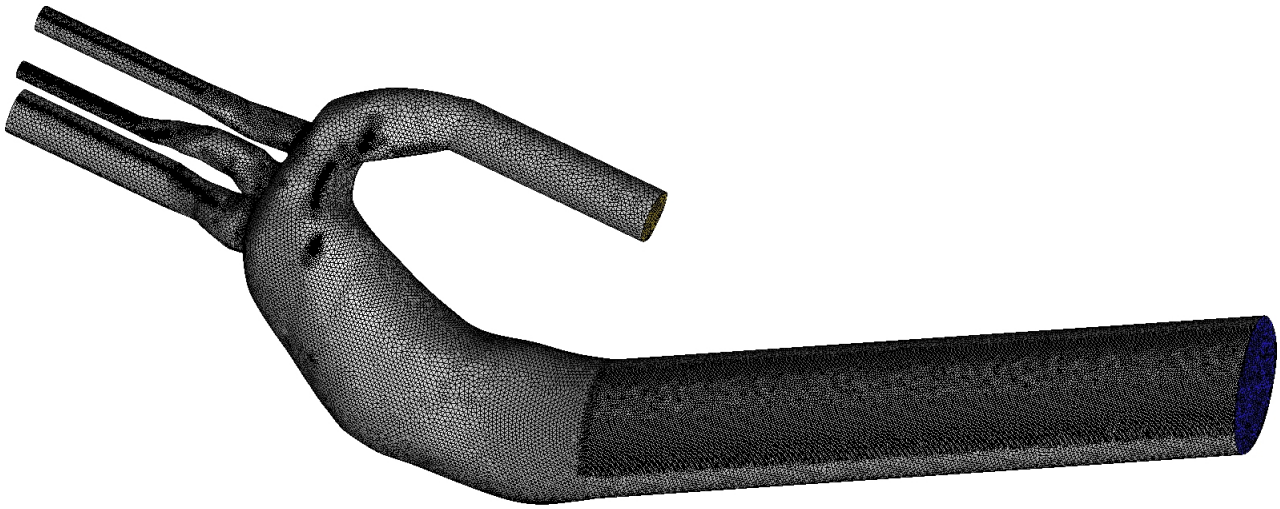

Figure 3.17: Mesh C, a fully unstructured mesh. The black parts suggest an augmented density of the tetrahedral elements due to particular changes in shape, for example, or due to irregularities in the geometry. They do not affect the results.

3.6 CFD Analysis

Computational fluid dynamics is probably the largest branch of Finite Elements Analysis (*FEA*), which is a part of the finite element method. FEA indicates a general analysis which uses a meshed domain such as mechanical structural stress analysis (eg. the interaction between a pedicle screw and a vertebra), heat transfer, acoustics problems and, indubitably, CFD analysis. The latter is the description of a fluid system produced by transforming, with powerful computers, the PDEs which govern fluid dynamics, into finite numbers in order to give a quantitative description of a complex problem. Evidently, describing the reality of complex problems is accomplished by high-performance computer technology, which has grown in the last two decades. Thanks to this technology, today CFD analysis can be viewed as the perfect complement when approaching a problem with an engineering perspective, being the middle ground between pure theory and laboratory experiment. As part of FEA, CFD uses finite elements to obtain a discrete solution of the governing equations of fluids. These equations are derived from the classical principles of physics applied to fluids (conservation of mass, conservation of momentum and conservation of energy) and are typically described in PDEs systems. In a finite elements approach, the continuous governing equations are applied to a finite volume, under certain conditions, which discretize the continuous domain. In this fashion, the PDEs systems are not resolved but are integrated, hence the solution is in integral form and not the solution of the PDEs in itself (which is quite impossible considering the continuous nature of these equations). In this project, the FEM was used to obtain the integral form of the PDEs. The FEM is often applied to CFD analysis as a method to resolve Navier-Stokes equations (PDEs) by approximating the solution with the Galërkin method. The latter is one of the most famous mathematical procedures, which turns a generic problem defined in a continuous domain into an integral form. It could be stated that the FEM is based on the Galërkin discretization. The error made while approximating the continuous solution into a discretized one using the Galërkin method is very poor. In fact, the Galërkin method substantially divides the continuous space, where the initial problem is defined, into a finite set of functional subspaces and the approximation error, which arises from this procedure, is orthogonal to the functional subspace leading to the best approximation possible for a given subspace. Converting this statement to FEM and, consequently to CFD, means not only will the discretized solution be precise (if the initial problem is well posed), but the Galërkin solution will converge in the discretized domain.

3.6.1 Boundary Conditions Overview

In CFD analysis, in order to obtain the convergence of the solution or, more generally, to better describe the problem, a number of conditions must be set. These conditions, namely boundary conditions, are fundamental in the definition of a CFD problem. They can be applied anywhere in the finite domain, but are usually applied to the contours, to the inlet and to the outlet of the model. Boundary conditions absolve the role of setting up the fluid dynamics problem, which in the case of vascular domain implies establishing quantities such as blood flow or velocity profile, pressure gradient, vessel wall conditions and several others. By describing the physics of the domain, these quantities lead the solution in the right direction, validating in a non-formal manner, the modeling work previously done.

At this stage, it is clear that the boundary conditions play a fundamental role in a CFD evaluation and, more generally, in the whole modeling process. Several works attempted to prescribe different boundary conditions in various vascular districts, such as the innovative work of Perktold *et al.* (1997) on a common carotid model where the velocity profile boundary conditions were imposed on both the inlet and the outlet ; Formaggia *et al.* (2002) demonstrated a method which intends to consider a set of boundary conditions valid (and so to maintain the problem well-posed), which he named defective boundary conditions, suggested by medical data obtained with non-invasive techniques such as doppler or magnetic resonance techniques.

The name defective is quite appropriate, referring to boundary conditions derived from average values published in literature, which for a patient-specific case or a small collection of patient-specific cases can be very limiting. Fluctuations of physiological and pathological data are indeed responsible for significant variations of quantities just as for flow rates, heart beat, pressure, *etc.* (Steinman, 2002). Even if these variations can be statistically determined for a large group of patients or normalized with indices, literature still lacks several pathological cases and, with regards to small groups of patients, certain values relative to the vascular domain cannot be fully supplied with averaged data. However, when imposing boundary conditions (and in many other possible examples), one should look at the phenomenon being investigated. Let us propose an example related to this thesis : even in a patient-specific case, if the research is more focused on finding specific values, which depend on particular conditions such as a local deformation, rather than absolute values describing the behavior of a human body part, average boundary conditions can be still used. Obviously, certain considerations should be made in order to make the findings consistent with the global fluid dynamics of the studied area.

Being a patient-specific case evaluation where values of WSS and blood velocity in a specific region were investigated, the model presented in this article should be coupled with

boundary conditions derived from magnetic resonance acquisitions data. Unfortunately, these data were not available for the selected patient and, among the 21 patients from the last selection, hemodynamics data were accessible for only seven patients. Moreover, looking at the statistical data of these seven patients, none were comparable with the selected patient (looking at the clinical panorama, at the BSA and at the z-score), which impedes the selection of similar data to apply to the case.

3.6.2 Applied Boundary Conditions

In order to provide valid boundary conditions for the model, the medical report of the selected patient was investigated. In this report, the left ventricle's functionality was described as normal and the hemodynamic values were in the physiological range. For this reason, data for pressure and blood flow rate were taken from literature. More specifically, the famous study by Ku (1997) concerning blood flow in arteries was coupled with Warren *et al.* (2006)'s findings to build the pressure outlet waveform, and with the study by Poutanen *et al.* (2003) to obtain blood velocity reference values in order to build the cardiac output waveform prescribed as the inlet boundary condition. The pressure waveform obtained, was prescribed as the outlet boundary condition in all the four outlets of the model. The resulting waveforms are shown in figures 3.18 and 3.19. A cardiac cycle of 0.8 s was assumed, which corresponds

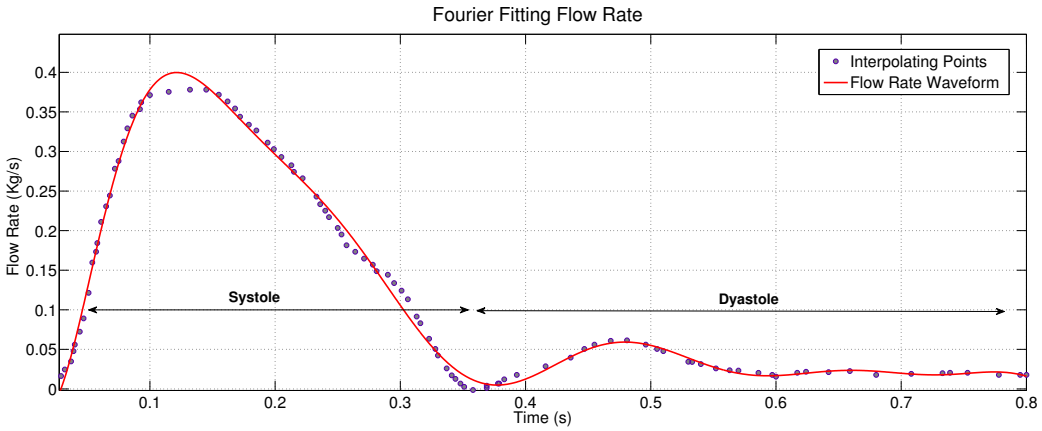

Figure 3.18: The flow rate fitting obtained with the software Matlab. The approximation is made at a 95% of confidence level.

to an average frequency of 0.75 bpm. The inlet flow rate waveform has a systole (first 0.35 s) to diastole (the remaining 0.45 s) ratio over than 1 : 1, that is considered physiological by the studies cited above. In order to translate the mass flow and the pressure waveform into a Fluent-friendly form, a function describing the two waveforms was written. In fact,

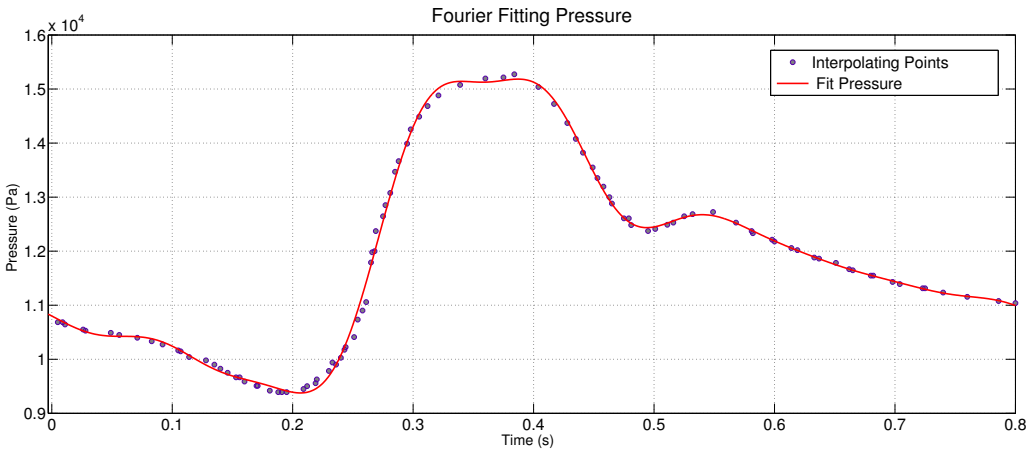

Figure 3.19: The pressure fitting obtained with the software Matlab. The approximation is made at a 95% of confidence level.

Fluent allows the user to write functions (often in C code) that can better set the problem in hand. These functions are called User Defined Functions (*UDFs*) and represent one of the most powerful tools in Fluent. The mass flow and pressure waveforms were therefore firstly converted to a mathematical function which approximates the wave trend and then translated to C code. Two different functions in the same UDF were written and hooked in Fluent.

As it is expected for the ascending aorta walls to be subjected to larger stresses when the blood flow has the greatest component of velocity and the vessels experience the highest pressure variation, we were particularly interested in changes that affect vessel walls during the systole. Consequently, aorta walls were modeled as rigid and impermeable even if it is known that arterial walls and even more aorta walls are compliant. However, in the book by Lighthill, concerning biofluid-dynamics (Lighthill, 1975) and in the numerical analysis on curved tubes by Berger *et al.* (1983), it is assessed that the fluid motion is barely influenced by wall compliance, even though the latter is primarily responsible for the pulse wave propagation and local pressure gradients. Furthermore, the relative motion of the ascending wall being attached to a moving entity (heart) was not considered in the CFD analysis. Presently, there is no sufficient proof in literature to determine an important cause-effect relation to hemodynamics due to the link between the aorta walls and the beating heart. Blood was assumed as a Newtonian fluid (which is a valid approximation for large vessels, (Perktold et Rappitsch, 1995)), incompressible, isothermal and homogeneous, with a density of ρ =1000 Kg/m and a constant viscosity of μ_N=0.0035 Kg/ms^{-1} (Antiga *et al.*, 2008). Under these assumptions and neglecting the effect of gravity, two conservation equations govern the fluid

dynamics of the region of the aorta : the conservation of mass and the conservation of momentum equations. Therefore, the fluid dynamics problem can be described as the combination of these two equations :

$$\begin{cases} \rho\left\{\left(\dfrac{\partial v_i}{\partial t}\right) + v_i\dfrac{\partial v_i}{\partial x} + v_j\dfrac{\partial v_j}{\partial y} + v_k\dfrac{\partial v_k}{\partial z}\right\} = F_i - \dfrac{\partial p}{\partial x_i} + \mu_N\nabla^2 v_i \\ \\ \dfrac{\partial \rho}{\partial t} + \rho\nabla\cdot\boldsymbol{v} = 0 \end{cases}$$

The second equation is the conservation of mass (mass continuity equation), which, considering the assumption of constant density (dealing with incompressible flow), leads to

$$\nabla\cdot\boldsymbol{v} = 0$$

This is Euler's popular conservation of mass equation where $\boldsymbol{v}$ = flow velocity (be reminded that speed is a scalar quantity while velocity indicates a vector quantity) and ∇ is the divergence operator. Euler's conservation of mass equation is an abridged form of the corresponding Navier-Stokes equation, having simplified the derivative term $\frac{\partial\rho}{\partial t}$ which involves density (ρ) changes over time and having assumed the fluid to be isothermal. The first equation is the three-dimensional Navier-Stokes equation where it is possible to simplify the terms F_i (which takes into account the effect of general external forces) for the absence gravity effects assumption (which are the only external forces acting on the problem). The other terms are the p for the pressure of the fluid and μ_N where N indicates the fluid is Newtonian. In other words, performing a Navier-Stokes equations based fluid simulation means solving this system of two equations for every finite volume of which the tridimensional mesh of the aorta model is made. The study by Formaggia *et al.* (2009) proved the validity of mathematically describing the blood system using Navier-Stokes equations, under certain assumptions.

3.6.3 Fluent Settings

The software Fluent version 14.5 (Fluent, Canonsburg, Pennsylvania) was used to perform a CFD analysis. This software was chosen because of its widely known capacity to deal with fluid dynamics problems ranging from the molecular (eg. drug delivery systems analysis) to the supersonic field (eg. in aeronautic simulation). Moreover, Fluent is now a part of the Ansys suite and is perfectly integrated with ICEM CFD and the Ansys WorkBench environment, in which part of this thesis was made. Through Fluent, the boundary conditions discussed above were applied, namely, the inlet blood flow waveform and the outlet pressure waveform, the blood density, the Newtonian blood viscosity. Furthermore, the rigid aorta walls condition

discussed before eliminates both the absolute and the relative component of the blood velocity of every finite volume immediately adjacent to the wall. This evidence was translated in prescribing the no-slip boundary condition in all the walls of the model $v|_{y=0} = 0$, where v=fluid velocity and y is again the distance between fluid and the boundary.

The time step chosen in order to accomplish a transient (unsteady) laminar calculation on Fluent was set to 0.001 s and 30 iterations per time step were considered. Convergence was enforced by reducing the residual of the continuity equation by 10^{-5} at all time steps. Thanks to the inlet extension added, the initial flat flow at the inlet entrance, became parabolic (Poiseuille shape flow) before entering into the real model, allowing to consider that, at the real inlet, the blood flow was already fully developed. The aortic valve was modeled in Fluent with a simple on/off mechanism, as proposed by Faggiano *et al.* (2012), meaning that the intermediate steps between the valve being fully opened and fully closed weren't modeled. Due to this mechanism, the valve results as completely closed (off modality) at the end of the diastolic phase, in which no mass flow is prescribed while it results as completely opened during the rest of the cardiac cycle.

3.6.4 Blood Streamlines, Speed and WSS

Post-processing the CFD analysis allows one to collect the required data. In this study, two data are collected : the blood speed and the WSS distribution during one cardiac cycle. To post-process Fluent results, Ansys CFX-Post (Ansys, Canonsburg, Pennsylvania) was used into the Ansys WorkBench environment. Within this environment is possible to import and export data from a software to the other, in this case from Fluent to CFX-Post. Blood speed results are displayed during one cardiac cycle, thus considering the whole speed distribution along the model and in particular in the aneurysm. This is in line with literature.

In terms of WSS, the simple data from the whole CFD simulation were considered. These data are representative of the WSS distribution during the cardiac cycle. In other words, this means to collect the WSS maximum contribute during all the cardiac cycle. This is in contrast with literature, where often WSS results are showed for the peak systole ($WSS_{systole}$), considered as the moment in which the WSS contribute is the most relevant, likewise the WSS trend is plotted using indices as the Oscillatory Shear Index (OSI) or the WSS space and time averaged $WSS_{\theta,t}$.

Finally, within CFX-Post, the blood streamlines as long as the WSS distribution in the whole set of meshes are displayed. This software is particularly powerful when analyzing post-processing findings as it contains tools that help with the graphic comprehension of the results. The Clip Plane tool, which focused on the streamlines entering and exiting from one defined aortic section.

3.7 Corroboration Methods

In this subsection, methods to accomplish the corroboration for the segmentation step, the CAD modeling and the mesh generation are described.

3.7.1 Segmentation Errors

To evaluate errors made during aorta segmentation, a simple method based on measured distances was applied. This method consists of creating a set of points along the segmented profile and then take measurements between pairs of points, as in figure 3.20 (left). These measurements are then compared with measurements taken in the same slice, but for the original set of images, before being segmented, figure 3.20 (right). To measure points on

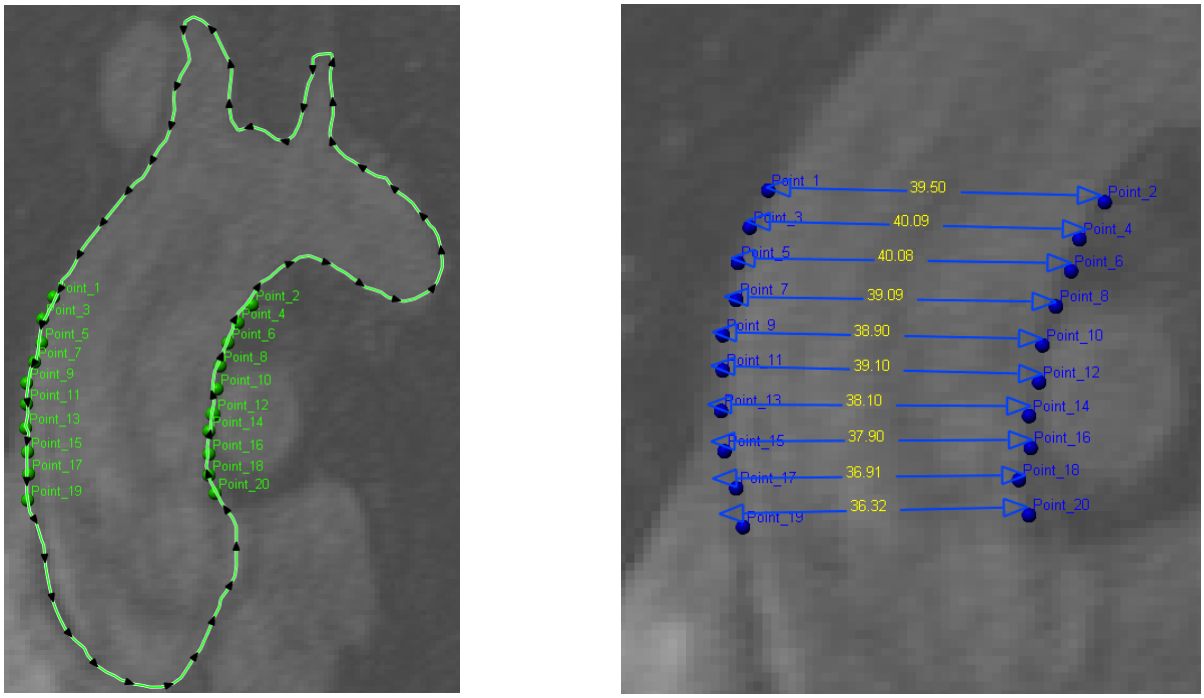

Figure 3.20: Left : Snake segmentation profile with the points used to take measurements. Right : For the same set of points, measures are taken. In Slice-O-Matic, different 2D measures can be taken within the feature Measurement in Modes.

the snake, the feature Point in the Tools was used and in particular, the 2D option was implemented. This option, gives the 2D coordinates of the points in a slice, thus allowing to collect distances between points. Then, the points were projected into the 3D reconstructed volume to obtain a better visualization on CATIA, figure 3.21.

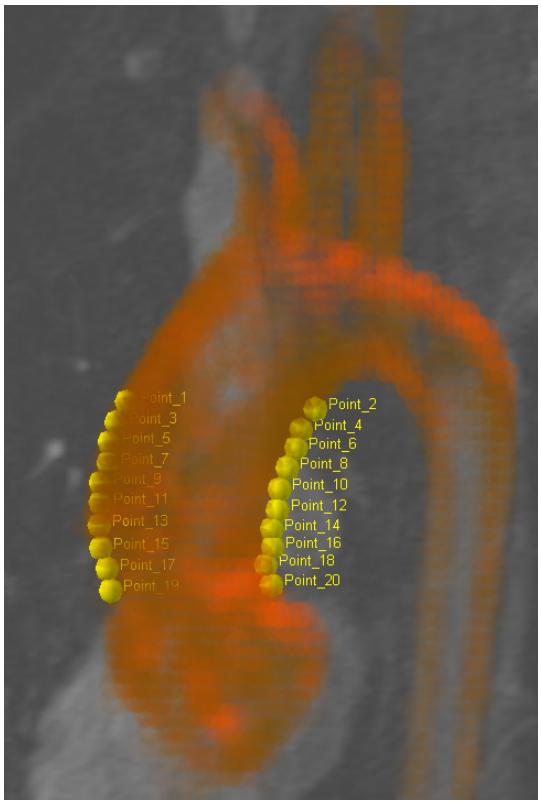

Figure 3.21: The rendered volume resulting from the segmentation, within the measurements points.

3.7.2 CAD Errors

Following the author's experience when assessing a patient-specific study, manual reconstruction techniques must be adopted, even if they could be time consuming. Moreover, part of the final result also depends on the CAD software used, because the precision of retro-engineering CAD techniques can vary (a lot) between one software and the next.

To quantify retro-engineering errors, the same approach used to evaluate segmentation errors was applied. From Slice-O-Matic, points were visually traced in a vertical line and then measurements were taken between pairs of points, as is showed in figure 3.22.

3.7.3 Mesh Errors

In section MESH Generation, the importance of generating a very good mesh was discussed. To assess the performance of each structure, two kinds of analyses were undertaken : mesh convergence and mesh sensitivity analysis. These two analyses are both based on the concept of establishing the independence of the CFD results over the mesh quality. In this particular case, quality is expressed by the smoothness of the mesh, in other words, by the

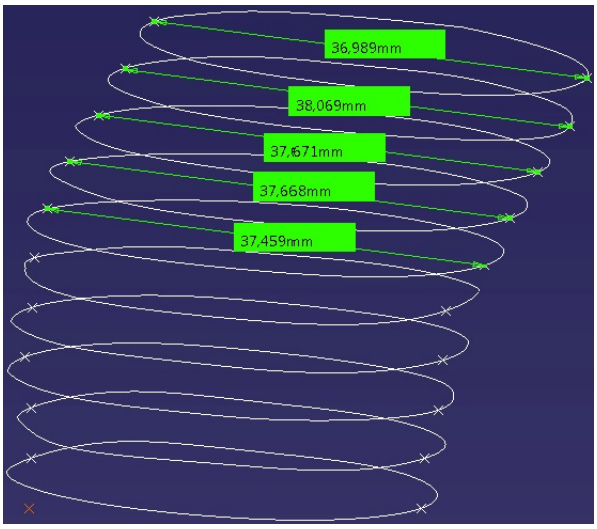

Figure 3.22: Measurements taken within CATIA. The measurements are show partially to make the image comprehensible.

number of elements which forms the mesh. Typically, such analyses are accomplished by incrementing the quality of the mesh, from a coarse to a very fine mesh. For our purposes, six different mesh configurations for meshes A, B and C were tested, for both the convergence and the sensitivity analysis.

The convergence analysis was done beginning with a very coarse mesh and incrementing the smoothness of the mesh by 25% for each further step, reaching 150% of augmented mesh density. This process needs to be done in two different ways, depending on the type of the mesh. Mesh density has to be handled in different ways, depending on the mesh structure. To be more specific, if the mesh is generated starting from a block schema, as for mesh A and for the hexahedral part of mesh B, the density has to be set for the edges of the blocks.

For an unstructured mesh like mesh C, density is determined by imposing the finite element maximum dimension in terms of various parameters such as height, width, etc. For a full or hybrid hexahedral (both structured and unstructured) mesh (mesh A and B), density is handled by ICEM CFD through the Pre-Mesh parameters panel, in different ways, the most precise one being the Edge Parameters option, which permits the selection of several parameters for regulating hexahedron distribution along one edge. In particular, the number of nodes and the spacing between them along one edge varied (in quantities proportional at 25%) for our tests.

For mesh C, density is handled by ICEM CFD with the Part Mesh Setup panel, in which it is possible to set dimensions for the single discrete element, even different for different part of the mesh. This is quite useful to save computing resources, if for example, the region where

the phenomenon varies the most is already known, instead of smoothing the whole mesh one can simply smooth only the interested region. The majority of the meshes converged after the first cardiac cycle (800 iterations per cardiac cycle, the solution is iterated 30 times).

For the sensitivity analysis, the value monitored was the maximum blood speed in the aneurysm region, at the end of one complete simulation (four cardiac cycles). Speed was chosen, instead of the most commonly used WSS (Prakash et Ethier, 2001), because it is already known from literature that WSS values strongly depend on the type of element, the results being more precise when dealing with a hexahedral mesh (De Santis *et al.*, 2010) rather than an unstructured mesh (typically tetrahedral).

CHAPTER 4

RESULTS

In this section, results from the CFD analysis of meshes A, B and C are presented. Furthermore, results from the non-pathological aortic model, generated using the parametric feature, are presented and a particular case concerning the WSS distribution is also shown. Moreover, results from the corroboration study are shown and discussed. All the simulations were produced with an Intel *Pentium* 7 based computer, with a CPU of 3.44 GHz and a RAM of 16 Gb.

4.1 CFD Results

The chosen meshes for the CFD analysis of blood velocity and wall shear stress were mesh A with 157226 elements, mesh B with 588567 elements, mesh C with 828176 elements and mesh B-1 with 559416 elements. Results of the blood velocity distribution for meshes A, B, C and B-1 are shown in figures 4.1 to 4.4. The blood velocity along with the WSS results for meshes A, B, C and B-1 of the aortic aneurysm, obtained from the CFD analysis, are shown in figures 4.5 to 4.8.

The WSS distribution for mesh B in the aneurysm differs from the WSS distribution seen in the other regions of mesh B due the two different techniques used when generating the mesh. As described in section MESH Generation, when assessing WSS distribution, the mesh type can vary results a lot. In general, tetra based meshes tend to overestimate WSS values resulting in a distribution that is not as realistic as the one obtained with hexahedral based meshes. Figure 4.9 shows the calculated WSS for the whole mesh B. Finally, table 4.1 helps visualizing results for mesh A, B, C and B-1.

Table 4.1: Blood speed and WSS maximum values for the whole set of meshes in the ascending aorta. Blood speed is in ms^{-1} and WSS in Pa. Mesh C tends to overestimate both the blood speed and the WSS results, while blood speed for the two structured pathological mesh A and B is the same.

	WSS	Blood Speed
Mesh A	37.2	1.2
Mesh B	38	1.2
Mesh C	39.2	1.4
Mesh B-1	8.6	0.61

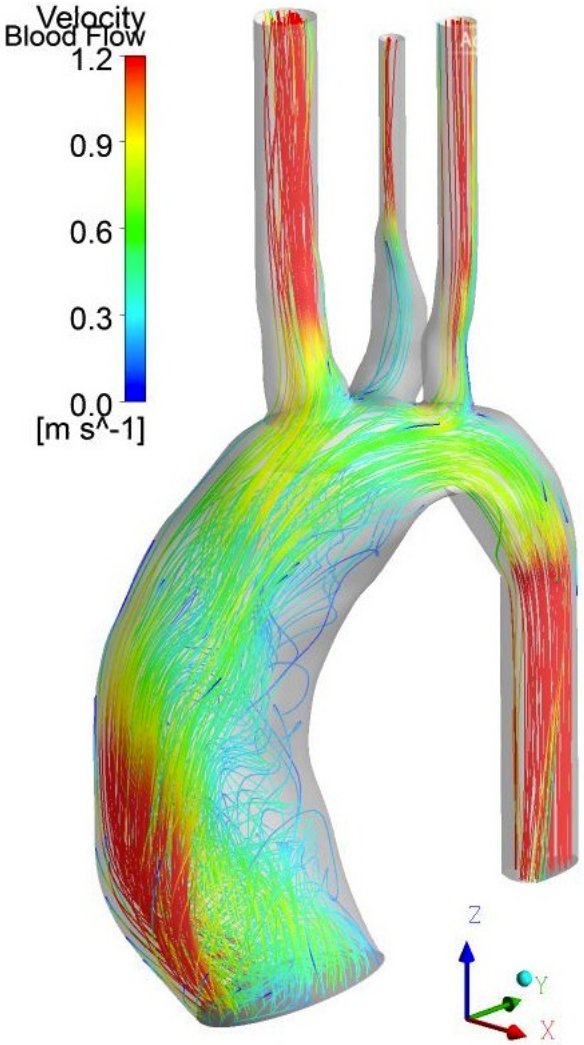

Figure 4.1: Mesh A blood streamlines in the whole model (except for the inflow). One can appreciate the blood jet which impacts the wall of the aneurysm at high speed.

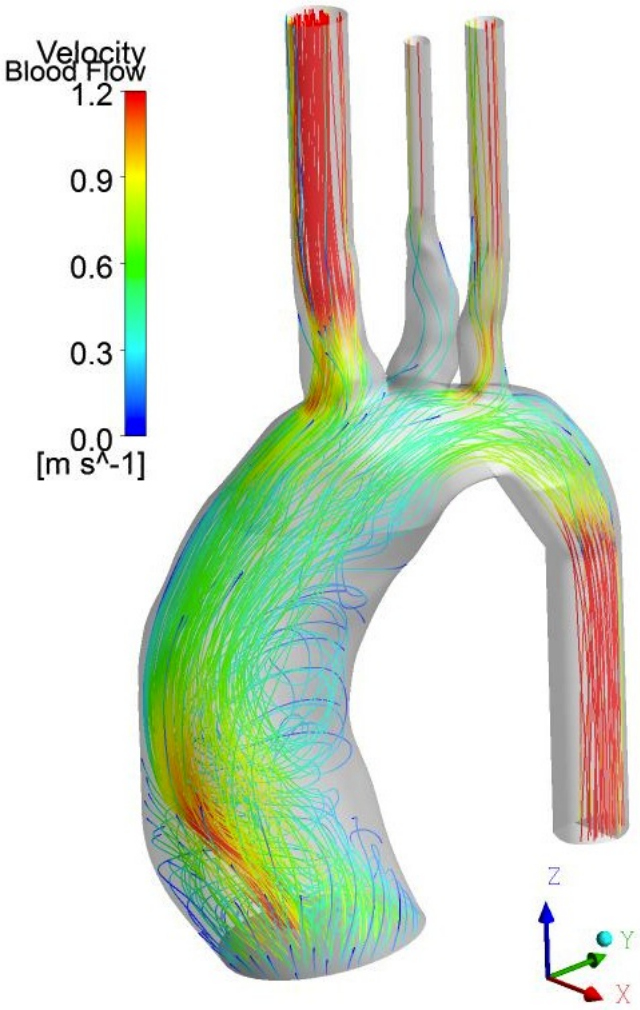

Figure 4.2: Mesh B blood streamlines in the whole model (except for the inflow). The blood jet impacting the wall of the aneurysm is even more visible than in mesh A.

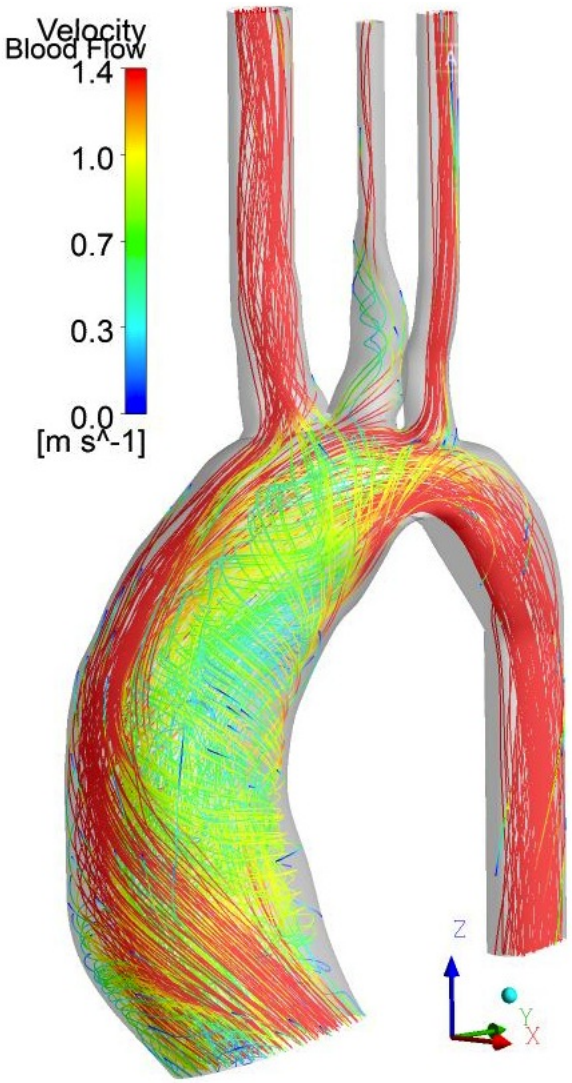

Figure 4.3: Mesh C blood streamlines in the whole model (except for the inflow). The values of blood speed are in general higher for mesh C compared to meshes A and B, for this reason, there are more red zones than in the other meshes.

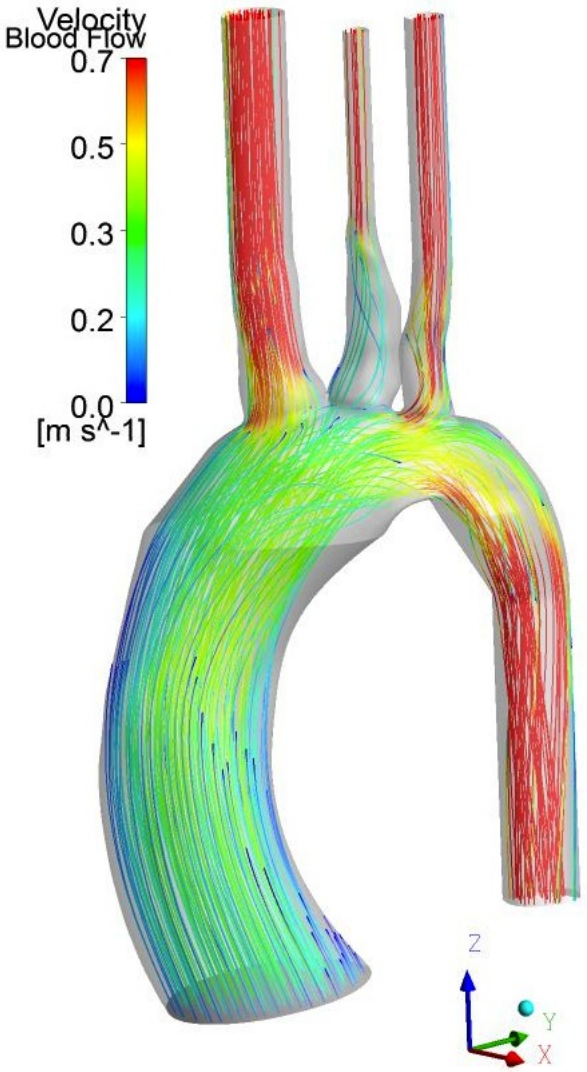

Figure 4.4: Mesh B-1 blood streamlines in the whole model (except for the inflow). In the physiological state, the blood jet does not have a major direction hitting the aneurysm, instead, blood is flowing with a principal direction along the z axis.

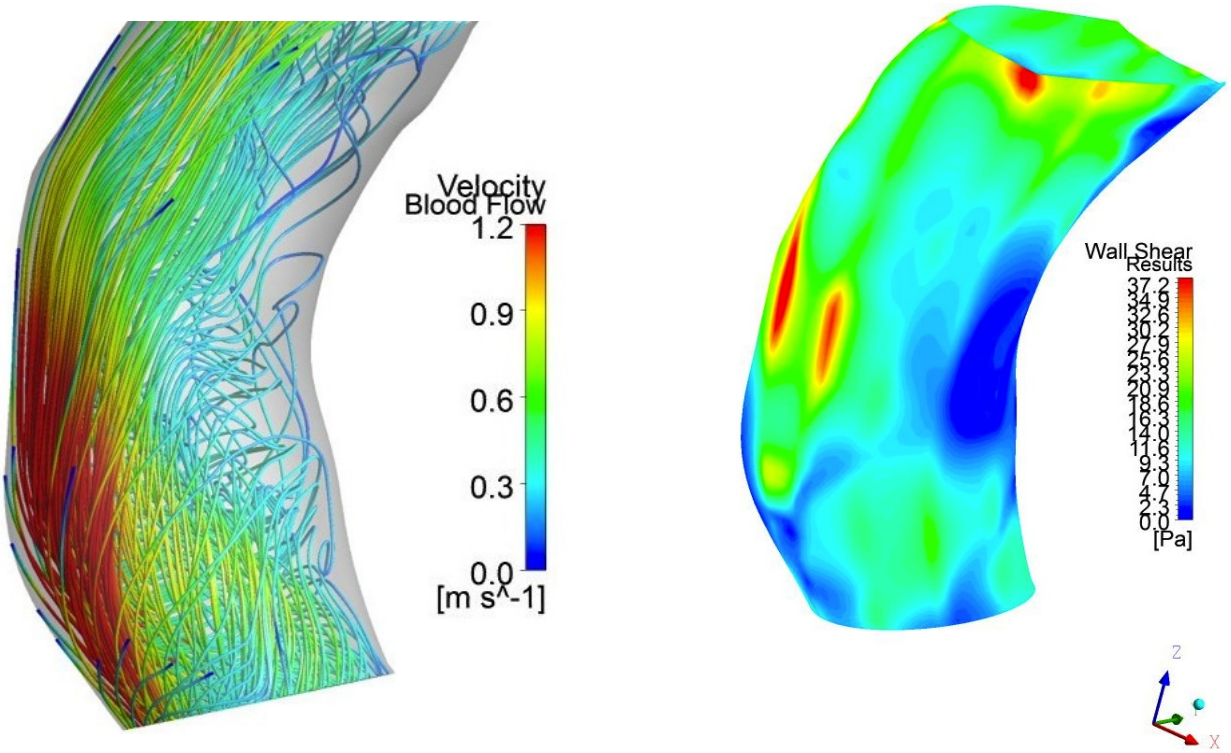

Figure 4.5: Left : Mesh A blood flow in the aneurysmal region. Right : Mesh A wall shear stress distribution in the aneurysm. It is evident that the region with the highest wall shear stress (in red) is the one impacted by the blood jet, which corresponds to the aneurysm's inner wall.

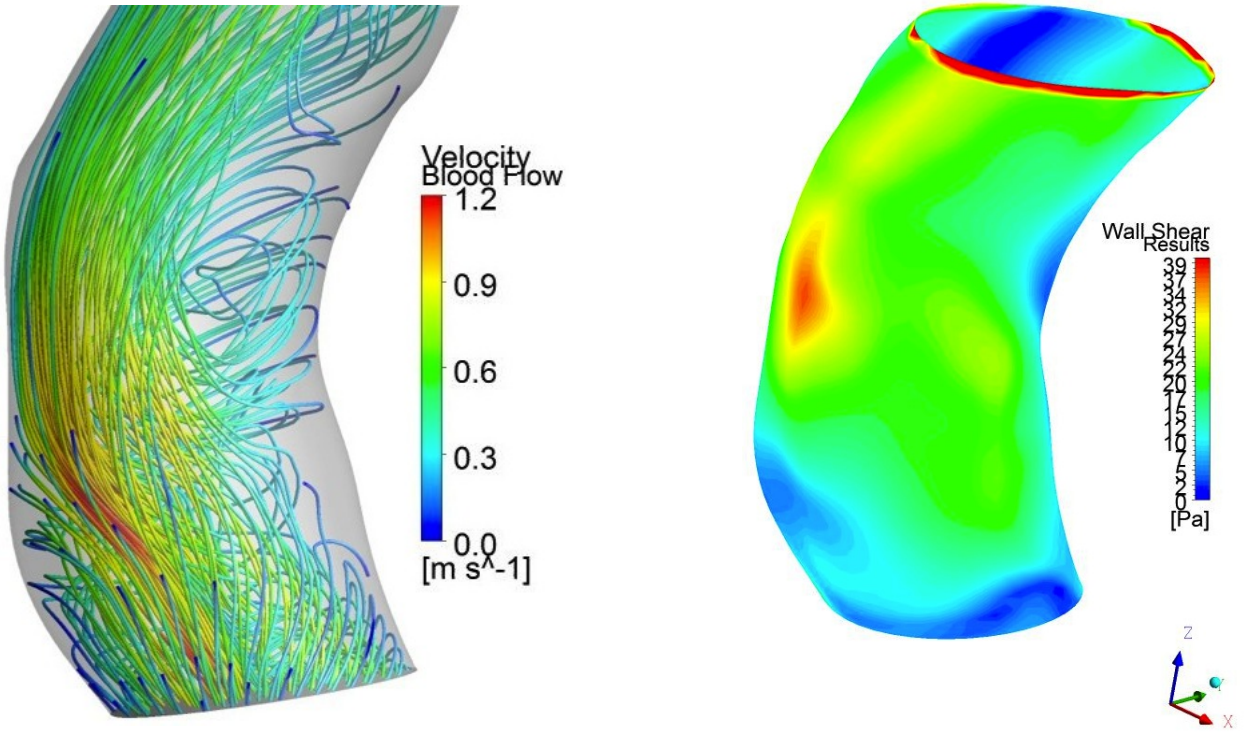

Figure 4.6: Left : Mesh B blood flow in the aneurysm. Right : Mesh B wall shear stress distribution in the aneurysm. Again, the aneurysm's inner wall region struck by the jet is the one with the highest wall shear stress value (in red).

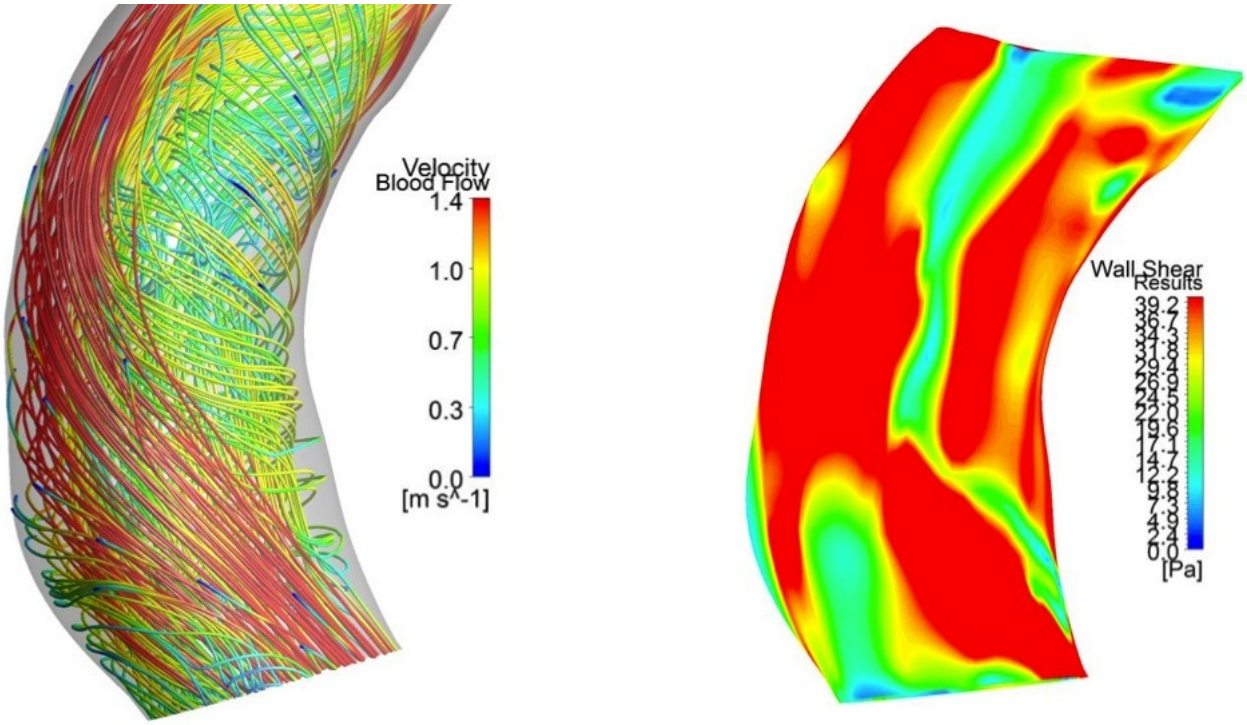

Figure 4.7: Left : Mesh C blood flow in the aneurysm. Right : Mesh C wall shear stress distribution in the aneurysm. From both images, it is evident that blood flow and WSS are overestimated if compared with the findings for meshes A and B. This is particularly evident for the WSS results, thus confirming the findings in (Prakash et Ethier, 2001), (De Santis *et al.*, 2010) and (Biswas et Strawn, 1998).

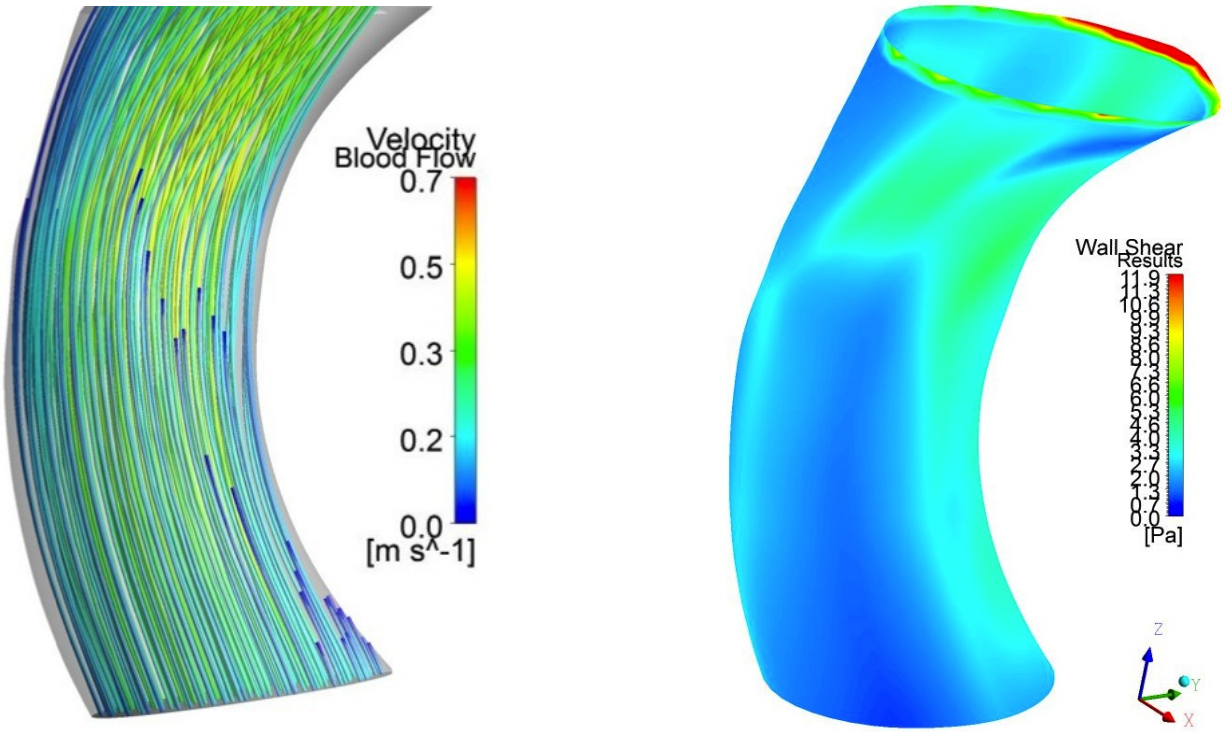

Figure 4.8: Left : Mesh B-1 blood flow in the aneurysm. Right : Mesh B-1 wall shear stress distribution in the aneurysm. In the physiological ascending aorta, the wall shear stress distribution does not have a relevant gradient and no zones with higher wall shear stress values can be appreciated.

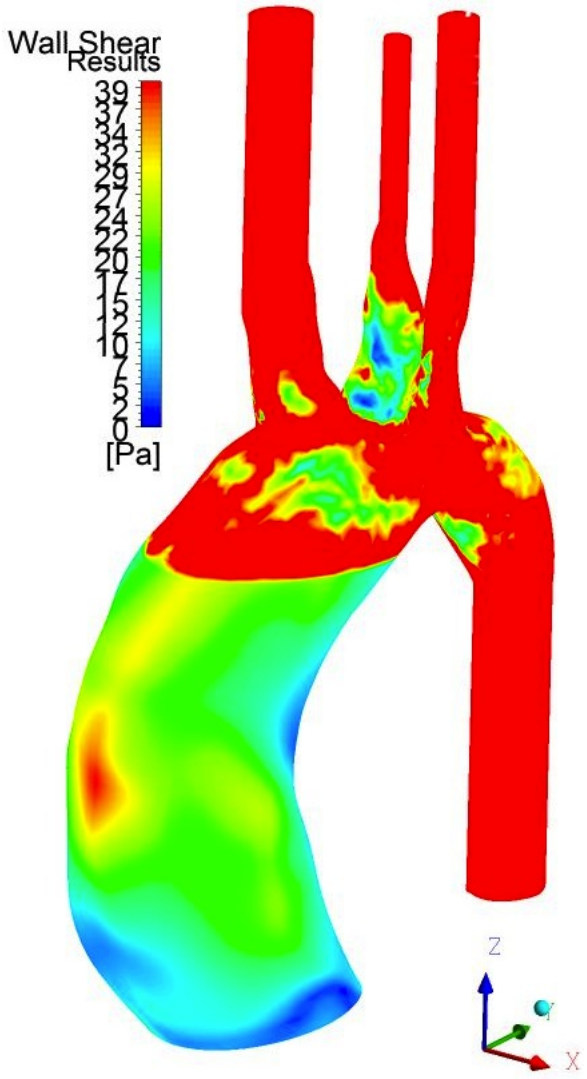

Figure 4.9: The WSS distribution in the whole mesh B shows how much impact have the different mesh elements (and meshing techniques) in the WSS results. Red zones, indicating higher WSS values, are much more present in the tetrahedral part of mesh B than in structured hexahedral part.

4.2 Corroboration Results

In this section, the results from a qualitative error analysis are displayed. More specifically, errors made during the segmentation step and the CAD modeling were considered. Furthermore, the convergence and sensitivity analyses for each of the meshes (A, B, C) built have been reported.

4.2.1 Segmentation and CAD Errors

Due to the lack of references in literature, the maximum error acceptable between MRI and segmented images and between MRI and CATIA model, was imposed to be less than or equal to 5%. This value was chosen considering the relative dimensions of the aorta, for which an error of more than 5% is a substantial approximation. Table 4.2 shows the whole set of measures taken to assess the errors made during the reconstruction. From the analysis of the averages, we can affirm that the reconstruction maintained almost the same size of the original images, as well as for the segmentation. In particular, the two principal errors, between the MRI images and the segmented images and between MRI images and CAD model, were under the 3%.

Table 4.2: Measurement taken in the three cases : the original MRI image, then the same image but with a snake segmentation and lastly measures taken within the CAD model. From the average, it is possible to notice the very low error made, which for all the cases is lower than 5%. All the measures are in mm.

Points	MRI	Segmentation	CAD
1-2	39.5	38.22	36.99
3-4	40.09	38.7	38.07
5-6	40.08	38.7	37.67
7-8	39.09	37.52	37.67
9-10	38.9	37.19	37.46
11-12	39.1	37.98	38.62
13-14	38.1	38.15	37.71
15-16	37.9	38.44	38.16
17-18	36.91	37.13	36.8
19-20	36.32	37.02	36.55
Average	38.6	37.9	37.57

4.2.2 Mesh Errors Results

As table 3.2 partially demonstrates, we were able to obtain three meshes high in quality. The dominating trend from the convergence and sensitivity analyses reports the superiority of mesh A (hexahedral structured mesh) when the convergence test is given, with comparable results between mesh B (hybrid mesh) and C (tetra mixed), for the sensitivity analysis. Figure 4.10 shows the graph resulting from the convergence analysis, while in the next figure (4.11) the results from the sensitivity analysis for the three meshes are plotted.

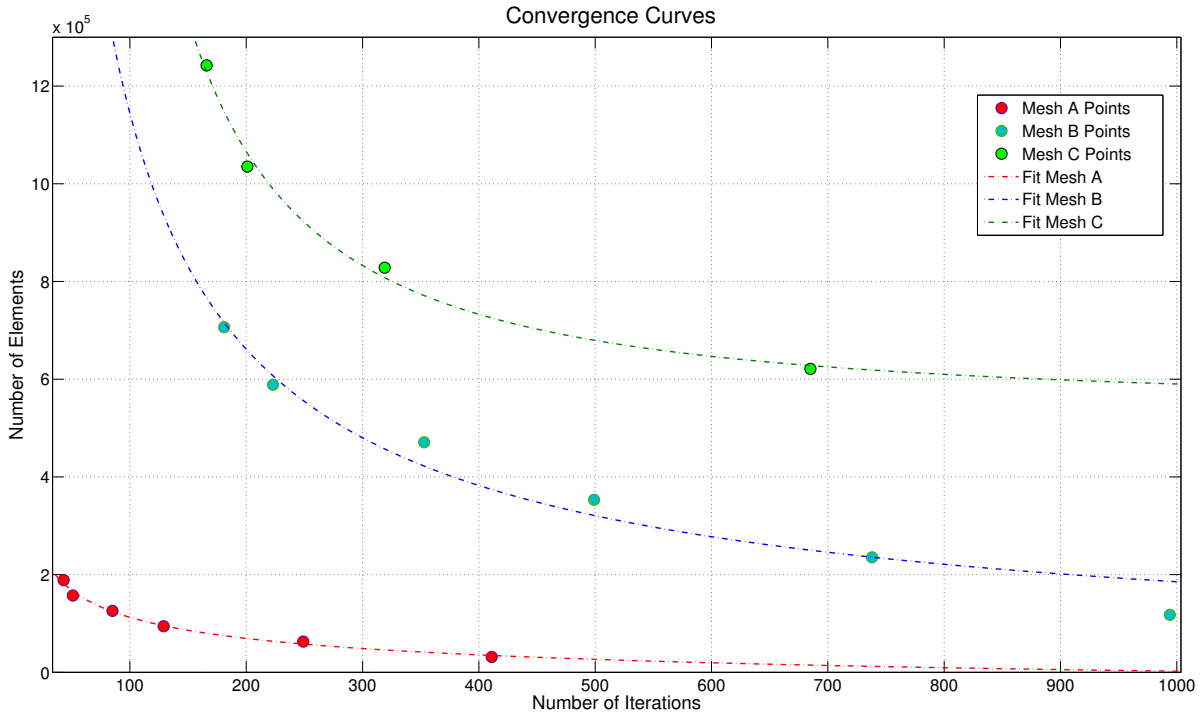

Figure 4.10: Mesh convergence analysis results. The graph shows the three interpolating curves, obtained with a Gaussian interpolation. The points indicate where the mesh reached the convergence (after the first cardiac cycle) for a specific mesh density. It is interesting to notice that meshes B and C are comparable, while mesh A reaches the convergence quickly, even for coarse configurations. The last two points (low density) for mesh C are not displayed, to better visualize the graph, but are included in the Gaussian interpolation.

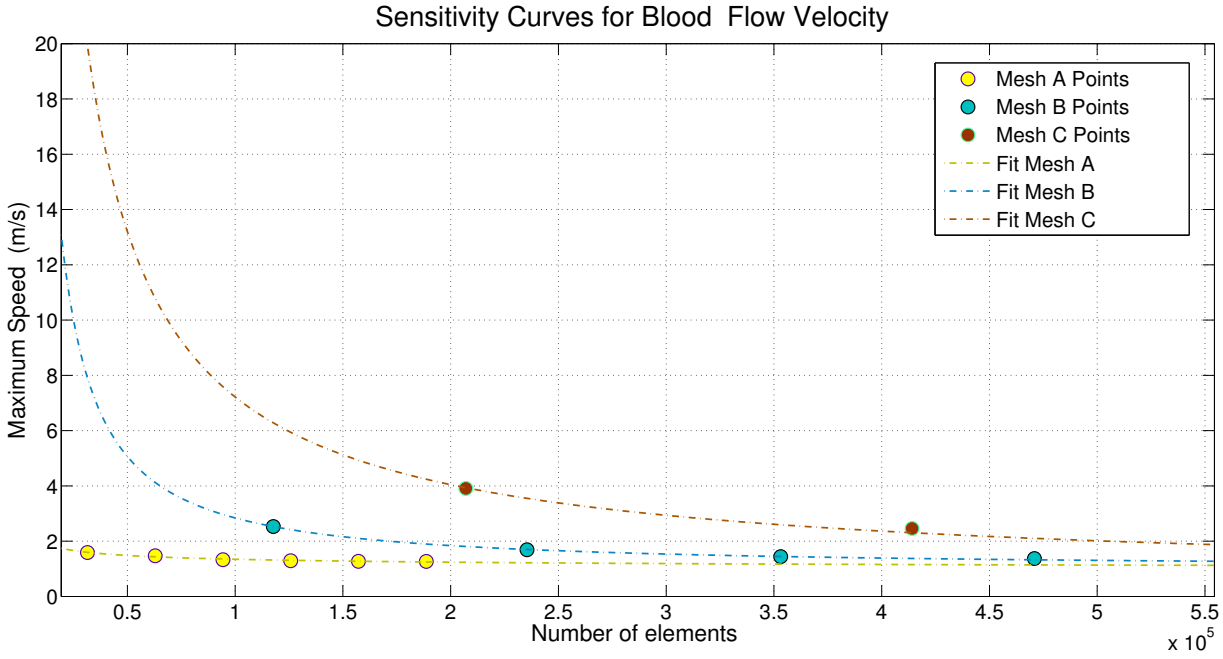

Figure 4.11: Mesh sensitivity analysis results. The graph shows the three interpolating curves, obtained with a Gaussian interpolation. The points indicate the values of maximum speed reached by the blood flow in function of the density of the mesh, at the end of the simulation. Again, meshes B and C are comparable, while mesh A shows similar speed values for almost all six configurations. For the best visualization, certain points of mesh B and mesh C were not included in the plotting, even if they were fitted by the Gaussian interpolation.

CHAPTER 5

DISCUSSION

THIS STUDY aimed to build a parametric CAD model of the human ascending aorta in a patient-specific case, in order to perform a fluid dynamics analysis within this model. To better follow the achievement of this global objective, five sub-objectives were formulated (Research Objectives). Having accomplished all the sub-objectives posed, we can affirm that the global objective was also attained. Thus, the originality of this research project is now evident, having built a parametric CAD model of the ascending aorta which is not, at the present time, seen in literature. In particular, the parametric feature developed, which is the second sub-objective, represents the most innovating aspect of this work justifying the effort spent building a CAD model instead of the more common models based solely on segmentation present in literature (see CAD and CFD Modeling).

While attaining the first sub-objective (to conceive a highly reliable CAD model), one of the most problematic factors was modeling the area between the aortic arch, the brachiocephalic artery and the left common carotid artery. The accurate CAD modeling of this trifurcation allows one to assess the extent of non-physiological change in the blood velocity streamlines and in the WSS. To solve this problem, the Fillet and Round feature in CATIA was implemented, combined with the Cut & Assembly feature. In literature, the few CAD models developed use other CAD softwares to resolve this issue, for instance, Pro/ENGINEER (Biadillah, 2005) or SolidWorks (Li et Kleinstreuer, 2006) or use the Center Line method (Antiga, 2005), (Xiong *et al.*, 2012).

The second sub-objective, to achieve the parameterization, was attained by parameterizing the aneurysm aROI. This technique, explained in Parameterization, showed its potential when meshes B and B-1 are compared, showing different behaviors in blood streamlines when passing through the pathological aorta or the physiological one. This result was accomplished without changing any settings in the CFD software, except for the loaded mesh (from B to B-1). The entire process of generating a new mesh for the parameterized aROI, followed by importing the mesh into Fluent was relatively easy and time saving, when compared with cases that need to reload all the geometry of the model or modify the segmentation to obtain a new model. In literature, there is no evidence of this kind of procedure.

The third sub-objective, to generate the most reliable mesh, was achieved by building a set of 3 different meshes. This set was widely tested during CFD evaluations and convergence and sensibility analyses. Having achieved reliable results from these latter analyses,

which constitute the fourth sub-objective of this thesis, we were able to affirm that mesh A (structured) is the best mesh to assess blood flow and WSS evaluations, even if mesh B is more adaptable in the case of changes in geometry (for example, when the model's shape is modified due to different parameterization settings). We considered mesh A better than the others meshes because of the quality of the results that we obtained in much less time. In literature, the majority of the studies establishing which mesh is the most reliable are focused on circulatory system in general (Prakash et Ethier, 2001) and not in the region of the aorta.

To reach the last sub-objective (obtain CFD results comparable with the literature), we compared our results with two studies previously cited in section LITERATURE REVIEW. Having considered that, to the best of our knowledge to date, there are no published studies based on the evaluation of hemodynamics and variations in wall properties in BAV and AAoA in young patients, to compare blood speed results, the article by Faggiano *et al.* (2012) was used as a reference. Similarly, the article by Barker *et al.* (2010) was used as a reference when comparing WSS results. In general, the blood speed obtained for meshes A, B and C showed strong agreement with the reference article, our highest blood speed value being 1.4 ms^{-1} found with mesh C, and 1.2 ms^{-1} in the cited article. On the other hand, when considering our best blood speed results, we find a complete agreement with the article seeing as the blood speed found with mesh A equals 1.2 ms^{-1}.

In terms of WSS, in the cited article, Barker shows the WSS distribution. We cannot display this distribution in our study, so we extracted the WSS result of Barker's distribution. To do this, we calculated the integral of the curve that Barker obtained by plotting the local WSS in one section of the ascending aorta. The integral was calculated for the grey curve (figure 5 of the cited article), which is the curve showing the maximum value used to compare with the maximum value that we found in our CFD simulations. The result from the integral, calculated by MatLab, was 34.1 Pa which is in accordance with the maximum value that we found for mesh C (39.2 Pa). If we consider mesh A, the WSS result is even more precise compared to the reference article. The difference between the reference value and our own is most likely due to the fact that the integral was calculated for the cardiac cycle described in Barker's article (approximately 0.6 s), which is slightly shorter than the cardiac cycle considered in this study (0.8 s).

The 157226, 588567 and 828176 element configurations were finally chosen for meshes A, B and C respectively, looking at both the convergence and at the sensitivity analysis results. As a matter of fact, even if mesh configurations with more elements have been tested, we noticed a slight improvement in the final results and convergence time, which in essence suggests that augmenting mesh elements and in turn, total simulation time, do not produce more accurate results.

A problematic factor, encountered during the CFD modeling, concerned the pressure gradients. In a physiological setting, gradients allow blood to flow across the aortic valve and be distributed uniformly along the aortic route. Only a certain variation in pressure allows the blood to flow properly in the supra-aortic branches. Typically, the pressure at the turn of the aortic valve ranges between 80 and 120 mmHg at the instant before systole (isovolumic contraction). This value is influenced by a multitude of factors that are an intrinsic part of the mechanism of the heart. Assuming that there are no diseases upstream, where the bicuspid aortic valve is concerned, the variation in pressure is not guaranteed and pressure gradients are then modified. To solve this problem, the valve was modeled with an on/off mechanism meaning that when the valve is on, the pressure gradient is the one prescribed by the boundary conditions while in the opposite situation (valve off), no pressure gradient is prescribed and no blood is flowing. In the studies of Vergara *et al.* (2012), Faggiano *et al.* (2012) and Viscardi *et al.* (2010), this method is performed to simulate a bicuspid aortic valve.

The modeling of the pulsatile flow maintaining, therefore, the transitory characteristics of hemodynamics in the cardiovascular region, was a problematic factor faced. In the ascending aorta, the flow can not be considered developed or constant and nor is it possible to do in the aneurysmal portion. A part of the fluid indeed, in the first section of the aorta, has mixed laminar and almost turbulent characteristics, that is necessary to take into account. The particular properties of the blood also do not allow the use of standard models with simplified assumptions of classical Newtonian fluid or the use of models that employ inviscid fluids, without preventively prescribing some important conditions. In this work, we prescribed an inlet transient flow and an outlet transient pressure by using the UDF feature in Fluent, having previously discretized the flow rate and pressure waveform as described in CFD Analysis. In literature, several studies ((Varghese *et al.*, 2003), (Paul et Larman, 2009), (Panta et Harvey, 2012)) applied the UDF method to accomplish the transient characteristic in blood flow.

Mesh A, as expected, gave the best performance. Three cardiac cycles were accomplished to reach a solution independent of transient effects and the fourth cycle was considered to be the solution, as reported in literature (Antiga, 2005), (Stefanov *et al.*, 2013). The simulated time was 3.2 s, the time step size was set to 0.001 s and the maximum number of iterations per time step was set equal to 30. The simulation time needed to perform four cardiac cycles with these settings was about 9 hours. Results for mesh A show that the blood jet impacts the aneurysm wall, with a maximum speed of about 1.2 ms^{-1}, producing a range of WSS values reaching its maximum at about 37.2 Pa in the aneurysm region. This is in accordance with the WSS theory and with the behavior reported in the two reference articles. Moreover, the

blood flow streamlines in the aneurysm follow a pattern which creates helicity, as commonly seen in literature and explained in section Changes in Blood Flow Patterns.

Four cardiac cycles were also performed with mesh B, with the same time step size and maximum number of iterations per time step as mesh A. The simulation time needed was measured to be about 13 hours. As expected, results showed the same helicity observed in the blood flow streamlines of mesh A, with a maximum speed in the order of 1.2 ms^{-1}. The WSS values in the aneurysmatic region was measured to have peaked at about 38 Pa.

As expected, obtaining results with mesh C took several hours more than mesh A and mesh B. Four cardiac cycles were performed as in the previous cases, considering the fourth cycle as representative of the solution. The simulation time needed was about 19 hours, an increment of 105.5% and 73% compared to meshes A and B, respectively. This increase is principally due to the type of mesh used in this case. Even if the majority of the elements in mesh C are hexahedral, they are not built in a structured fashion, resulting in a unstructured or disoriented mesh, which has a notably lower performance when compared to a structured mesh. However, the precision of the results was not evidently affected (maximum speed and WSS 1.4 ms^{-1} and 39.2 Pa, respectively). The blood flow streamlines in the aneurysm follow the same pattern seen in meshes A and B, hitting the aneurysm wall and then creating helicity when blood flows upper.

Finally, for mesh B-1, which is a hybrid hexahedral and tetrahedral mesh, composed by 559416 elements and 123614 nodes, three cycles were performed before achieving a solution damped from transitoriness. The simulation time needed to accomplish this solution was about 12.5 hours. No helicity was noticed, but the major jet exited the valve (which is not modeled) and did not hit the arterial walls in a strong way. The blood flow streamlines in fact, showed a maximum speed of 0.61 ms^{-1} , which is physiological as well as the wall shear stress values, which remain in the normal physiologic ranges. Having achieved physiological results with a model built from a non-physiological one suggests that the parametrization feature worked and can be used further in this model.

In conclusion, although a well posed reference study for our work is still missing in literature, we did not noticed any particular difference between the values obtained in this study and the correspondent values of the two reference studies considered. Moreover, considering results from other studies already cited (Faggiano *et al.*, 2012), (Viscardi *et al.*, 2010), we can affirm that this study, even with its innovative parametrization aspect, can produce results that are aligned with similar ones published in literature.

CHAPTER 6

CONCLUSION

6.1 Summary

In this thesis, a patient specific case was investigated. The patient suffers from both an aneurysm of the ascending aorta and a bicuspid aortic valve. In order to build a three-dimensional CAD model, the biomedical images of the patient were segmented. The most innovative aspect of this model is the possibility to parametrize any part of it. To test the quality of the parameterization, the most important part of the model (the ascending aorta aneurysm) has been parameterized and tested in a CFD analysis. The parameterization consisted of transforming the aneurysm (maximum diameter of 40 mm) into a normal ascending aorta (maximum diameter of 25 mm).

To achieve the CFD analysis, a volume mesh was generated for both the pathological and the non-pathological models. For the pathological model, three different meshes obtained by three different meshing techniques were generated in order to understand which mesh offers the best performance, in terms of convergence and accuracy of results. The three generated meshes were a structured hexahedral mesh (mesh A), a hybrid hexahedral and tetrahedral mesh (mesh B) and a mixed hexahedral, tetrahedral and prismatic mesh (mesh C). To quantify mesh quality, two kinds of analyses were performed : mesh convergence and mesh sensitivity analysis. The two analyses were achieved by incrementing the density of the mesh by a constant quantity (25%, starting from a very coarse mesh).

For the mesh convergence analysis, the number of iterations needed by the mesh to converge after the first 800 iterations was noted (one cardiac cycle, the solution is iterated 30 times per time-step) and, for the sensitivity mesh analysis, the values for blood flow speed obtained at the end of one entire simulation were also noted (4 cardiac cycles, 3200 iterations, solution iterated 30 times per time-step). Results from the two analyses proved the superiority of mesh A, over meshes B and C. The non-pathological mesh (mesh B-1) showed the same behavior as mesh B (from which it was derived). Finally, a CFD assessment was accomplished for the set of four meshes measuring the average wall shear stress and the blood flow speed after four cardiac cycles. Results showed that blood flow streamlines follow the same path as it was described in literature. Moreover, blood flow speed and wss values agreed with comparable values found in literature.

During the modeling process of this study, particular emphasis was placed on the mesh

generation step since it is the author's conviction that the global quality of the mesh plays a fundamental role in the CFD analysis. Unfortunately, achieving a reliable mesh when dealing with human structures constitutes a challenge that, only few years ago, was hardly even conceivable. Nevertheless, several new meshing techniques and meshing softwares were recently proposed. For example, the highly interesting *vmtk* project, in development since 2004, is a collection of python based libraries that, thanks to their considerable flexibility, are becoming more and more popular in biomedical engineering.

CAD parametric modeling is an important feature developed in this project. The vast majority of CFD studies are carried out in segmentation based models, since they are relatively easier to obtain if compared to CAD models and, consequently, are more time-saving. Furthermore, as they require less user intervention, these segmentation based models are supposed to end up with less potential errors. However, these kinds of models often come as they are and cannot be directly manipulated. Even if some corrections are still possible, both for the segmentation and the model, the available operations are very limited and, in any case, not comparable with the ones available within a CAD modeling software. Parametrization, for example, is a feature that no segmentation software or a similar one can afford. The possibility of parametrizing almost every single part of a CAD model is the key feature of this developed model. Through the parametrization of the diameter of the aneurysm, the diameter of the patient-specific case was changed to a physiological value. Then, by importing the modified geometry into the meshing software, a mesh was generated only for the desired geometry, which permitted to save time.

Another problem inherent to the case studied in this project is the reliability of the model's representation of reality. This obstacle, which summarizes in itself the great dilemma of computer-assisted modeling in the biomedical field, becomes of particular importance. It is known that a model, even if it is as advanced as it is described by the best equations currently known, it will always maintain a certain margin of error, albeit infinitesimal. For this reason, the question posed is always how to build a faithful model, how to estimate reality accurately. This question becomes of primary importance in the biomedical field where the incorrect interpretation of a phenomenon can generate significant damage. In this research project, tests for the estimation of the most critical steps in the modeling process have been carried out as proof of validation. It is evident that, until human intervention characterizes the creation of an engineering model, the error will be intrinsic to the modeling and it will be interesting to estimate and to control it.

6.2 Study Limitations

Despite our best effort to achieve all the objectives in the most accurate way, this study contains certain limitations. For each step of the reconstruction process, limitations of the study can be found in the form of approximation or intrinsic limitations. Approximations typically concern user skills, experience or time constraints while intrinsic limitations can include the number of patients investigated, the quality of the device used to take measurements or images, the availability of softwares or the software's internal behavior. For this study, we experienced both approximation and intrinsic limitations.

Limitations in this study as a result of approximations can be found in the lack of a repeatability analysis for the segmentation process. In general, repeatability analyses are considered to be more valid than an analysis based on the comparison between segmentation and original images, but require the presence of other persons in order to repeat the segmentation resulting in a very time consuming process.

Another limitation can be due to the reconstruction technique used when building the CAD model. As a matter of fact, other techniques exist, such as the techniques based on Center Lines, which produce a series of splines built around a common segment (Center Line) that follows the blood path. CATIA possesses many tools to perform a Center Line based reconstruction, which can, in turn, produce powerful models. Furthermore, during the CAD step, the aortic valve was modeled as rigid, an assumption that does not completely match reality and that can vary the results considering that a normal aortic valve and a bicuspid aortic valve exhibit different mechanical behaviors (Weinberg et Kaazempur Mofrad, 2008). Finally, a CAD model of the aorta which also accounts for wall deformations (no rigid walls assumption) will better simulate the reality of this region and, assuming the aorta walls to be rigid should be considered an approximation even if WSS results seem to be influenced by a maximum of 10% as a result of this approximation (Jin *et al.*, 2003).

Due to the author's inexperience in calculating values of OSI or of WSS in other temporal or spatial configurations, a result for WSS was found which requires further integration for it to be directly comparable with the WSS results in literature. This calculation can be difficult or approximative if data concerning the WSS trend are not displayed in the reference article.

In the CFD process, a number of approximations were made, beginning by approximating the blood viscosity with a Newtonian blood model chosen to perform the CFD analysis. This assumption, even if it is quite realistic in the region of the aorta, does not reflect reality at one hundred percent seeing as the blood is a non-Newtonian fluid. Another assumption was made in CFD post-processing. Because of the limitation in the user experience, the oscillatory shear stress index was not assessed. This index has been found to be important, especially

in atherosclerosis investigation (Ku *et al.*, 1985) and can offer a better comprehension when assessing WSS. To improve the calculation time in Fluent, the Semi-Implicit Method for Pressure Linked Equations (SIMPLE) algorithm was used to couple pressure and velocity. Additionally, a Second Order Upwind algorithm was used to discretize the momentum. A more complex algorithm, which produces a better approximation, could have been used to assess the final results.

The most relevant intrinsic limitation of this study relies on the fact that this is a patient-specific study. Even if CFD investigations are usually made for patient-specific cases, the same investigation made on a group of patients could improve the global quality of the results thus increasing the power of the study. However, a study involving a group of patients requires significant resources and that cannot be assessed within the time frame of a Master's degree. Another intrinsic limitation can be found in the quality of the MRI images, that, as discussed in section Second Selection, was poor due to various factors unrelated to the author.

6.3 Future Improvements

This work can be considered concluded in the terms of this Master's project, but leaves several aspects that can be further developed. In essence, the CFD analysis can be performed with a more powerful post-processing in order to investigate the correlation between the results with known fluid dynamics quantities such as the Reynolds number, the Womersley number and the Dean number. These three quantities are strictly correlated with the hemodynamics in the thoracic aorta and it would be interesting to quantify the dependence of the results, obtained with the developed aorta model, on these three quantities.

Furthermore, a study focused on finding a semi-automatic CAD reconstruction technique, which requires little time spent (and few interventions) by the user, could be a great improvement. Coupling this semi-automatic reconstruction process with the semi-automatic segmentation algorithm already developed by ((Zheng *et al.*, 2010), (Kurkure *et al.*, 2008) and (Rueckert *et al.*, 1997)) leads to the possibility of increasing the number of patients processed and therefore eliminating one of the greatest limitations of this study (and many more).

In addition, the parameterization in this study was made for the aneurysm aROI since the AAoA was one of the topics of this study. With the same parameterization technique, other parts can be parameterized, especially the geometric characteristics of the valve instead of its orientation in the aortic root. Achieving a fully parameterized thoracic aorta CAD model implies the possibility to study the dependence of the fluid dynamics results on parameters that can be simultaneously changed in order to evaluate multiple configurations.

Moreover, a study which accounts for Fluid-Structure Interaction (FSI) can be conceived

starting from the CAD model already developed. This kind of analysis, which are more realistic compared to ones where rigid walls are assumed, represents one of the most interesting field of biomechanics. It is a known fact that interaction between vessel walls and blood flow can be relevant in the arterial three (Mortazavinia *et al.*, 2012).

Lastly, the growing world of rapid prototyping nowadays allows the obtention of a physical phantom from a virtual model in few hours and without excessive costs. Thus, can be very interesting to test the developed CAD model within an *in-vitro* configuration, simulating the same conditions that were simulated in this thesis. Hence, comparing results obtained by the CFD analysis with the *in-vitro* fluid dynamics analysis will yield more valuable results.

REFERENCES

ABSI, T. S., SUNDT III, T. M., TUNG, W. S., MOON, M., LEE, J. K., DAMIANO JR, R. R. et THOMPSON, R. W. (2003). Altered patterns of gene expression distinguishing ascending aortic aneurysms from abdominal aortic aneurysms : complementary dna expression profiling in the molecular characterization of aortic disease. *The Journal of Thoracic and Cardiovascular Surgery*, 126, 344–357.

ACHNECK, H., MODI, B., SHAW, C., RIZZO, J., ALBORNOZ, G., FUSCO, D. et ELEFTERIADES, J. (2005). Ascending thoracic aneurysms are associated with decreased systemic atherosclerosis. *CHEST Journal*, 128, 1580–1586.

AGMON, Y., KHANDHERIA, B. et MEISSNER, I. (2004). Is aortic dilatation an atherosclerosis-related process ? clinical, laboratory, and transesophageal echocardiographic correlates of thoracic aortic dimensions in the population with implications for thoracic aortic aneurysm formation. *ACC Current Journal Review*, 13, 27.

AI, L. et VAFAI, K. (2005). An investigation of stokes' second problem for non-newtonian fluids. *Numerical Heat Transfer, Part A*, 47, 955–980.

AICHER, D., URBICH, C., ZEIHER, A., DIMMELER, S. et SCHÄFERS, H.-J. (2007). Endothelial nitric oxide synthase in bicuspid aortic valve disease. *The Annals of thoracic surgery*, 83, 1290–1294.

ALCORN, H. G., WOLFSON, S. K., SUTTON-TYRRELL, K., KULLER, L. H. et O'LEARY, D. (1996). Risk factors for abdominal aortic aneurysms in older adults enrolled in the cardiovascular health study. *Arteriosclerosis, thrombosis, and vascular biology*, 16, 963–970.

ANTIGA, L. (2005). *Patient-specific modeling of geometry and blood flow in large arteries*. Thèse de doctorat, Politecnico di Milano.

ANTIGA, L., PICCINELLI, M., BOTTI, L., ENE-IORDACHE, B., REMUZZI, A. et STEINMAN, D. A. (2008). An image-based modeling framework for patient-specific computational hemodynamics. *Medical & biological engineering & computing*, 46, 1097–1112.

BAKER, T. J., PEBAY, P. et POUSIN, J. (2002). Dynamic meshing for finite element based segmentation of cardiac imagery. *WCCM V-Fifth World Congress on Computational Mechanics, Vienna*.

BALLYK, P., STEINMAN, D. et ETHIER, C. (1993). Simulation of non-newtonian blood flow in an end-to-side anastomosis. *Biorheology*, 31, 565–586.

BARBOUR, J. R., SPINALE, F. G. et IKONOMIDIS, J. S. (2007). Proteinase systems and thoracic aortic aneurysm progression. *Journal of Surgical Research*, 139, 292–307.

BARKER, A. J., LANNING, C. et SHANDAS, R. (2010). Quantification of hemodynamic wall shear stress in patients with bicuspid aortic valve using phase-contrast mri. *Annals of biomedical engineering*, 38, 788–800.

BARKER, A. J., MARKL, M., BÜRK, J., LORENZ, R., BOCK, J., BAUER, S., SCHULZ-MENGER, J. et VON KNOBELSDORFF-BRENKENHOFF, F. (2012). Bicuspid aortic valve is associated with altered wall shear stress in the ascending aorta. *Circulation : Cardiovascular Imaging*, 5, 457–466.

BASKURT, O. K. et MEISELMAN, H. J. (1997). Cellular determinants of low-shear blood viscosity. *Biorheology*, 34, 235–247.

BASKURT, O. K. et MEISELMAN, H. J. (2003). Blood rheology and hemodynamics. *Seminars in thrombosis and hemostasis*. New York : Stratton Intercontinental Medical Book Corporation, c1974-, vol. 29, 435–450.

BASSO, C., BOSCHELLO, M., PERRONE, C., MECENERO, A., CERA, A., BICEGO, D., THIENE, G. et DE DOMINICIS, E. (2004). An echocardiographic survey of primary school children for bicuspid aortic valve. *The American journal of cardiology*, 93, 661–663.

BECKER, A. E., BECKER, M. J. et EDWARDS, J. E. (1970). Anomalies associated with coarctation of aorta particular reference to infancy. *Circulation*, 41, 1067–1075.

BEIGHTON, P., PAEPE, A. D., STEINMANN, B., TSIPOURAS, P. et WENSTRUP, R. J. (1998). Ehlers-danlos syndromes : revised nosology, villefranche, 1997. *American journal of medical genetics*, 77, 31–37.

BERGER, S., TALBOT, L. et YAO, L. (1983). Flow in curved pipes. *Annual Review of Fluid Mechanics*, 15, 461–512.

BERGWERFF, M., VERBERNE, M. E., DERUITER, M. C., POELMANN, R. E. et GITTENBERGER-DE GROOT, A. C. (1998). Neural crest cell contribution to the developing circulatory system implications for vascular morphology ? *Circulation research*, 82, 221–231.

BEROUKHIM, R. S., KRUZICK, T. L., TAYLOR, A. L., GAO, D. et YETMAN, A. T. (2006). Progression of aortic dilation in children with a functionally normal bicuspid aortic valve. *The American journal of cardiology*, 98, 828–830.

BIADILLAH, Y. (2005). *Hemodynamics of an Anatomically Realistic Human Aorta*. McGill University.

BIEGING, E. T., FRYDRYCHOWICZ, A., WENTLAND, A., LANDGRAF, B. R., JOHNSON, K. M., WIEBEN, O. et FRANÇOIS, C. J. (2011). In vivo three-dimensional mr wall shear stress estimation in ascending aortic dilatation. *Journal of Magnetic Resonance Imaging*, 33, 589–597.

BISSELL, M. M., HESS, A. T., BIASIOLLI, L., GLAZE, S. J., LOUDON, M., PITCHER, A., DAVIS, A., PRENDERGAST, B., MARKL, M., BARKER, A. J. *ET AL.* (2013). Aortic dilation in bicuspid aortic valve disease : Flow pattern is a major contributor and differs with valve fusion type. *Circulation : Cardiovascular Imaging*.

BISWAS, R. et STRAWN, R. C. (1998). Tetrahedral and hexahedral mesh adaptation for cfd problems. *Applied Numerical Mathematics*, 26, 135–151.

BONDERMAN, D., GHAREHBAGHI-SCHNELL, E., WOLLENEK, G., MAURER, G., BAUMGARTNER, H. et LANG, I. M. (1999). Mechanisms underlying aortic dilatation in congenital aortic valve malformation. *Circulation*, 99, 2138–2143.

BONOW, R. O., MANN, D. L., ZIPES, D. P. et LIBBY, P. (2011). *Braunwald's Heart Disease : A Textbook of Cardiovascular Medicine, 2-Volume Set*. Elsevier Health Sciences.

BRAUN, D. D. et ROSEN, M. R. (2008). *Rheology Modifiers Handbook : Practical Use and Applilcation*. Access Online via Elsevier.

BROOKE, B. S., HABASHI, J. P., JUDGE, D. P., PATEL, N., LOEYS, B. et DIETZ III, H. C. (2008). Angiotensin ii blockade and aortic-root dilation in marfan's syndrome. *New England Journal of Medicine*, 358, 2787–2795.

BROOKSHIER, K. et TARBELL, J. (1993). Evaluation of a transparent blood analog fluid : aqueous xanthan gum/glycerin. *Biorheology*, 30, 107.

BÜRK, J., BLANKE, P., STANKOVIC, Z., BARKER, A., RUSSE, M., GEIGER, J., FRYDRYCHOWICZ, A., LANGER, M., MARKL, M. *ET AL.* (2012). Evaluation of 3d blood flow patterns and wall shear stress in the normal and dilated thoracic aorta using flow-sensitive 4d cmr. *Journal of Cardiovascular Magnetic Resonance*, 14, 84.

BURMAN, E. D., KEEGAN, J. et KILNER, P. J. (2008). Aortic root measurement by cardiovascular magnetic resonance specification of planes and lines of measurement and corresponding normal values. *Circulation : Cardiovascular Imaging*, 1, 104–113.

BUSUTTIL, R. W., RINDERBRIECHT, H., FLESHER, A. et CARMACK, C. (1982). Elastase activity : the role of elastase in aortic aneurysm formation. *Journal of Surgical Research*, 32, 214–217.

C, F. Y. (1993). *Biomechanics : Mechanical Properties of Living Tissues*. Springer.

CAMPA, J., GREENHALGH, R. et POWELL, J. T. (1987). Elastin degradation in abdominal aortic aneurysms. *Atherosclerosis*, 65, 13–21.

CARTWRIGHT, N., CARTWRIGHT, N. et CARTWRIGHT, N. (1983). *How the laws of physics lie*. Cambridge Univ Press.

CHAN, W., DING, Y. et TU, J. (2007). Modeling of non-newtonian blood flow through a stenosed artery incorporating fluid-structure interaction. *Anziam Journal*, 47, C507–C523.

CHEN, H.-Q., ZHONG, G., LI, L., WANG, X.-Y., ZHOU, T. et CHEN, Z. (1991). Effects of gender and age on thixotropic properties of whole blood from healthy adult subjects. *Biorheology*, 28, 177.

CHENG, C., TEMPEL, D., VAN HAPEREN, R., VAN DER BAAN, A., GROSVELD, F., DAEMEN, M. J., KRAMS, R. et DE CROM, R. (2006). Atherosclerotic lesion size and vulnerability are determined by patterns of fluid shear stress. *Circulation*, 113, 2744–2753.

CHIASTRA, C., MORLACCHI, S., PEREIRA, S., DUBINI, G. et MIGLIAVACCA, F. (2012). Computational fluid dynamics of stented coronary bifurcations studied with a hybrid discretization method. *European Journal of Mechanics-B/Fluids*, 35, 76–84.

CHIEN, S., USAMI, S., DELLENBACK, R. J. et GREGERSEN, M. I. (1970). Shear-dependent deformation of erythrocytes in rheology of human blood. *American Journal of Physiology–Legacy Content*, 219, 136–142.

CHO, Y. et KENSEY, K. (1990). Effects of the non-newtonian viscosity of blood on flows in a diseased arterial vessel. part 1 : Steady flows. *Biorheology*, 28, 241–262.

CHOUDHURY, N., BOUCHOT, O., ROULEAU, L., TREMBLAY, D., CARTIER, R., BUTANY, J., MONGRAIN, R. et LEASK, R. L. (2009). Local mechanical and structural properties of healthy and diseased human ascending aorta tissue. *Cardiovascular Pathology*, 18, 83–91.

CLOUSE, W. D., HALLETT JR, J. W., SCHAFF, H. V., GAYARI, M. M., ILSTRUP, D. M. et MELTON III, L. J. (1998). Improved prognosis of thoracic aortic aneurysms. *JAMA : the journal of the American Medical Association*, 280, 1926–1929.

COADY, M. A., DAVIES, R. R., ROBERTS, M., GOLDSTEIN, L. J., ROGALSKI, M. J., RIZZO, J. A., HAMMOND, G. L., KOPF, G. S. et ELEFTERIADES, J. A. (1999). Familial patterns of thoracic aortic aneurysms. *Archives of Surgery*, 134, 361.

CORNONI-HUNTLEY, J. C., HARRIS, T. B., EVERETT, D. F., ALBANES, D., MICOZZI, M. S., MILES, T. P. et FELDMAN, J. J. (1991). An overview of body weight of older persons, including the impact on mortality the national health and nutrition examination survey i-epidemiologic follow-up study. *Journal of clinical epidemiology*, 44, 743–753.

COSOLO, W. C., MORGAN, D. J., SEEMAN, E., ZIMET, A. S., MCKENDRICK, J. J. et ZALCBERG, J. R. (1994). Lean body mass, body surface area and epirubicin kinetics. *Anti-cancer drugs*, 5, 293–297.

CROWLEY, T. A. et PIZZICONI, V. (2005). Isolation of plasma from whole blood using planar microfilters for lab-on-a-chip applications. *Lab on a Chip*, 5, 922–929.

DANIELS, S. R., KIMBALL, T. R., MORRISON, J. A., KHOURY, P. et MEYER, R. A. (1995). Indexing left ventricular mass to account for differences in body size in children and adolescents without cardiovascular disease. *The American journal of cardiology*, 76, 699–701.

DAVIES, R. R., KAPLE, R. K., MANDAPATI, D., GALLO, A., BOTTA JR, D. M., ELEFTERIADES, J. A. et COADY, M. A. (2007). Natural history of ascending aortic aneurysms in the setting of an unreplaced bicuspid aortic valve. *The Annals of Thoracic Surgery*, 83, 1338–1344.

DE GRUTTOLA, S., BOOMSMA, K. et POULIKAKOS, D. (2005). Computational simulation of a non-newtonian model of the blood separation process. *Artificial organs*, 29, 949–959.

DE SA, M., MOSHKOVITZ, Y., BUTANY, J. et DAVID, T. E. (1999). Histologic abnormalities of the ascending aorta and pulmonary trunk in patients with bicuspid aortic valve disease : clinical relevance to the ross procedure. *The Journal of Thoracic and Cardiovascular Surgery*, 118, 588–596.

DE SANTIS, G., DE BEULE, M., VAN CANNEYT, K., SEGERS, P., VERDONCK, P. et VERHEGGHE, B. (2011). Full-hexahedral structured meshing for image-based computational vascular modeling. *Medical engineering & physics*, 33, 1318–1325.

DE SANTIS, G., MORTIER, P., DE BEULE, M., SEGERS, P., VERDONCK, P. et VERHEGGHE, B. (2010). Patient-specific computational fluid dynamics : structured mesh generation from coronary angiography. *Medical & biological engineering & computing*, 48, 371–380.

DEN REIJER, P. M., SALLEE, D., VAN DER VELDEN, P., ZAAIJER, E. R., PARKS, W. J., RAMAMURTHY, S., ROBBIE, T. Q., DONATI, G., LAMPHIER, C., BEEKMAN, R. P. *ET AL.* (2010). Hemodynamic predictors of aortic dilatation in bicuspid aortic valve by velocity-encoded cardiovascular magnetic resonance. *J Cardiovasc Magn Reson*, 12.

DUDZINSKI, D. M., IGARASHI, J., GREIF, D. et MICHEL, T. (2006). The regulation and pharmacology of endothelial nitric oxide synthase. *Annu. Rev. Pharmacol. Toxicol.*, 46, 235–276.

EKNOYAN, G. (2008). Adolphe quetelet (1796–1874) ?the average man and indices of obesity. *Nephrology Dialysis Transplantation*, 23, 47–51.

ELEFTERIADES, J. A. (2002). Natural history of thoracic aortic aneurysms : indications for surgery, and surgical versus nonsurgical risks. *The Annals of thoracic surgery*, 74, S1877–S1880.

FAGGIANO, E., ANTIGA, L., PUPPINI, G., QUARTERONI, A., LUCIANI, G. B. et VERGARA, C. (2012). Helical flows and asymmetry of blood jet in dilated ascending aorta with normally functioning bicuspid valve. *Biomechanics and modeling in mechanobiology*, 1–13.

FERZIGER, J. H. et PERIĆ, M. (1996). *Computational methods for fluid dynamics*, vol. 3. Springer Berlin.

FILLINGER, M. F., MARRA, S. P., RAGHAVAN, M. et KENNEDY, F. E. (2003). Prediction of rupture risk in abdominal aortic aneurysm during observation : wall stress versus diameter. *Journal of Vascular Surgery*, 37, 724–732.

FILLINGER, M. F., RAGHAVAN, M., MARRA, S. P., CRONENWETT, J. L. et KENNEDY, F. E. (2002). In vivo analysis of mechanical wall stress and abdominal aortic aneurysm rupture risk. *Journal of Vascular Surgery*, 36, 589–597.

FORMAGGIA, L., GERBEAU, J.-F., NOBILE, F. et QUARTERONI, A. (2002). Numerical treatment of defective boundary conditions for the navier–stokes equations. *SIAM Journal on Numerical Analysis*, 40, 376–401.

FORMAGGIA, L., QUARTERONI, A. M. et VENEZIANI, A. (2009). *Cardiovascular Mathematics : Modeling and simulation of the circulatory system*, vol. 1. Springer.

FRANCO, K. L. et VERRIER, E. D. (2003). *Advanced Therapy of Cardiac Surgery*. PMPH-USA.

FREY, P. et GEORGE, P. (2010). *Mesh Generation*. Wiley.

GEWALTIG, M. T. et KOJDA, G. (2002). Vasoprotection by nitric oxide : mechanisms and therapeutic potential. *Cardiovascular research*, 55, 250–260.

GHORPADE, A. et BAXTER, B. T. (1996). Biochemistry and molecular regulation of matrix macromolecules in abdominal aortic aneurysms. *Annals of the New York Academy of Sciences*, 800, 138–150.

GIJSEN, F., ALLANIC, E., VAN DE VOSSE, F. et JANSSEN, J. (1999). The influence of the non-newtonian properties of blood on the flow in large arteries : unsteady flow in a 90 curved tube. *Journal of biomechanics*, 32, 705–713.

GIRDAUSKAS, E., BORGER, M. A., SECKNUS, M.-A., GIRDAUSKAS, G. et KUNTZE, T. (2011). Is aortopathy in bicuspid aortic valve disease a congenital defect or a result of abnormal hemodynamics ? a critical reappraisal of a one-sided argument. *European Journal of Cardio-Thoracic Surgery*, 39, 809–814.

GITTENBERGER-DE GROOT, A. C., DERUITER, M. C., BERGWERFF, M. et POELMANN, R. E. (1999). Smooth muscle cell origin and its relation to heterogeneity in development and disease. *Arteriosclerosis, thrombosis, and vascular biology*, 19, 1589–1594.

GLEASON, T. G. (2005). Heritable disorders predisposing to aortic dissection. *Seminars in thoracic and cardiovascular surgery*. Elsevier, vol. 17, 274–281.

HALLYNCK, T., SOEP, H., THOMIS, J., BOELAERT, J., DANEELS, R. et DETTLI, L. (1981). Should clearance be normalised to body surface or to lean body mass ? *British journal of clinical pharmacology*, 11, 523–526.

HARLOFF, A., NUßBAUMER, A., BAUER, S., STALDER, A. F., FRYDRYCHOWICZ, A., WEILLER, C., HENNIG, J. et MARKL, M. (2010). In vivo assessment of wall shear stress in the atherosclerotic aorta using flow-sensitive 4d mri. *Magnetic Resonance in Medicine*, 63, 1529–1536.

HE, R., GUO, D.-C., ESTRERA, A. L., SAFI, H. J., HUYNH, T. T., YIN, Z., CAO, S.-N., LIN, J., KURIAN, T., BUJA, L. *ET AL.* (2006). Characterization of the inflammatory and apoptotic cells in the aortas of patients with ascending thoracic aortic aneurysms and dissections. *The Journal of thoracic and cardiovascular surgery*, 131, 671–678.

HIRATZKA, L. F., BAKRIS, G. L., BECKMAN, J. A., BERSIN, R. M., CARR, V. F., CASEY, D. E., EAGLE, K. A., HERMANN, L. K., ISSELBACHER, E. M., KAZEROONI, E. A. *ET AL.* (2010). 2010 accf/aha/aats/acr/asa/sca/scai/sir/sts/svm guidelines for the diagnosis and management of patients with thoracic aortic disease. *Journal of the American College of Cardiology*, 55, e27–e129.

HO, V. B., BAKALOV, V. K., COOLEY, M., VAN, P. L., HOOD, M. N., BURKLOW, T. R. et BONDY, C. A. (2004). Major vascular anomalies in turner syndrome prevalence and magnetic resonance angiographic features. *Circulation*, 110, 1694–1700.

HOLLISTER, S. J., LEVY, R. A., CHU, T.-M., HALLORAN, J. W. et FEINBERG, S. E. (2000). An image-based approach for designing and manufacturing craniofacial scaffolds. *International Journal of Oral & Maxillofacial Surgery*, 29, 67–71.

HOLMES, K. W., LEHMANN, C. U., DALAL, D., NASIR, K., DIETZ, H. C., RAVEKES, W. J., THOMPSON, W. R. et SPEVAK, P. J. (2007). Progressive dilation of the ascending aorta in children with isolated bicuspid aortic valve. *The American journal of cardiology*, 99, 978–983.

HOPE, M. D., HOPE, T. A., MEADOWS, A. K., ORDOVAS, K. G., URBANIA, T. H., ALLEY, M. T. et HIGGINS, C. B. (2010). Bicuspid aortic valve : four-dimensional mr evaluation of ascending aortic systolic flow patterns. *Radiology*, 255, 53–61.

HOPE, T. A., MARKL, M., WIGSTRÖM, L., ALLEY, M. T., MILLER, D. C. et HERFKENS, R. J. (2007). Comparison of flow patterns in ascending aortic aneurysms and volunteers using four-dimensional magnetic resonance velocity mapping. *Journal of Magnetic Resonance Imaging*, 26, 1471–1479.

HOSHINA, K., SHO, E., MIEN, S., NAKAHASHI, T. K. et DALMAN, R. L. (2003). Wall shear stress and strain modulate experimental aneurysm cellularity. *Journal of vascular surgery*, 37, 1067–1074.

HUANG, C., PAN, W., CHEN, H. et COPLEY, A. (1986). Thixotropic properties of whole blood from healthy human subjects. *Biorheology*, 24, 795–801.

ISHIDA, T., TAKAHASHI, M., CORSON, M. A. et BERK, B. C. (1997). Fluid shear stress-mediated signal transduction : How do endothelial cells transduce mechanical force into biological responses ? *Annals of the New York Academy of Sciences*, 811, 12–24.

ITO, Y., COREY SHUM, P., SHIH, A. M., SONI, B. K. et NAKAHASHI, K. (2006). Robust generation of high-quality unstructured meshes on realistic biomedical geometry. *International Journal for Numerical Methods in Engineering*, 65, 943–973.

JIN, S., OSHINSKI, J. et GIDDENS, D. P. (2003). Effects of wall motion and compliance on flow patterns in the ascending aorta. *Journal of biomechanical engineering*, 125, 347–354.

JOHNSTON, B. M., JOHNSTON, P. R., CORNEY, S. et KILPATRICK, D. (2004). Non-newtonian blood flow in human right coronary arteries : steady state simulations. *Journal of biomechanics*, 37, 709–720.

JOHNSTON, B. M., JOHNSTON, P. R., CORNEY, S. et KILPATRICK, D. (2006). Non-newtonian blood flow in human right coronary arteries : transient simulations. *Journal of biomechanics*, 39, 1116–1128.

JUDGE, D. P. et DIETZ, H. C. (2005). Marfan's syndrome. *The Lancet*, 366, 1965–1976.

KANG, I. S. (2002). A microscopic study on the rheological properties of human blood in low concentration limit. *Korea-Australia Rheology Journal*, 14, 77–86.

KASS, M., WITKIN, A. et TERZOPOULOS, D. (1988). Snakes : Active contour models. *International journal of computer vision*, 1, 321–331.

KEANE, M. G., WIEGERS, S. E., PLAPPERT, T., POCHETTINO, A., BAVARIA, J. E. et SUTTON, M. G. S. J. (2000). Bicuspid aortic valves are associated with aortic dilatation out of proportion to coexistent valvular lesions. *Circulation*, 102, Iii–35.

KIRBY, M. L. et WALDO, K. L. (1990). Role of neural crest in congenital heart disease. *Circulation*, 82, 332–340.

KOULLIAS, G., MODAK, R., TRANQUILLI, M., KORKOLIS, D. P., BARASH, P. et ELEFTERIADES, J. A. (2005). Mechanical deterioration underlies malignant behavior of aneurysmal human ascending aorta. *The Journal of thoracic and cardiovascular surgery*, 130, 677–e1.

KU, D. N. (1997). Blood flow in arteries. *Annual Review of Fluid Mechanics*, 29, 399–434.

KU, D. N., GIDDENS, D. P., ZARINS, C. K. et GLAGOV, S. (1985). Pulsatile flow and atherosclerosis in the human carotid bifurcation. positive correlation between plaque location and low oscillating shear stress. *Arteriosclerosis, thrombosis, and vascular biology*, 5, 293–302.

KURKURE, U., AVILA-MONTES, O. C. et KAKADIARIS, I. A. (2008). Automated segmentation of thoracic aorta in non-contrast ct images. *Biomedical Imaging : From Nano to Macro, 2008. ISBI 2008. 5th IEEE International Symposium on*. IEEE, 29–32.

LADAK, H. M., MILNER, J. S. et STEINMAN, D. A. (2000). Rapid 3d segmentation of the carotid bifurcation from serial mr images. *ASME J. Biomech. Eng*, 122, 96–99.

LAL, P. et SUN, W. (2004). Computer modeling approach for microsphere-packed bone scaffold. *Computer-Aided Design*, 36, 487–497.

LAWRENCE, E. J. (2005). The clinical presentation of ehlers-danlos syndrome. *Advances in neonatal care*, 5, 301–314.

LEE, I.-M., MANSON, J. E., HENNEKENS, C. H. et PAFFENBARGER JR, R. S. (1993). Body weight and mortality. *JAMA : the journal of the American Medical Association*, 270, 2823–2828.

LEE, S.-W. et STEINMAN, D. A. (2007). On the relative importance of rheology for image-based cfd models of the carotid bifurcation. *Journal of Biomechanical Engineering*, 129, 273.

LEONDES, C. T. (2000). *Biomechanical Systems : Techniques and Applications, Volume IV : Biofluid Methods in Vascular and Pulmonary Systems*. Taylor & Francis.

LESAUSKAITE, V., TANGANELLI, P., SASSI, C., NERI, E., DICIOLLA, F., IVANOVIENE, L., EPISTOLATO, M. C., LALINGA, A. V., ALESSANDRINI, C. et SPINA, D. (2001). Smooth muscle cells of the media in the dilatative pathology of ascending thoracic aorta : morphology, immunoreactivity for osteopontin, matrix metalloproteinases, and their inhibitors. *Human pathology*, 32, 1003–1011.

LEVEY, A. S., BOSCH, J. P., LEWIS, J. B., GREENE, T., ROGERS, N. et ROTH, D. (1999). A more accurate method to estimate glomerular filtration rate from serum creatinine : a new prediction equation. *Annals of internal medicine*, 130, 461–470.

LI, Z. et KLEINSTREUER, C. (2006). Analysis of biomechanical factors affecting stent-graft migration in an abdominal aortic aneurysm model. *Journal of biomechanics*, 39, 2264–2273.

LIBBY, P., RIDKER, P. M. et MASERI, A. (2002). Inflammation and atherosclerosis. *Circulation*, 105, 1135–1143.

LIGHTHILL, J. (1975). *Mathematical Biofluiddynamics*. Society for Industrial and Applied Mathematics.

LIN, F. Y., DEVEREUX, R. B., ROMAN, M. J., MENG, J., JOW, V. M., JACOBS, A., WEINSAFT, J. W., SHAW, L. J., BERMAN, D. S., GILMORE, A. *ET AL.* (2008). Assessment of the thoracic aorta by multidetector computed tomography : age-and sex-specific reference values in adults without evident cardiovascular disease. *Journal of Cardiovascular Computed Tomography*, 2, 298–308.

LIU, Y., PEKKAN, K., JONES, S. C. et YOGANATHAN, A. P. (2004). The effects of different mesh generation methods on computational fluid dynamic analysis and power loss assessment in total cavopulmonary connection. *Journal of biomechanical engineering*, 126, 594–603.

LLOYD-JONES, D., ADAMS, R. J., BROWN, T. M., CARNETHON, M., DAI, S., DE SIMONE, G., FERGUSON, T. B., FORD, E., FURIE, K., GILLESPIE, C. *ET AL.* (2010). Heart disease and stroke statistics ?2010 update a report from the american heart association. *Circulation*, 121, e46–e215.

LOEYS, B. L., CHEN, J., NEPTUNE, E. R., JUDGE, D. P., PODOWSKI, M., HOLM, T., MEYERS, J., LEITCH, C. C., KATSANIS, N., SHARIFI, N. *ET AL.* (2005). A syndrome of altered cardiovascular, craniofacial, neurocognitive and skeletal development caused by mutations in tgfbr1 or tgfbr2. *Nature genetics*, 37, 275–281.

LOEYS, B. L., SCHWARZE, U., HOLM, T., CALLEWAERT, B. L., THOMAS, G. H., PANNU, H., DE BACKER, J. F., OSWALD, G. L., SYMOENS, S., MANOUVRIER, S. *ET AL.* (2006). Aneurysm syndromes caused by mutations in the tgf-β receptor. *New England Journal of Medicine*, 355, 788–798.

LONG, D. S., SMITH, M. L., PRIES, A. R., LEY, K. et DAMIANO, E. R. (2004). Microviscometry reveals reduced blood viscosity and altered shear rate and shear stress profiles in microvessels after hemodilution. *Proceedings of the National Academy of Sciences of the United States of America*, 101, 10060–10065.

MALEK, A. M., ALPER, S. L. et IZUMO, S. (1999). Hemodynamic shear stress and its role in atherosclerosis. *JAMA : the journal of the American Medical Association*, 282, 2035–2042.

MANSON, J. E., STAMPFER, M. J., HENNEKENS, C. H. et WILLETT, W. C. (1987). Body weight and longevity. *JAMA : the journal of the American Medical Association*, 257, 353–358.

MATURA, L. A., HO, V. B., ROSING, D. R. et BONDY, C. A. (2007). Aortic dilatation and dissection in turner syndrome. *Circulation*, 116, 1663–1670.

MAZUMDAR, J. N. (1992). *Biofluids Mechanics*. World Scientific.

MOHAMED, S. A., RADTKE, A., SARAEI, R., BULLERDIEK, J., SORANI, H., NIMZYK, R., KARLUSS, A., SIEVERS, H. H. et BELGE, G. (2012). Locally different endothelial nitric oxide synthase protein levels in ascending aortic aneurysms of bicuspid and tricuspid aortic valve. *Cardiology research and practice*, 2012.

MOORE, J., STEINMAN, D., HOLDSWORTH, D. et ETHIER, C. (1999). Accuracy of computational hemodynamics in complex arterial geometries reconstructed from magnetic resonance imaging. *Annals of biomedical engineering*, 27, 32–41.

MOORE, J. A., STEINMAN, D. A. et ROSS ETHIER, C. (1997). Computational blood flow modelling : Errors associated with reconstructing finite element models from magnetic resonance images. *Journal of Biomechanics*, 31, 179–184.

MORBIDUCCI, U. (2007). Does flow dynamics of the magnetic vascular coupling for distal anastomosis in coronary artery bypass grafting contribute to the risk of graft failure ? *International Journal of Artificial Organs*, 30, 628–639.

MORBIDUCCI, U., PONZINI, R., RIZZO, G., CADIOLI, M., ESPOSITO, A., DE COBELLI, F., DEL MASCHIO, A., MONTEVECCHI, F. M. et REDAELLI, A. (2009). In vivo quantification of helical blood flow in human aorta by time-resolved three-dimensional cine phase contrast magnetic resonance imaging. *Annals of biomedical engineering*, 37, 516–531.

MORTAZAVINIA, Z., GOSHTASBI RAD, E., EMDAD, H., SHARIFKAZEMI, M., ZARE, A. et MEHDIZADEH, A. (2012). Study of pulsatile non-newtonian blood flow through abdominal aorta and renal arteries incorporating fluid-structure interaction. *Journal of Biomedical Physics and Engineering*, 2.

NEREM, R. M., ALEXANDER, R. W., CHAPPELL, D. C., MEDFORD, R. M., VARNER, S. E. et TAYLOR, W. R. (1998). The study of the influence of flow on vascular endothelial biology. *The American journal of the medical sciences*, 316, 169–175.

NISTRI, S., BASSO, C., MARZARI, C., MORMINO, P. et THIENE, G. (2005). Frequency of bicuspid aortic valve in young male conscripts by echocardiogram. *The American journal of cardiology*, 96, 718–721.

NIWA, K., PERLOFF, J. K., BHUTA, S. M., LAKS, H., DRINKWATER, D. C., CHILD, J. S. et MINER, P. D. (2001). Structural abnormalities of great arterial walls in congenital heart disease light and electron microscopic analyses. *Circulation*, 103, 393–400.

O'CALLAGHAN, S., WALSH, M. et MCGLOUGHLIN, T. (2006). Numerical modelling of newtonian and non-newtonian representation of blood in a distal end-to-side vascular bypass graft anastomosis. *Medical engineering & physics*, 28, 70–74.

ORESKES, N., SHRADER-FRECHETTE, K., BELITZ, K. *ET AL.* (1994). Verification, validation, and confirmation of numerical models in the earth sciences. *Science*, 263, 641–646.

OTSU, N. (1975). A threshold selection method from gray-level histograms. *Automatica*, 11, 23–27.

PANTA, Y. et HARVEY, M. (2012). Technical brief : Computational fluid dynamic (cfd) analysis of blood flow through human arter-ies. *Journal of Computational Simulation and Modeling, ISSN*, 2231–3494.

PAPE, L. A., TSAI, T. T., ISSELBACHER, E. M., OH, J. K., O'GARA, P. T., EVANGELISTA, A., FATTORI, R., MEINHARDT, G., TRIMARCHI, S., BOSSONE, E. *ET AL.* (2007). Aortic diameter $\geq$ 5.5 cm is not a good predictor of type a aortic dissection observations from the international registry of acute aortic dissection (irad). *Circulation*, 116, 1120–1127.

PATEL, H. J. et DEEB, G. M. (2008). Ascending and arch aorta pathology, natural history, and treatment. *Circulation*, 118, 188–195.

PAUL, M. C. et LARMAN, A. (2009). Investigation of spiral blood flow in a model of arterial stenosis. *Medical engineering & physics*, 31, 1195–1203.

PEDLEY, T. J. (1980). *The fluid mechanics of large blood vessels*, vol. 1. Cambridge University Press Cambridge.

PEPIN, M., SCHWARZE, U., SUPERTI-FURGA, A. et BYERS, P. H. (2000). Clinical and genetic features of ehlers–danlos syndrome type iv, the vascular type. *New England Journal of Medicine*, 342, 673–680.

PERKTOLD, K., HOFER, M., RAPPITSCH, G., LOEW, M., KUBAN, B. et FRIEDMAN, M. (1997). Validated computation of physiologic flow in a realistic coronary artery branch. *Journal of biomechanics*, 31, 217–228.

PERKTOLD, K. et RAPPITSCH, G. (1995). Computer simulation of local blood flow and vessel mechanics in a compliant carotid artery bifurcation model. *Journal of biomechanics*, 28, 845–856.

POUTANEN, T., TIKANOJA, T., SAIRANEN, H. et JOKINEN, E. (2003). Normal aortic dimensions and flow in 168 children and young adults. *Clinical physiology and functional imaging*, 23, 224–229.

PRADO, C. M., RAMOS, S. G., ALVES-FILHO, J. C., ELIAS JR, J., CUNHA, F. Q. et ROSSI, M. A. (2006). Turbulent flow/low wall shear stress and stretch differentially affect aorta remodeling in rats. *Journal of hypertension*, 24, 503–515.

PRAKASH, S. et ETHIER, C. R. (2001). Requirements for mesh resolution in 3d computational hemodynamics. *Journal of biomechanical engineering*, 123, 134–144.

RANJAN, V., XIAO, Z. et DIAMOND, S. L. (1995). Constitutive nos expression in cultured endothelial cells is elevated by fluid shear stress. *American Journal of Physiology-Heart and Circulatory Physiology*, 269, H550–H555.

RAO, M. A. (2007). *Rheology of fluid and semisolid foods*. Springer.

REYNOLDS, H. R., TUNICK, P. A., KORT, S., ROSENZWEIG, B. P., FREEDBERG, R. S., KATZ, E. S., APPLEBAUM, R. M., PORTNAY, E. L., ADELMAN, M. A., ATTUBATO, M. J. *ET AL.* (2001). Abdominal aortic aneurysms and thoracic aortic atheromas. *Journal of the American Society of Echocardiography*, 14, 1127–1131.

RIMM, E. B., STAMPFER, M. J., GIOVANNUCCI, E., ASCHERIO, A., SPIEGELMAN, D., COLDITZ, G. A. et WILLETT, W. C. (1995). Body size and fat distribution as predictors of coronary heart disease among middle-aged and older us men. *American Journal of Epidemiology*, 141, 1117–1127.

ROBERTS, W. C. (1981). Dissection of the aorta associated with congenital malformation of the aortic valve. *American Heart Journal*, 101, 195–214.

RODKIEWICZ, C., SINHA, P. et KENNEDY, J. (1990). On the application of a constitutive equation for whole human blood. *Journal of biomechanical engineering*, 112, 198–206.

ROMAN, M. J., DEVEREUX, R. B., KRAMER-FOX, R. et O'LOUGHLIN, J. (1989). Two-dimensional echocardiographic aortic root dimensions in normal children and adults. *The American journal of cardiology*, 64, 507–512.

RUECKERT, D., BURGER, P., FORBAT, S., MOHIADDIN, R. et YANG, G.-Z. (1997). Automatic tracking of the aorta in cardiovascular mr images using deformable models. *Medical Imaging, IEEE Transactions on*, 16, 581–590.

SANTARPIA, G., SCOGNAMIGLIO, G., DI SALVO, G., D'ALTO, M., SARUBBI, B., ROMEO, E., INDOLFI, C., COTRUFO, M. et CALABRÒ, R. (2012). Aortic and left ventricular remodeling in patients with bicuspid aortic valve without significant valvular dysfunction : A prospective study. *International journal of cardiology*, 158, 347–352.

SCHMID, F.-X., BIELENBERG, K., SCHNEIDER, A., HAUSSLER, A., KEYSER, A. et BIRNBAUM, D. (2003). Ascending aortic aneurysm associated with bicuspid and tricuspid aortic valve : involvement and clinical relevance of smooth muscle cell apoptosis and expression of cell death-initiating proteins. *European journal of cardio-thoracic surgery*, 23, 537–543.

SHAHCHERAGHI, N., DWYER, H. A., CHEER, A. Y., BARAKAT, A. I. et RUTAGANIRA, T. (2002). Unsteady and three-dimensional simulation of blood flow in the human aortic arch. *Journal of biomechanics*, 124, 378–387.

SHIMIZU, K., MITCHELL, R. N. et LIBBY, P. (2006). Inflammation and cellular immune responses in abdominal aortic aneurysms. *Arteriosclerosis, thrombosis, and vascular biology*, 26, 987–994.

SHO, E., SHO, M., HOSHINA, K., KIMURA, H., NAKAHASHI, T. K. et DALMAN, R. L. (2004). Hemodynamic forces regulate mural macrophage infiltration in experimental aortic aneurysms. *Experimental and molecular pathology*, 76, 108–116.

SILVERMAN, D. I., BURTON, K. J., GRAY, J., BOSNER, M. S., KOUCHOUKOS, N. T., ROMAN, M. J., BOXER, M., DEVEREUX, R. B. et TSIPOURAS, P. (1995). Life expectancy in the marfan syndrome. *The American journal of cardiology*, 75, 157–160.

STALDER, A., RUSSE, M., FRYDRYCHOWICZ, A., BOCK, J., HENNIG, J. et MARKL, M. (2008). Quantitative 2d and 3d phase contrast mri : optimized analysis of blood flow and vessel wall parameters. *Magnetic resonance in medicine*, 60, 1218–1231.

STEFANOV, F., MCGLOUGHLIN, T., DELASSUS, P. et MORRIS, L. (2013). Hemodynamic variations due to spiral blood flow through four patient-specific bifurcated stent graft configurations for the treatment of abdominal aortic aneurysms. *International journal for numerical methods in biomedical engineering*, 29, 179–196.

STEINMAN, D. A. (2002). Image-based computational fluid dynamics modeling in realistic arterial geometries. *Annals of biomedical engineering*, 30, 483–497.

STEWART, W. J., KING, M. E., GILLAM, L. D., GUYER, D. E. et WEYMAN, A. E. (1984). Prevalence of aortic valve prolapse with bicuspid aortic valve and its relation to aortic regurgitation : a cross-sectional echocardiographic study. *The American journal of cardiology*, 54, 1277–1282.

SUN, W., DARLING, A., STARLY, B. et NAM, J. (2004). Computer-aided tissue engineering : overview, scope and challenges. *Biotechnology and Applied Biochemistry*, 39, 29–47.

TADROS, T. M., KLEIN, M. D. et SHAPIRA, O. M. (2009). Ascending aortic dilatation associated with bicuspid aortic valve pathophysiology, molecular biology, and clinical implications. *Circulation*, 119, 880–890.

TAGUCHI, M. et CHIDA, K. (2003). Computer reconstruction of the three-dimensional structure of mouse cerebral ventricles. *Brain research protocols*, 12, 10–15.

TANG, P. C., COADY, M. A., LOVOULOS, C., DARDIK, A., ASLAN, M., ELEFTERIADES, J. A. et TELLIDES, G. (2005). Hyperplastic cellular remodeling of the media in ascending thoracic aortic aneurysms. *Circulation*, 112, 1098–1105.

TAYLOR, C. A., DRANEY, M. T., KU, J. P., PARKER, D., STEELE, B. N., WANG, K. et ZARINS, C. K. (1999). Predictive medicine : computational techniques in therapeutic decision-making. *Computer Aided Surgery*, 4, 231–247.

TUTAR, E., EKICI, F., ATALAY, S. et NACAR, N. (2005). The prevalence of bicuspid aortic valve in newborns by echocardiographic screening. *American heart journal*, 150, 513–515.

VAN DE VOSSE, F., DE HART, J., VAN OIJEN, C., BESSEMS, D., GUNTHER, T., SEGAL, A., WOLTERS, B., STIJNEN, J. et BAAIJENS, F. (2003). Finite-element-based computational methods for cardiovascular fluid-structure interaction. *Journal of engineering mathematics*, 47, 335–368.

VARGHESE, S. S., FRANKEL, S. H. *ET AL.* (2003). Numerical modeling of pulsatile turbulent flow in stenotic vessels. *TRANSACTIONS-AMERICAN SOCIETY OF MECHANICAL ENGINEERS JOURNAL OF BIOMECHANICAL ENGINEERING*, 125, 445–460.

VERBRAECKEN, J., VAN DE HEYNING, P., DE BACKER, W. et VAN GAAL, L. (2006). Body surface area in normal-weight, overweight, and obese adults. a comparison study. *Metabolism*, 55, 515–524.

VERGARA, C., VISCARDI, F., ANTIGA, L. et LUCIANI, G. B. (2012). Influence of bicuspid valve geometry on ascending aortic fluid dynamics : a parametric study. *Artificial organs*, 36, 368–378.

VINCHURKAR, S. et LONGEST, P. (2008). Evaluation of hexahedral, prismatic and hybrid mesh styles for simulating respiratory aerosol dynamics. *Computers & Fluids*, 37, 317–331.

VISCARDI, F., VERGARA, C., ANTIGA, L., MERELLI, S., VENEZIANI, A., PUPPINI, G., FAGGIAN, G., MAZZUCCO, A. et LUCIANI, G. B. (2010). Comparative finite element model analysis of ascending aortic flow in bicuspid and tricuspid aortic valve. *Artificial organs*, 34, 1114–1120.

WALSH, M., WALLIS, F. et GRACE, P. (2005). 3-d numerical simulation of blood flow through models of the human aorta. *Journal of biomechanical engineering*, 127, 767.

WARD, C. (2000). Clinical significance of the bicuspid aortic valve. *Heart*, 83, 81–85.

WARREN, A. E., BOYD, M. L., O'CONNELL, C. et DODDS, L. (2006). Dilatation of the ascending aorta in paediatric patients with bicuspid aortic valve : frequency, rate of progression and risk factors. *Heart*, 92, 1496–1500.

WEIGANG, E., KARI, F. A., BEYERSDORF, F., LUEHR, M., ETZ, C. D., FRYDRYCHOWICZ, A., HARLOFF, A. et MARKL, M. (2008). Flow-sensitive four-dimensional magnetic resonance imaging : flow patterns in ascending aortic aneurysms. *European Journal of Cardio-Thoracic Surgery*, 34, 11–16.

WEINBERG, E. J. et KAAZEMPUR MOFRAD, M. R. (2008). A multiscale computational comparison of the bicuspid and tricuspid aortic valves in relation to calcific aortic stenosis. *Journal of biomechanics*, 41, 3482–3487.

WILLETT, W. C., STAMPFER, M., MANSON, J. et VANITALLIE, T. (1991). New weight guidelines for americans : justified or injudicious ? *The American journal of clinical nutrition*, 53, 1102.

XIONG, G., CHOI, G. et TAYLOR, C. A. (2012). Virtual interventions for image-based blood flow computation. *Computer-Aided Design*, 44, 3–14.

YASUDA, H., NAKATANI, S., STUGAARD, M., TSUJITA-KURODA, Y., BANDO, K., KOBAYASHI, J., YAMAGISHI, M., KITAKAZE, M., KITAMURA, S. et MIYATAKE, K. (2003). Failure to prevent progressive dilation of ascending aorta by aortic valve replacement in patients with bicuspid aortic valve : comparison with tricuspid aortic valve. *Circulation*, 108, II–291.

YUN, K. (2002). Ascending aortic aneurysm and aortic root disease. *Coronary artery disease*, 13, 79.

ZÉLICOURT, D. D., GE, L., WANG, C., SOTIROPOULOS, F., GILMANOV, A. et YOGANATHAN, A. (2009). Flow simulations in arbitrarily complex cardiovascular anatomies–an unstructured cartesian grid approach. *Computers & Fluids*, 38, 1749–1762.

ZHENG, Y., JOHN, M., LIAO, R., BOESE, J., KIRSCHSTEIN, U., GEORGESCU, B., ZHOU, S. K., KEMPFERT, J., WALTHER, T., BROCKMANN, G. *ET AL.* (2010). Automatic aorta segmentation and valve landmark detection in c-arm ct : application to aortic valve implantation. *Medical Image Computing and Computer-Assisted Intervention–MICCAI 2010*, Springer. 476–483.

ZYDNEY, A., OLIVER III, J. et COLTON, C. (1991). A constitutive equation for the viscosity of stored red cell suspensions : Effect of hematocrit, shear rate, and suspending phase. *Journal of Rheology*, 35, 1639.